Dissecting paraventricular hypothalamic neural circuits involved in energy balance control

by

Amy K. Sutton

A dissertation submitted in partial fulfillment
of the requirements for the degree of
Doctor of Philosophy
(Molecular and Integrative Physiology)
in the University of Michigan
2016

Doctoral Committee:

Assistant Professor David P. Olson, Co-Chair
Professor Martin G. Myers Jr., Co-Chair
Professor Suzanne M. Moenter
Associate Professor Geoffrey G. Murphy
Professor Audrey F. Seasholtz

“Tough it out, darlin’”-Fred Richard Sutton

Dedicated to:

Michelle Bremer Newsome,

Fred Richard Sutton II,

and

Fred Richard Sutton, my hero

Acknowledgements

Most importantly, thank you to my mentor, David Olson, for his never-ending support, friendship, and substantial investment in my development. I am forever indebted to Dave, who continually pushes me to become the best scientist and, more importantly, person I can be. Additionally, thank you to my co-mentor, Martin Myers Jr., for his continuous support and for teaching me the value of being strong in your convictions.

The collaborative environment of the Myers and Olson labs, developed by both Martin and Dave, fueled a training culture with hard-working individuals that set great examples of leadership. I am beyond lucky and grateful to have entered the lab with one of the best leaders training me in Megan Greenwald-Yarnell. Thank you also to my partner in crime, Meg Allison, for her friendship and support throughout the graduate school process. I am so grateful to Paula Goforth for her friendship, support, and for continually broadening my scientific viewpoint. I want to also thank other members of the Myers and Olson labs for their support over the years, both in and out of the lab, including Hongjuan Pei, Jonathan Flak, Jessica Adams, Justin Jones, and Tammy Barnes. Additionally, thanks to Korri Burnett for her significant scientific contribution to my projects, many of which I would not have completed without her assistance.

I'd like to thank Christa Polidori for her unwavering support and friendship from my days as a mess-up rotation student, to some of the hardest times of my life, and now through my final year in graduate school and beyond. I am lucky to consider Christa and Vince Polidori a part of my family.

I would like to acknowledge my sources of funding throughout graduate school: Ruth L. Kirschstein National Research Service Award (F31 NS 082027), National Institutes of Health; Rackham Pre-Doctoral Fellowship, Rackham School of Graduate Studies, University of Michigan; and the Systems and Integrative Biology Training Grant, National Institutes of Health.

Special thanks to my committee members for their significant support and time: Dr. Suzanne Moenter, Dr. Geoffrey Murphy, Dr. Audrey Seasholtz, and my co-chairs Dr. Martin Myers and Dr. David Olson. I would also like to thank Dr. Edward Stuenkel for his mentorship and friendship throughout my time in Michigan.

I owe gratitude to the Molecular and Integrative Physiology Department for the time, energy, and resources devoted to the continued success of graduate students. A special thanks to Michele Boggs for providing me with a significant amount of administrative support during my graduate studies.

Thank you to my classmates in the MIP and Neuroscience programs, and friends both near and far. I am grateful for the army of support I've had throughout the process. You all have continually pushed me to reach higher than I ever thought possible, and are always there to catch me when life goes sideways. I am beyond proud to call you all my friends.

Lastly, but certainly not least, thank you to my family. Thank you for giving me the strength I often needed, and the courage to continue. Throughout my life, you have taught me the value of education, dedication, and perseverance. You instilled in me the belief that success knows only one thing: hard work. I carry these values with me each and every day, at the end of which I hope to always make you proud.

Table of Contents

List of Figures

Figure:

Abstract

The dramatic increase in obesity and its comorbidities in recent years highlight the critical importance of understanding the factors contributing to dysregulated energy balance. While a relatively small percentage of genetic loci have been correlated with bodyweight, the genetic variations that have been characterized with obesity highlight hypothalamic circuits in the central nervous system (CNS) as an essential regulator of energy homeostasis. The paraventricular nucleus of the hypothalamus (PVH) is a necessary node in satiety regulation, since alterations in PVH development or function in mice and humans result in hyperphagic obesity. Yet, as a heterogenous nucleus, little is known about the specific cell-types used by the PVH to coordinate feeding suppression and/or energy expenditure. Therefore, we first identified the circuitry of genetically-defined PVH subpopulations in order to hypothesize their functional relevance based on projection targets. We combined this methodology with chemogenetic activation and neuronal ablation techniques to determine the function of separate PVH neuronal subpopulations in distinct energy balance parameters. Finally, we attempted to characterize the neural circuit map of afferent inputs to specific PVH cell populations based on their projection targets with the hypothesis that disparate PVH physiologic outputs may be regulated by non-overlapping neural populations.

First, we identify a genetic PVH population expressing *neuronal nitric oxide synthase 1* (Nos1) that is capable of feeding suppression, presumably through

projections to hindbrain regions known to be involved in feeding control. Moreover, while PVH oxytocin (OXT) neurons, a subset of the $Nos1^{PVH}$ field, do not control feeding behavior, they are capable of increasing energy expenditure, likely through connections to the spinal cord. We then characterize a non-Nos1, non-OXT PVH population expressing *insulin receptor substrate 4* (IRS4) that is necessary for normal feeding. $IRS4^{PVH}$ neurons also regulate energy expenditure, highlighting the significance of multiple, mutually exclusive, PVH populations in both feeding and energy expenditure control. Lastly, we highlight the dense interconnectivity of PVH subpopulations, with numerous PVH subtypes directly upstream of centrally-projecting PVH populations. Altogether, our results suggest the relevance of a complex intra-PVH network engaging distinct PVH subpopulations in order to ultimately coordinate feeding and energy expenditure regulation.

Chapter I

Introduction: Hypothalamic circuits coordinating energy balance regulation

As the prevalence of obesity and its complications continue to rise worldwide, so too do the associated financial and medical consequences. Obesity is not merely a cosmetic issue, as it is associated with an increased incidence of type II diabetes, cardiovascular disease, cancer, sleep apnea, and a variety of mental health conditions, including depression (1-3). In addition to contributing to other economic and societal burdens, obesity-related illness underlies 10% of current annual health care expenditures in the United States (4). It is therefore crucial that we understand the mechanisms contributing to the development and maintenance of obesity and its complications, as well as potential points of therapeutic intervention for this disease.

The effort to study and cure obesity is complicated by common misperceptions: that obesity is a cosmetic rather than a medical concern and that obesity is the result of personal shortcomings (i.e., poor self-control), rather than the result of biologically-encoded processes. Most “common” obesity likely results from complicated alterations in multiple gene products (to date, genome wide association studies (GWAS) have identified over 90 genetic regions that contain polymorphisms linked to the control of body weight) whose effects are unmasked by the ubiquitous availability of calories in modern society (5). The recent modest success of a number of weight-loss drugs that modulate systems known to participate in body weight control suggests the utility of

more thoroughly understanding these systems to identify additional potential therapeutic targets.

The principles underlying the control of body weight are straightforward: simply stated, homeostasis is achieved when the amount of energy consumed (by eating) equals that expended (by the combination of basal metabolic rate and physical activity). Increasing energy intake relative to energy expenditure results in positive energy balance and the storage of surplus calories as fat; negative energy balance is a result of decreasing food intake relative to energy expenditure (as in dieting) and decreases fat stores. Both energy intake and energy expenditure are largely governed by the central nervous system (CNS); this is supported by the fact that the obesity-linked genes identified in monogenetic syndromes and in human GWAS studies are expressed in the CNS to a much larger degree than other physiologic systems(5). Indeed, many of these genes have aided in the identification and analysis of the CNS circuits that control feeding and/or body weight(6). As research uncovers the specific genes affecting bodyweight control, it is increasingly clear that many of these target genes are important for the development and regulation of neural circuits(5). To further investigate these circuits, significant technological advancements have been made in genetic reagents that can be used in combination with more specified rodent models.

Hypothalamic circuits regulate feeding behavior and overall energy balance

Targeted chemical and electrolytic lesions of specific hypothalamic regions, including the ventromedial hypothalamus (VMH) and paraventricular nucleus of the hypothalamus (PVH), in rodents result in the rapid onset of robust obesity due to altered feeding

behavior and energy expenditure (7, 8). Indeed, many of the genetic markers identified to play a role in bodyweight regulation in humans are expressed in the hypothalamus, a limbic region coordinating endocrine, metabolic, and autonomic responses (5). While initial lesioning results suggested that the VMH in particular was the primary site coordinating satiety responses, more directed mechanical lesions or more specific genetic disruption of the PVH in mice and rats resulted in hyperphagic obesity, thus proving the PVH as the essential hypothalamic nucleus controlling feeding suppression (7, 9, 10). Later studies determined this to be due, in part, to dense PVH innervation from the arcuate nucleus of the hypothalamus (ARC) (11-14). ARC neurons lie adjacent to the median eminence (ME), a site near the base of the brain with permeable vasculature, and are positioned to detect circulating factors that convey information about peripheral energy stores. For example, ARC neurons contain receptors for both leptin and ghrelin, hormones relaying information about adiposity levels and hunger, respectively (15). ARC projections then transfer this information to the PVH, the primary hypothalamic output (Figure 5.1) (16, 17). The significance of the PVH in coordinating these ARC signals with other hypothalamic inputs to mediate feeding suppression is underlined by the fact that PVH disruption results in substantial hyperphagic obesity (18).

The PVH is a heterogeneous nucleus containing both parvocellular and magnocellular populations. Magnocellular PVH neurons are defined by both their size and direct projections to the posterior pituitary and are therefore capable of releasing neuropeptides immediately into the circulation. Conversely, parvocellular PVH neurons project within the brain and fall into two categories: 1) endocrine PVH neurons

projecting to the median eminence and depositing neuropeptides into the hypophyseal portal system to regulate anterior pituitary function, and 2) PVH neurons projecting throughout the brain, including the hindbrain, that regulate a broad range of behaviors and autonomic responses. Considerable research has focused on the neurosecretory PVH populations, since endocrine populations have distinct magnocellular or parvocellular electrophysiologic patterns that are commonly used to identify PVH cell types in brain slices, therefore providing valuable insight that relates neuronal physiology to endocrine function (19). Yet, fewer studies to date have examined the role of centrally-projecting circuits in energy balance regulation.

PVH control of energy balance and the melanocortin system

In addition to historic lesioning studies that identified the PVH as an essential node in the control of bodyweight, recent genetic studies have highlighted the importance of this site. Haploinsufficiency of *Sim1*, a transcription factor required for the development of the PVH (and the amygdala), results in an anatomically abnormal PVH and hyperphagic obesity in mice and humans (20, 21). Energy balance control by the PVH is further highlighted by the dense expression of *melanocortin 4 receptor* (Mc4R), a necessary gene in feeding suppression and energy balance regulation (22). Indeed, genetic alterations in Mc4R represent the most common monogenetic form of severe human obesity, underlying the phenotype of 1-2.5% of morbidly obese patients (23, 24). This hyperphagic obesity phenotype is replicated in Mc4R knock-out rodent models (25).

The endogenous melanocortins capable of binding and regulating Mc4R activity arise from ARC neurons expressing either *proopiomelanocortin* (POMC) or *agouti-*

related peptide (AgRP) (26, 27). Cleavage of the POMC peptide results in production of the anorexigenic α-MSH peptide, the predominant agonist of Mc4R (28). Conversely, separate ARC neurons release the orexigenic AgRP peptide, a Mc4R antagonist, in the PVH (26). The importance of the melanocortinergic ARC-PVH circuit is demonstrated by both the necessity and sufficiency of Mc4R signaling in the PVH for normal feeding behavior (29-31). Moreover, inhibition of PVH neuronal activity is consistently shown to be required for AgRP-induced feeding behavior (32, 33). Furthermore, Mc4R re-expression exclusively in neurons expressing *Sim1*, a transcription factor necessary for PVH development, in *Mc4R*-null mice normalizes feeding and reduces obesity by 60% (29). The persistence of modest obesity following restoration of *Mc4R* expression in PVH cells suggests that the melanocortin-dependent regulation of energy expenditure is likely carried out by non-PVH *Mc4R*-expressing neurons, some of which are located in the hindbrain and express choline acetyltransferase (34).

Although melanocortin signaling in the PVH does not appear to control energy expenditure, studies altering PVH function broadly suggest that the PVH controls sympathetic outflow (11, 35). Certainly, energy expenditure is a critical component of homeostasis, since alterations in physical activity, thermogenesis, or basal metabolic rate (BMR) can affect adiposity. However, defining the potential role of the PVH in energy expenditure regulation has been problematic since many genetic PVH alterations lead to robust obesity early in development, and assessments of energy expenditure in the obese state are complicated. Therefore, it is difficult to ascertain if PVH alterations directly decrease energy expenditure, or if energy expenditure deficits following PVH manipulations are instead all a result of hyperphagic obesity. Yet,

ablation of $Sim1^{PVH}$ neurons in adult animals decreases oxygen consumption prior to the onset of obesity, suggesting a role for the PVH in driving energy expenditure (36).

PVH circuits regulating energy balance

Neuronal subpopulations of the PVH

Although the majority of research on the PVH has been performed in animal models, the same heterogenous PVH populations have been identified in the adult human PVH as well, suggesting the relevance of studies performed in rodents (37). Large cells that make up the magnocellular PVH subdivision include those producing either arginine vasopressin (AVP) or oxytocin (OXT). Release of OXT or AVP in the neurohypophysis is directly controlled by neuronal activity in response to physiologic stimuli (38). Specifically, AVP is released due to alterations in serum osmolality or peripheral blood pressure in order to ultimately increase renal water absorption and vasoconstriction (39). While OXT can be co-released with AVP in the posterior pituitary due to blood pressure changes, it is primarily released in significant amounts during reproductive functions including parturition and lactation (19, 40).

Neurons producing corticotropin releasing hormone (CRH) are the primary parvocellular PVH population studied to date, since they coordinate the stress response through the hypothalamic-pituitary-adrenal (HPA) axis. Briefly, secretion of CRH by CRH^{PVH} neurons into the hypophyseal portal system at the median eminence causes portal transport into the anterior pituitary and a corresponding release of adrenocorticotropic hormone (ACTH) into the systemic circulation by pituitary corticotropes. ACTH then acts on the adrenal glands to cause cortisol release (41).

Similar to CRH, parvocellular thyrotropin-releasing hormone (TRH) neurons in the PVH regulate the pituitary in order to stimulate thyrotropin-stimulating hormone (TSH) and prolactin release from the anterior pituitary to regulate metabolism and reproductive functions, respectively (42). Additional parvocellular PVH populations capable of regulating ACTH production through the HPA axis likely include both OXT and AVP, though there is less understanding of how these neuropeptides affect anterior pituitary function (43).

The characterization of centrally-projecting parvocellular PVH neurons continues to develop with the increasing number of research tools available to study individual PVH populations in rodent models. Significant research has been performed on parvocellular OXT neurons, since centrally-administered OXT causes a variety of behavioral responses including decreased feeding, decreased anxiety-like behaviors, increased social behaviors, and decreased stress responses (44-47). More recently, intranasal OXT administration has been studied in humans in an effort to treat diseases including autism, obesity, and obsessive-compulsive disorder (48-50). Given the diverse functions associated with OXT action and the wide expression of OXT receptors (OXTR) throughout the brain, it is perhaps not surprising that the neurobiology of central OXT is particularly complex. In relation to feeding regulation, OXT neurons are implicated as connectors between peripheral sensing neurons in the ARC and satiety centers in brainstem regions including the nucleus of the solitary tract (NTS). Indeed, OXT peptide immunoreactivity (IR) can be detected in the NTS, a site with OXTR localization (51). Furthermore, retrograde tracing studies employing fluorogold and cholera toxin B have identified OXT^{PVH} neuronal projections to the NTS in the rat (52).

Some of these NTS-projecting OXT^{PVH} neurons are activated following peripheral leptin treatment, further suggesting a role for these cells in conveying the ARC-PVH signal to the NTS and potentially signaling satiety (53). Consistently, hyperphagic obese *Sim1* haploinsufficient mice demonstrate decreased *Oxt* expression (54, 55).

While these studies suggest the importance of OXT^{PVH} neurons in PVH-mediated control of energy feeding, OXT knock-out and OXT neuron ablation studies do not support these findings. Specifically, elimination of the OXT or OXT receptor (OXTR) genes in mice has little effect on body weight regulation (56, 57). In fact, these mice display only a slight enhancement of diet-induced obesity which is due to decreased energy expenditure, but not hyperphagia (57). This lack of a feeding phenotype is not a consequence of developmental compensation, since genetic ablation of OXT neurons in adult mice produces similar results (58). Moreover, the re-expression of *Mc4R* in OXT neurons fails to abrogate hyperphagia or obesity in Mc4R-null mice, suggesting that the control of feeding by the PVH and PVH melanocortin signaling is independent of OXT neurons (30). $Mc4R^{PVH}$ neurons express little if any OXT, further supporting these findings (33).

While centrally-projecting parvocellular PVH populations are diverse, AVP^{PVH} and TRH^{PVH} neurons are the only other PVH populations that have been shown to directly regulate energy balance. Specifically, chemogenetic AVP^{PVH} neuronal activation slightly decreases feeding, whereas driving TRH^{PVH} neuronal activity results in increased food intake through activation of feeding circuits in the ARC (59, 60). Less is known regarding the ability of CRH^{PVH} neurons to control energy balance, since CRH is more widely produced throughout the brain therefore making it difficult to determine

PVH-specific CRH effects. Moreover, CRH knock-out animals do not demonstrate a bodyweight phenotype (61). Thus, while it is clear that central CRH administration is anorexigenic and thermogenic, it is not known if this is carried out by CRH^{PVH} neurons (62, 63). Furthermore, neither CRH^{PVH} nor AVP^{PVH} neuronal re-expression of *Mc4R* rescues the obesity due to knock-out of Mc4R (30).

Intra-PVH connectivity: characterization of the PVH microenvironment

As an essential node in the regulation of the stress response, PVH neurons are plastic and therefore capable of expressing combinations of neuropeptides in different physiologic paradigms. While populations are considered to be mutually exclusive in the basal state, CRH^{PVH} neurons can upregulate AVP expression in order to co-release AVP and CRH in context with decreased peripheral corticosteroid levels (64). Although OXT release has been identified in the hypophyseal portal system, and is increased as a result of CRH administration, it is not clear if this is due to co-release of CRH and OXT from the same neurons following chronic stress (43, 65, 66). Moreover, physiologic stressors can cause morphological plasticity in the PVH. In particular, lactation causes alterations in dendritic branching in AVP and OXT neurons as well as changes in the excitatory and inhibitory inputs to these neurons (67-69).

The PVH is also highly interconnected, with multiple neuropeptide populations communicating with one another in a complex intra-PVH network. This was originally discovered using Golgi staining methods that identified axonal collaterals between parvocellular PVH populations (70). Further studies employed light and electron micrographic techniques to validate interconnected PVH populations, including CRH^{PVH}

neurons that synapse on other PVH neurons (71-73). More recently, electrophysiologic studies have characterized glutamatergic PVH interneuron populations capable of regulating other parvocellular PVH neurons (74, 75). These excitatory PVH interneurons are required for the changes in magnocellular PVH neuronal activity observed in response to neurochemical inputs such as norepinephrine, orexin, and angiotensin as well as physiologic inputs such as restraint stress (75-78). Similarly, parvocellular PVH neurons projecting to the spinal cord have been shown to receive glutamatergic input, likely from neurons within the PVH (79).

Aside from axonal connections, PVH neurons also have the ability to release neuropeptides through dendrites, with dendritic processes extending within different PVH subnuclei (72, 80). Microdialysis studies first demonstrated intranuclear AVP and OXT release in the PVH in various physiologic paradigms including stress responses and lactation (81, 82). Furthermore, some of these stress-induced intra-PVH increases in AVP do not alter circulating levels of AVP, suggesting that the relevance of intranuclear neuropeptide release on local PVH circuits is independent of endocrine output (83). Although these studies did not demonstrate direct dendritic neuropeptide release, further electrophysiologic studies employed caged NMDA strategies to confirm dendritic release of AVP on pre-sympathetic PVH populations (80). Taken together, these studies suggest dense intra-PVH connectivity between glutamatergic PVH interneurons, neuropeptide populations, and pre-autonomic PVH outputs.

Neuroanatomy of PVH outputs and energy balance control

The circuitry engaged by PVH populations enables it to control pituitary function, feeding and sympathetic output. As previously mentioned, PVH projections to the median eminence and neurohypophysis regulate pituitary function. PVH projections throughout the CNS are widely considered to be the relevant circuits for energy balance control. Specifically, PVH projections to three sites are likely significant in these processes: hindbrain sites including the parabrachial nucleus (PBN) and NTS, and the intermediolateral column of the thoracic spinal cord (IML).

Nucleus of the Solitary Tract (NTS)

In general, the brainstem integrates neural and hormonal signals from the periphery, especially those derived from the gut. The brainstem relays these signals to forebrain, hypothalamic, and cortical regions to coordinate appropriate behavioral and physiologic responses. For the regulation of satiety, projections from the PVH to the NTS are of particular interest, since the NTS is anatomically close to the area postrema (AP), a site adjacent to the fourth ventricle that lacks a blood brain barrier. The adjacent NTS is therefore the primary CNS site of visceral input as it receives both AP- and vagally-derived gut signals of acute and chronic nutritional state, which it passes on to the dorsal motor nucleus of the vagus (DMV) to control gut motility and vagal reflexes (84). The NTS integrates both hypothalamic (through inputs from the PVH and, to a lesser extent, other hypothalamic sites) and vagal signals to coordinate the satiety response following ingestion of a meal. The circuitry engaged by the NTS to achieve the satiety response is largely unknown, although direct glutamatergic projections to the PBN and reciprocal connections back to the PVH have the potential to play a role (85-90).

Although PVH-NTS projections are primarily thought of in the regulation of feeding behavior, the NTS also has the potential to regulate sympathetic activity, since it is also indirectly connected to brown adipose tissue (BAT) (91). BAT is the primary driver of thermogenesis, and therefore a key contributor to basal metabolic rate (BMR) and overall energy expenditure. Indeed, the NTS has also been shown to control sympathetic outflow, and more recently sympathetic outflow specifically to BAT (92, 93). Additionally, reciprocal connections back to the PVH, including onto spinally-projecting PVH neurons, could contribute to energy expenditure regulation by the NTS (94). In fact, leptin-responsive ARC neurons regulate thermogenesis via the release of GABA into the PVH (95). Moreover, this ARC-PVH regulation of energy expenditure appears to be modulated by NTS-projecting PVH neurons, therefore establishing at least one PVH circuit potentially regulating energy expenditure via the NTS (95).

Although many neuroanatomical studies have aimed to identify the specific PVH populations projecting to the NTS, there still is not a clear consensus on the genetic or neuropeptide identity of NTS-projecting PVH neurons. As mentioned above, retrograde tract tracing has resulted in conflicting results on whether OXT^{PVH} neurons are a component of the PVH population capable of regulating NTS function. In particular, whether OXT peptide expression in the NTS/DMV reflects fibers of passage or synaptic terminals is unclear, since many retrograde reagents used to identify the NTS/DMV innervation by OXT^{PVH} neurons have been shown to infect fibers of passage (96, 97) (98). Additionally, AVP^{PVH} and CRH^{PVH} neurons are consistently not identified upstream of NTS neurons (99, 100). Moreover, although anatomical data shows projections to the NTS, channelrhodopsin-assisted circuit mapping (CRACM) techniques demonstrate

few glutamatergic PVH synaptic connections to the NTS (30, 33). In contrast, similar CRACM experiments demonstrate that optogenetic activation of excitatory PVH neurons, including those containing Mc4R, in slices are capable of inducing direct excitatory post-synaptic currents (EPSCs) in neurons of the adjacent DMV (30, 33). Yet, *in vivo* optogenetic techniques show that $Mc4R^{PVH}$ neuronal projections to the NTS/DMV are unable to control feeding behavior (33). Since PVH neurons project to both the NTS and DMV, and given the dense interconnectivity of these two adjacent regions, it is likely that PVH regulation of the NTS and DMV in the regulation of feeding and energy expenditure is more complex than originally thought.

Parabrachial Nucleus (PBN)

The PBN also integrates a variety of signals from the periphery and from other brainstem sites (e.g. periaqueductal gray (PAG), NTS) as well as the spinal column (101). Although this circuit has been less studied than the PVH-NTS connection, retrograde tracing studies reveal PBN afferents from the PVH (88). Moreover, PBN lesions result in hyperphagic obesity, suggesting the potential for PBN circuits as the primary output in PVH-regulated feeding suppression (102). Moreover, direct projections from AgRP neurons to the PBN can control anorexia (103). More recently, novel *in vivo* optogenetic studies displayed the ability of direct $Mc4R^{PVH}$ projections to the PBN to suppress feeding (33). While this finding puts $Mc4R^{PVH}$ connections to the PBN at the forefront of research pertaining to PVH-mediated feeding suppression, it is still not established if other, non-Mc4R, PVH neurons project to the PBN in order to regulate feeding behavior.

Although the mechanism of PBN-induced feeding suppression is somewhat unknown, the PBN sends projections to sites throughout the brain implicated in feeding behavior including the ventromedial hypothalamus (VMH), central nucleus of the amygdala (CeA) and bed nucleus of the stria terminalis (BNST) (104-107). Taken together, these data support a role for PVH-PBN connections in the PVH's ability to control feeding behavior. Conversely, little is known regarding the control of energy expenditure by the PBN. Recent studies demonstrate the physiologic relevance of PBN projections to the VMH in controlling sympathetic output, but whether this connection controls energy expenditure is unknown (107, 108).

Intermediolateral column of the spinal cord (IML)

While the PVH clearly plays a critical role in the regulation of feeding behavior, much less is known about the potential control of energy expenditure by the PVH. Studies have demonstrated PVH innervation of spinal cord regions, specifically in the thoracic IML, the main site of pre-ganglionic cholingergic neurons (i.e. expressing cholineacetyltransferase, ChAT) that regulate sympathetic outflow (16, 109, 110). The majority of studies have used neuroanatomical approaches with the idea that projections to sites important for sympathetic outflow (e.g. IML) are likely functionally relevant as it pertains to energy expenditure regulation. Initial studies aiming to determine whether the PVH is relevant for the control of thermogenesis used transsynaptic retrograde tracing reagents placed in BAT. Indeed, PVH populations are indirectly connected to BAT, and therefore have the potential to regulate thermogenesis and overall energy expenditure in the Siberian hamster (91). Although studies have

identified direct connections between the PVH and the IML, whether direct PVH-IML projections contact $ChAT^{+}$ neurons projecting to and regulating BAT has yet to be formally demonstrated.

In contrast with other PVH projection sites, some of the PVH populations projecting to the IML have been characterized. This was demonstrated by co-labeling of both OXT and AVP IR-neurons with IML-projecting PVH neurons labeled by retrograde tracing reagents (99, 109). More recently, studies demonstrated innervation of the IML by $Mc4R^{PVH}$ neurons (33). While relatively sparse, the relevance of this connection is intriguing, since $Mc4R^{PVH}$ neuronal activation fails to alter energy expenditure *in vivo* (33).

Inputs to and regulation of PVH neurons in energy balance control

Aside from the well-characterized ARC-PVH circuit previously described, PVH neurons also receive input from sites throughout the hypothalamus, forebrain, and hindbrain. While few studies have tested the function of these inputs, it is nonetheless useful to consider the functional relevance of distinct circuits upstream of the PVH, since these circuits could ultimately provide information about the ability to manipulate discrete energy balance parameters (i.e. feeding vs. energy expenditure) through distinct regulatory circuits.

Hypothalamic inputs to the PVH

In general, the hypothalamus is essential for maintaining overall homeostasis, and therefore receives significant amounts of peripheral and central information regarding

an organism's current physiologic environment. To this effect, hypothalamic neurons, especially those within the ARC that are close to the median eminence, express a variety of receptors for circulating hormones and signals (e.g. leptin, ghrelin, glucagon-like peptide, insulin, and serotonin) (15). Given the dense innervation of the PVH by ARC populations, ARC input to the PVH is widely felt to be the primary circuit important for PVH-mediated feeding and energy balance control. Yet, given the number of other hypothalamic inputs to the PVH, it is conceivable that other hypothalamic circuits control energy balance parameters via the PVH. PVH input arises from other hypothalamic sites, including the VMH, DMH and LHA, which are capable of detecting peripheral and metabolic signals (90). While receptors for most peripheral signals in these sites are less dense, receptors for leptin can be detected widely throughout all of these nuclei (111). Similarly, the hunger-promoting hormone ghrelin is capable of regulating both LHA and VMH function (15). These hypothalamic circuits also express a variety of metabolically-important receptors (e.g., Mc3/4R, cannabinoid receptors, CCK receptor) that are critical for feeding regulation (Figure 1.2) (15).

While the neurochemical composition of these discrete hypothalamic inputs is not known, the functional significance of these circuits can be hypothesized based on a combination of historical lesioning studies combined with more recent genetic approaches. In general, the DMH has been identified to regulate a variety of physiological processes also mediated by the PVH, including sympathetic output, feeding, the growth axis, and cardiovascular function (112). DMH neurons terminate in the parvocellular PVH subdivisions that project to spinal cord regions, and therefore have the potential to regulate sympathetic output and energy expenditure (113-115).

Moreover, DMH neurons with direct PVH projections are activated following leptin treatment, and DMH leptin action is capable of increasing sympathetic tone to BAT, highlighting this pathway as a potential integrator of peripheral signals with PVH circuits controlling energy expenditure (116, 117).

The VMH is commonly associated with its control of autonomic outflow and the counterregulatory response (118). While lesioning studies demonstrated conflicting results on the ability of the VMH to control feeding behavior, more recent studies employing genetic mouse models demonstrate the necessity of leptin signaling in the VMH in the prevention of diet-induced obesity (119). While the obesity due to disruption of VMH signaling pathways is not to the same degree as that observed upon PVH manipulation, it seems reasonable that the VMH controls both feeding and energy expenditure (120, 121). Glutamatergic VMH neurons project throughout the anterior and posterior PVH (122). Since VMH manipulations consistently result in decreased sympathetic tone, it is conceivable that the excitatory VMH inputs to the PVH drive sympathetic output, though this has not been determined (123, 124).

The PVH also receives robust innervation from the LHA, a site characterized for its role in reward processing mediated by the midbrain (125). LHA lesions result in aphagia and bodyweight loss leading to the classification of the LHA as a feeding center (126). However, recent optogenetic studies demonstrate the LHA as a heterogenous nucleus in feeding regulation since activation of GABAergic LHA neurons drives robust feeding whereas LHA glutamatergic neurons are capable of suppressing feeding (127, 128). In addition, LHA neurons are capable of dramatically increasing motivated behaviors such as locomotor activity (129-132). LHA populations are heterogenous,

with multiple combinations of neuropeptide and neurotransmitter neuronal contents. In particular, orexin neurons in the LHA have been implicated in regulating energy balance, since orexin drives feeding when injected in the CNS (133). Specifically, orexin neurons in the LHA are synaptically connected to the PVH, and orexin infusion in the PVH increases both physical activity and feeding duration (77, 134). Yet, the function of this and other LHA populations, including those producing neurotensin, melanin concentrating hormone, GABA, and glutamate, in the regulation of PVH outputs is still largely unknown.

Forebrain inputs to the PVH

Since the PVH is widely viewed as the main pre-autonomic hypothalamic output, non-hypothalamic inputs to the PVH are often overlooked. Yet, sites within the forebrain display dense connectivity with PVH neurons. In particular, neurons throughout the bed nucleus of the stria terminalis (BNST) are routinely labeled upstream of PVH populations by retrograde tracing reagents including fluorogold and modified rabies virus(122, 125). BNST populations are also heterogenous, with both excitatory and inhibitory neuronal populations. While GABAergic BNST neurons have been shown to project within the hypothalamus, clarification is still needed on whether PVH innervation by the BNST originates from inhibitory or excitatory BNST neurons (127). The BNST is also well characterized in the ability to control both appetitive and aversive responses (135). Certainly, recent reports suggest the intersection of food intake and appetitive and aversive behaviors (33, 136, 137). Therefore, while not well understood, BNST

connections to the PVH have the potential to integrate complex behaviors likely connected to feeding control.

Hindbrain inputs to the PVH

Although the majority of research on PVH circuitry is focused on PVH outputs to the brainstem, reciprocal connections from the hindbrain to the PVH have been described. The significance of these reciprocal connections in energy balance is largely unknown; however, it is tempting to consider that different populations of PVH neurons integrate these inputs and therefore coordinate an ultimate autonomic response depending on peripheral energy stores. In particular, glutamatergic neurons of the PAG, PBN and zona incerta (ZI) project to the PVH (113, 138-142). The function of zona incerta neurons is largely unknown, though it is possible that these neurons could supply the PVH with dopaminergic input, highlighting the potential for integration of motivational circuits with satiety and autonomic circuits in the PVH (143). Though traditionally considered in the context of pain, PAG connections to the PVH provide an additional input capable of relaying information surrounding stress responses, and sympathetic output (144). Additionally, catecholaminergic brainstem populations in the rostral ventrolateral medulla (RVLM) innervate parvocellular PVH populations, and are therefore capable of relaying sensory information in the control of sympathetic output (89). Specifically, A1-A6 (noradrenergic) and C1-C3 (adrenergic) RVLM cell groups project throughout the PVH, though the specific populations innervated by these cell groups is largely unknown (145, 146)

GABA shell

The PVH also receives local inhibitory input from a GABAergic shell surrounding the PVH. These inputs help sustain a tonic inhibitory tone on magnocellular and parvocellular PVH neurons (70, 147-149). Research to date on the function of these inhibitory inputs has primarily focused on regulation of the HPA axis, demonstrated by altered endocrine responses and increased CRH neuronal activity following pharmacologic administration of GABA receptor antagonists in the PVH (150, 151). Retrograde tracing studies identified innervation of pre-autonomic PVH neurons by neurons within the GABA shell, demonstrating the potential for the GABA shell to regulate PVH energy balance circuits (152). The GABA shell also has the potential to serve as an intermediary between the PVH and cortical structures that do not have direct PVH projections (150).

Future Directions

A molecular and cellular understanding of the mechanisms used by PVH circuits to control energy balance has advanced significantly in recent years, largely due to the development of novel rodent models used in combination with *in vivo* tools, including chemogenetic and optogenetic reagents. Yet, this new framework underlines additional questions regarding the capability and necessity of PVH neuronal subsets to regulate distinct energy balance parameters. The possibility to dissect the circuitry and function of neuronal subpopulations in the PVH provides an opportunity to characterize the component parts of a complex nucleus that is essential for obesity prevention. Although the anatomical structure of parvocellular and magnocellular PVH subnuclei has long

been characterized, the understanding of how these different PVH structures coordinate physiologic outputs is unknown. For this reason, it is crucial to identify and interrogate PVH neurocircuitry through the analysis of PVH subsets. The understanding of PVH subpopulation projection targets and upstream inputs will allow for the understanding of how multiple components of neural circuits used by the PVH control feeding suppression and/or sympathetic output. Moreover, identifying PVH markers that are functionally relevant in the control of distinct aspects of energy balance has the potential to highlight novel markers that could contribute to the development of more targeted therapeutics. Since the PVH is not uniform in nature, therapeutic intervention of the entire heterogenous PVH might have broad side effects that offset the desired energy balance changes. Therefore, the careful dissection of genetically-defined PVH circuits and their necessity or sufficiency in energy balance parameters is pertinent.

Recent studies have characterized the importance of $Mc4R^{PVH}$ neurons projections to the PBN in mediating the satiety response (33). Moreover, $Mc4R^{PVH}$ neurons are necessary for obesity prevention through feeding suppression (29, 30). While significant research has been performed on the $Mc4R^{PVH}$ population, less has been focused on non-$Mc4R^{PVH}$ neurons. Certainly, *Mc4R* re-expression on CRH, OXT, or AVP neurons is not sufficient to rescue the obesity phenotype of Mc4R null mice (30). Yet, the connectivity of these non-$Mc4R^{PVH}$ neuronal populations, both with one another and outside of the PVH is not understood. Furthermore, significant research suggests that OXT^{PVH} neurons might control feeding energy expenditure (32, 53). Additionally, since centrally-projecting AVP, OXT and CRH PVH populations comprise just 25% of PVH neurons, it is likely that unidentified PVH neurons are capable of regulating energy

balance parameters(109). Furthermore, control of energy expenditure by the PVH is often overlooked due to the clarification of $Mc4R^{PVH}$ neuronal function in feeding, but not energy expenditure (29, 33). While spinal cord projections from PVH populations suggest the possibility for PVH-regulated sympathetic outflow, the physiologic role of distinct PVH neurons in energy expenditure is largely unstudied (109).

To address some of these issues, we employed genetic mouse models in combination with anterograde and retrograde tracing reagents to investigate the circuitry of PVH neuronal subsets in energy balance control. First, we characterized the role of a novel PVH subset expressing *neuronal nitric oxide synthase* (Nos1) in the regulation of both feeding and energy expenditure. Furthermore, we clarify the circuitry and capability of OXT^{PVH} neurons, a subset of the $Nos1^{PVH}$ field, to control both feeding and energy expenditure parameters. We then identify a unique genetic marker, insulin receptor substrate 4 (IRS4) and test the sufficiency and necessity of the $IRS4^{PVH}$ neuronal population in bodyweight regulation. Lastly, we characterize projection-specific inputs to OXT^{PVH}, $IRS4^{PVH}$, $Nos1^{PVH}$, or $Sim1^{PVH}$ neurons in order to identify upstream modulators of NTS-projecting, PBN-projecting, or IML-projecting PVH neuronal subsets. Overall, we demonstrate that genetic dissection of PVH cell types allows for assessment of the functional relevance of PVH neurons in energy balance parameters. We superimpose these questions with circuit analyses of both downstream targets and potential upstream modifiers to ultimately construct circuit maps that engage PVH subsets projecting to disparate hindbrain or spinal cord sites.

References

1. Onyike CU, Crum RM, Lee HB, Lyketsos CG, Eaton WW. 2003. Is obesity associated with major depression? Results from the Third National Health and Nutrition Examination Survey. *Am. J. Epidemiol.* 158(12):1139–47
2. Calle EE, Thun MJ. 2004. Obesity and cancer. *Oncogene*. 23(38):6365–78
3. Romero-Corral A, Caples SM, Lopez-Jimenez F, Somers VK. 2010. Interactions between obesity and obstructive sleep apnea: implications for treatment. *Chest*. 137(3):711–19
4. Finkelstein EA, Trogdon JG, Cohen JW, Dietz W. 2009. Annual medical spending attributable to obesity: payer-and service-specific estimates. *Health Aff (Millwood)*. 28(5):w822–31
5. Locke AE, Kahali B, Berndt SI, Justice AE, Pers TH, et al. 2015. Genetic studies of body mass index yield new insights for obesity biology. *Nature*. 518(7538):197–206
6. Schwartz MW, Woods SC, Porte D, Seeley RJ, Baskin DG. 2000. Central nervous system control of food intake. *Nature*. 404(6778):661–71
7. Gold RM. 1973. Hypothalamic obesity: the myth of the ventromedial nucleus. *Science*. 182(4111):488–90
8. Hetherington AW, Ranson SW. 1940. Hypothalamic lesions and adiposity in the rat. *The Anatomical Record*
9. Sims JS, Lorden JF. 1986. Effect of paraventricular nucleus lesions on body weight, food intake and insulin levels. *Behav. Brain Res.*
10. Weingarten HP, Chang PK, McDonald TJ. 1985. Comparison of the metabolic and behavioral disturbances following paraventricular- and ventromedial-hypothalamic lesions. *Brain Res. Bull.* 14(6):551–59
11. Cowley MA, Pronchuk N, Fan W, Dinulescu DM, Colmers WF, Cone RD. 1999. Integration of NPY, AGRP, and melanocortin signals in the hypothalamic paraventricular nucleus: evidence of a cellular basis for the adipostat. *Neuron*. 24(1):155–63
12. Zheng H, Patterson LM, Rhodes CJ, Louis GW, Skibicka KP, et al. 2010. A potential role for hypothalamomedullary POMC projections in leptin-induced suppression of food intake. *Am. J. Physiol. Regul. Integr. Comp. Physiol.* 298(3):R720–28
13. Broberger C, Johansen J, Johansson C, Schalling M, Hökfelt T. 1998. The neuropeptide Y/agouti gene-related protein (AGRP) brain circuitry in normal, anorectic, and monosodium glutamate-treated mice. *Proceedings of the National Academy of Sciences*. 95(25):15043–48
14. Bouret SG, Draper SJ, Simerly RB. 2004. Formation of projection pathways from the arcuate nucleus of the hypothalamus to hypothalamic regions implicated in the neural control of feeding behavior in mice. *J. Neurosci.* 24(11):2797–2805
15. Yeo GSH, Heisler LK. 2012. Unraveling the brain regulation of appetite: lessons from genetics. *Nat. Neurosci.* 15(10):1343–49
16. Saper CB, Loewy AD, Swanson LW, Cowan WM. 1976. Direct hypothalamo-autonomic connections. *Brain Research*. 117(2):305–12
17. Swanson LW, Kuypers HG. 1980. The paraventricular nucleus of the

hypothalamus: cytoarchitectonic subdivisions and organization of projections to the pituitary, dorsal vagal complex, and spinal cord as demonstrated by retrograde fluorescence double-labeling methods. *J. Comp. Neurol.* 194(3):555–70
18. Sawchenko PE. 1998. Toward a new neurobiology of energy balance, appetite, and obesity: the anatomists weigh in. *J. Comp. Neurol.*
19. Renaud LP, Bourque CW. 1991. Neurophysiology and neuropharmacology of hypothalamic magnocellular neurons secreting vasopressin and oxytocin. *Prog. Neurobiol.* 36(2):131–69
20. Michaud JL, Rosenquist T, May NR, Fan CM. 1998. Development of neuroendocrine lineages requires the bHLH-PAS transcription factor SIM1. *Genes Dev.* 12(20):3264–75
21. Holder JL, Butte NF, Zinn AR. 2000. Profound obesity associated with a balanced translocation that disrupts the SIM1 gene. *Hum. Mol. Genet.* 9(1):101–8
22. Kishi T, Aschkenasi CJ, Lee CE, Mountjoy KG, Saper CB, Elmquist JK. 2003. Expression of melanocortin 4 receptor mRNA in the central nervous system of the rat. *J. Comp. Neurol.* 457(3):213–35
23. Vaisse C, Clement K, Guy-Grand B, Froguel P. 1998. A frameshift mutation in human MC4R is associated with a dominant form of obesity. *Nat. Genet.* 20(2):113–14
24. Loos RJF, Lindgren CM, Li S, Wheeler E, Zhao JH, et al. 2008. Common variants near MC4R are associated with fat mass, weight and risk of obesity. *Nat. Genet.* 40(6):768–75
25. Huszar D, Lynch CA, Fairchild-Huntress V, Dunmore JH, Fang Q, et al. 1997. Targeted disruption of the melanocortin-4 receptor results in obesity in mice. *Cell*. 88(1):131–41
26. Ollmann MM, Wilson BD, Yang YK, Kerns JA, Chen Y, et al. 1997. Antagonism of central melanocortin receptors in vitro and in vivo by agouti-related protein. *Science*. 278(5335):135–38
27. Cheung CC, Clifton DK, Steiner RA. 1997. Proopiomelanocortin neurons are direct targets for leptin in the hypothalamus. *Endocrinology*. 138(10):4489–92
28. Hruby VJ, Lu D, Sharma SD, Castrucci AL, Kesterson RA, et al. 1995. Cyclic lactam alpha-melanotropin analogues of Ac-Nle4-cyclo[Asp5, D-Phe7,Lys10] alpha-melanocyte-stimulating hormone-(4-10)-NH2 with bulky aromatic amino acids at position 7 show high antagonist potency and selectivity at specific melanocortin receptors. *J. Med. Chem.* 38(18):3454–61
29. Balthasar N, Dalgaard LT, Lee CE, Yu J, Funahashi H, et al. 2005. Divergence of melanocortin pathways in the control of food intake and energy expenditure. *Cell*. 123(3):493–505
30. Shah BP, Vong L, Olson DP, Koda S, Krashes MJ, et al. 2014. MC4R-expressing glutamatergic neurons in the paraventricular hypothalamus regulate feeding and are synaptically connected to the parabrachial nucleus. *Proc. Natl. Acad. Sci. U.S.A.* 111(36):13193–98
31. Marsh DJ, Hollopeter G, Huszar D, Laufer R, Yagaloff KA, et al. 1999. Response of melanocortin-4 receptor-deficient mice to anorectic and orexigenic

peptides. *Nat. Genet.* 21(1):119–22
32. Atasoy D, Betley JN, Su HH, Sternson SM. 2012. Deconstruction of a neural circuit for hunger. *Nature*. 488(7410):172–77
33. Garfield AS, Li C, Madara JC, Shah BP, Webber E, et al. 2015. A neural basis for melanocortin-4 receptor-regulated appetite. *Nat. Neurosci.* 18(6):863–71
34. Rossi J, Balthasar N, Olson D, Scott M, Berglund E, et al. 2011. Melanocortin-4 receptors expressed by cholinergic neurons regulate energy balance and glucose homeostasis. *Cell Metab.* 13(2):195–204
35. Tolson KP, Gemelli T, Meyer D, Yazdani U, Kozlitina J, Zinn AR. 2014. Inducible neuronal inactivation of Sim1 in adult mice causes hyperphagic obesity. *Endocrinology*. 155(7):en20132125–444
36. Xi D, Gandhi N, Lai M, Kublaoui BM. 2012. Ablation of Sim1 neurons causes obesity through hyperphagia and reduced energy expenditure. *PLoS ONE*. 7(4):e36453
37. Koutcherov Y, Mai JK, Ashwell KW, Paxinos G. 2000. Organization of the human paraventricular hypothalamic nucleus. *J. Comp. Neurol.* 423(2):299–318
38. Cunningham ET, Sawchenko PE. 1991. Reflex control of magnocellular vasopressin and oxytocin secretion. *Trends in Neurosciences*. 14(9):406–11
39. Treschan TA, Peters J. 2006. The vasopressin system: physiology and clinical strategies. *Anesthesiology*. 105(3):599–612–quiz639–40
40. Poulain DA, Wakerley JB. 1982. Electrophysiology of hypothalamic magnocellular neurones secreting oxytocin and vasopressin. *Neuroscience*. 7(4):773–808
41. Smith SM, Vale WW. 2006. The role of the hypothalamic-pituitary-adrenal axis in neuroendocrine responses to stress. *Dialogues Clin Neurosci*. 8(4):383–95
42. Feuerstein G, Hassen AH, Faden AI. 1983. TRH: cardiovascular and sympathetic modulation in brain nuclei of the rat. *Peptides*. 4(5):617–20
43. Gibbs DM, Vale W, Rivier J, Yen SS. 1984. Oxytocin potentiates the ACTH-releasing activity of CRF(41) but not vasopressin. *Life Sci.* 34(23):2245–49
44. Windle RJ, Shanks N, Lightman SL, Ingram CD. 1997. Central oxytocin administration reduces stress-induced corticosterone release and anxiety behavior in rats. *Endocrinology*. 138(7):2829–34
45. Arletti R, Benelli A, Bertolini A. 1989. Influence of oxytocin on feeding behavior in the rat. *Peptides*. 10(1):89–93
46. Olson BR, Drutarosky MD, Chow MS, Hruby VJ, Stricker EM, Verbalis JG. 1991. Oxytocin and an oxytocin agonist administered centrally decrease food intake in rats. *Peptides*. 12(1):113–18
47. Witt DM, Winslow JT, Insel TR. 1992. Enhanced social interactions in rats following chronic, centrally infused oxytocin. *Pharmacol. Biochem. Behav.* 43(3):855–61
48. Zhang H, Wu C, Chen Q, Chen X, Xu Z, et al. 2013. Treatment of obesity and diabetes using oxytocin or analogs in patients and mouse models. *PLoS ONE*. 8(5):e61477
49. Anagnostou E, Soorya L, Brian J, Dupuis A, Mankad D, et al. 2014. Intranasal oxytocin in the treatment of autism spectrum disorders: a review of literature and early safety and efficacy data in youth. *Brain Research*. 1580:188–98

50. Epperson CN, McDougle CJ, Price LH. 1996. Intranasal oxytocin in obsessive-compulsive disorder. *Biol. Psychiatry*. 40(6):547–49
51. Barberis C, Tribollet E. 1996. Vasopressin and oxytocin receptors in the central nervous system. *Critical Reviews™ in Neurobiology*
52. Blevins JE, Eakin TJ, Murphy JA, Schwartz MW, Baskin DG. 2003. Oxytocin innervation of caudal brainstem nuclei activated by cholecystokinin. *Brain Research*. 993(1-2):30–41
53. Blevins JE, Schwartz MW, Baskin DG. 2004. Evidence that paraventricular nucleus oxytocin neurons link hypothalamic leptin action to caudal brain stem nuclei controlling meal size. *Am. J. Physiol. Regul. Integr. Comp. Physiol.* 287(1):R87–R96
54. Tolson KP, Gemelli T, Gautron L, Elmquist JK, Zinn AR, Kublaoui BM. 2010. Postnatal Sim1 deficiency causes hyperphagic obesity and reduced Mc4r and oxytocin expression. *J. Neurosci.* 30(10):3803–12
55. Kublaoui BM, Gemelli T, Tolson KP, Wang Y, Zinn AR. 2008. Oxytocin deficiency mediates hyperphagic obesity of Sim1 haploinsufficient mice. *Mol. Endocrinol.* 22(7):1723–34
56. Takayanagi Y, Kasahara Y, Onaka T, Takahashi N, Kawada T, Nishimori K. 2008. Oxytocin receptor-deficient mice developed late-onset obesity. *Neuroreport*. 19(9):951–55
57. Camerino C. 2009. Low sympathetic tone and obese phenotype in oxytocin-deficient mice. *Obesity (Silver Spring)*. 17(5):980–84
58. Wu Z, Xu Y, Zhu Y, Sutton AK, Zhao R, et al. 2012. An obligate role of oxytocin neurons in diet induced energy expenditure. *PLoS ONE*. 7(9):e45167
59. Pei H, Sutton AK, Burnett KH, Fuller PM, Olson DP. 2014. AVP neurons in the paraventricular nucleus of the hypothalamus regulate feeding. *Mol Metab*. 3(2):209–15
60. Krashes MJ, Shah BP, Madara JC, Olson DP, Strochlic DE, et al. 2014. An excitatory paraventricular nucleus to AgRP neuron circuit that drives hunger. *Nature*. 507(7491):238–42
61. CRH-deficient mice have a normal anorectic response to chronic stress. 1999. CRH-deficient mice have a normal anorectic response to chronic stress. 84(1-3):69–74
62. Morley JE, Levine AS. 1982. Corticotrophin releasing factor, grooming and ingestive behavior. *Life Sci.*
63. Krahn DD, Gosnell BA, Grace M, Levine AS. 1986. CRF antagonist partially reverses CRF- and stress-induced effects on feeding. *Brain Res. Bull.* 17(3):285–89
64. Swanson LW. 1991. Biochemical switching in hypothalamic circuits mediating responses to stress. *Prog. Brain Res.* 87:181–200
65. Plotsky PM, Sawchenko PE. 1987. Hypophysial-portal plasma levels, median eminence content, and immunohistochemical staining of corticotropin-releasing factor, arginine vasopressin, and oxytocin after pharmacological adrenalectomy. *Endocrinology*. 120(4):1361–69
66. Holmes MC, Antoni FA, Aguilera G, Catt KJ. 1986. Magnocellular axons in passage through the median eminence release vasopressin. *Nature*.

319(6051):326–29
67. Stern JE, Armstrong WE. 1998. Reorganization of the dendritic trees of oxytocin and vasopressin neurons of the rat supraoptic nucleus during lactation. *Journal of Neuroscience*. 18(3):841–53
68. Theodosis DT. 2002. Oxytocin-secreting neurons: A physiological model of morphological neuronal and glial plasticity in the adult hypothalamus. *Front Neuroendocrinol*. 23(1):101–35
69. Theodosis DT, Poulain DA. 1993. Activity-dependent neuronal-glial and synaptic plasticity in the adult mammalian hypothalamus. *Neuroscience*. 57(3):501–35
70. van den Pol AN. 1982. The magnocellular and parvocellular paraventricular nucleus of rat: intrinsic organization. *J. Comp. Neurol.* 206(4):317–45
71. Liposits Z, Paull WK, Sétáló G, Vigh S. 1985. Evidence for local corticotropin releasing factor (CRF)-immunoreactive neuronal circuits in the paraventricular nucleus of the rat hypothalamus. An electron microscopic immunohistochemical analysis. *Histochemistry*. 83(1):5–16
72. Rho JH, Swanson LW. 1989. A morphometric analysis of functionally defined subpopulations of neurons in the paraventricular nucleus of the rat with observations on the effects of colchicine. *Journal of Neuroscience*. 9(4):1375–88
73. Silverman AJ, Hou-Yu A, Chen WP. 1989. Corticotropin-releasing factor synapses within the paraventricular nucleus of the hypothalamus. *Neuroendocrinology*. 49(3):291–99
74. Csáki A, Kocsis K, Halász B, Kiss J. 2000. Localization of glutamatergic/aspartatergic neurons projecting to the hypothalamic paraventricular nucleus studied by retrograde transport of [3H]D-aspartate autoradiography. *Neuroscience*. 101(3):637–55
75. Daftary SS, Boudaba C, Szabó K, Tasker JG. 1998. Noradrenergic excitation of magnocellular neurons in the rat hypothalamic paraventricular nucleus via intranuclear glutamatergic circuits. *Journal of Neuroscience*. 18(24):10619–28
76. Latchford KJ, Ferguson AV. 2004. ANG II-induced excitation of paraventricular nucleus magnocellular neurons: a role for glutamate interneurons. *Am. J. Physiol. Regul. Integr. Comp. Physiol.* 286(5):R894–902
77. Follwell MJ, Ferguson AV. 2002. Cellular mechanisms of orexin actions on paraventricular nucleus neurones in rat hypothalamus. *The Journal of Physiology*. 545(Pt 3):855–67
78. Ziegler DR, Herman JP. 2000. Local integration of glutamate signaling in the hypothalamic paraventricular region: regulation of glucocorticoid stress responses. 141(12):4801–4
79. Li D-P, Chen S-R, Pan H-L. 2004. VR1 receptor activation induces glutamate release and postsynaptic firing in the paraventricular nucleus. *J. Neurophysiol.* 92(3):1807–16
80. Son SJ, Filosa JA, Potapenko ES, Biancardi VC, Zheng H, et al. 2013. Dendritic Peptide Release Mediates Interpopulation Crosstalk between Neurosecretory and Preautonomic Networks. *Neuron*. 78(6):1036–49
81. Neumann I, Russell JA, Landgraf R. 1993. Oxytocin and vasopressin release within the supraoptic and paraventricular nuclei of pregnant, parturient and lactating rats: a microdialysis study. *Neuroscience*. 53(1):65–75

82. Wotjak CT, Kubota M, Liebsch G, Montkowski A, Holsboer F, et al. 1996. Release of vasopressin within the rat paraventricular nucleus in response to emotional stress: a novel mechanism of regulating adrenocorticotropic hormone secretion? *Journal of Neuroscience*. 16(23):7725–32
83. Wotjak CT, Ganster J, Kohl G, Holsboer F, Landgraf R, Engelmann M. 1998. Dissociated central and peripheral release of vasopressin, but not oxytocin, in response to repeated swim stress: new insights into the secretory capacities of peptidergic neurons. *Neuroscience*. 85(4):1209–22
84. Grill HJ, Hayes MR. 2012. Hindbrain neurons as an essential hub in the neuroanatomically distributed control of energy balance. *Cell Metab.* 16(3):296–309
85. Norgren R. 1978. Projections from the nucleus of the solitary tract in the rat. *Neuroscience*. 3(2):207–18
86. Herbert H, Moga MM, Saper CB. 1990. Connections of the parabrachial nucleus with the nucleus of the solitary tract and the medullary reticular formation in the rat. *J. Comp. Neurol.* 293(4):540–80
87. Jhamandas JH, Harris KH. 1992. Excitatory amino acids may mediate nucleus tractus solitarius input to rat parabrachial neurons. *Am. J. Physiol.* 263(2 Pt 2):R324–30
88. Tokita K, Inoue T, Boughter JD. 2009. Afferent connections of the parabrachial nucleus in C57BL/6J mice. *Neuroscience*. 161(2):475–88
89. McKellar S, Loewy AD. 1981. Organization of some brain stem afferents to the paraventricular nucleus of the hypothalamus in the rat. *Brain Research*. 217(2):351–57
90. Sawchenko PE, Swanson LW. 1983. The organization and biochemical specificity of afferent projections to the paraventricular and supraoptic nuclei. *Prog. Brain Res.* 60:19–29
91. Bamshad M, Song CK, Bartness TJ. 1999. CNS origins of the sympathetic nervous system outflow to brown adipose tissue. *Am. J. Physiol.* 276(6 Pt 2):R1569–78
92. Cao W-H, Madden CJ, Morrison SF. 2010. Inhibition of brown adipose tissue thermogenesis by neurons in the ventrolateral medulla and in the nucleus tractus solitarius. *Am. J. Physiol. Regul. Integr. Comp. Physiol.* 299(1):R277–90
93. Morrison SF, Madden CJ, Tupone D. 2014. Central neural regulation of brown adipose tissue thermogenesis and energy expenditure. *Cell Metab.* 19(5):741–56
94. Affleck VS, Coote JH, Pyner S. 2012. The projection and synaptic organisation of NTS afferent connections with presympathetic neurons, GABA and nNOS neurons in the paraventricular nucleus of the hypothalamus. *Neuroscience*. 219:48–61
95. Kong D, Tong Q, Ye C, Koda S, Fuller PM, et al. 2012. GABAergic RIP-Cre neurons in the arcuate nucleus selectively regulate energy expenditure. *Cell*. 151(3):645–57
96. Dado RJ, Burstein R, Cliffer KD, Giesler GJ. 1990. Evidence that Fluoro-Gold can be transported avidly through fibers of passage. *Brain Research*. 533(2):329–33

97. Chen S, Aston-Jones G. 1995. Evidence that cholera toxin B subunit (CTb) can be avidly taken up and transported by fibers of passage. *Brain Research*. 674(1):107–11
98. Swanson LW. 1977. Immunohistochemical evidence for a neurophysin-containing autonomic pathway arising in the paraventricular nucleus of the hypothalamus. *Brain Research*. 128(2):346–53
99. Biag J, Huang Y, Gou L, Hintiryan H, Askarinam A, et al. 2012. Cyto- and chemoarchitecture of the hypothalamic paraventricular nucleus in the C57BL/6J male mouse: a study of immunostaining and multiple fluorescent tract tracing. *J. Comp. Neurol.* 520(1):6–33
100. Swanson LW, Sawchenko PE, Rivier J, Vale WW. 1983. Organization of ovine corticotropin-releasing factor immunoreactive cells and fibers in the rat brain: an immunohistochemical study. *Neuroendocrinology*. 36(3):165–86
101. Becskei C, Grabler V, Edwards GL, Riediger T, Lutz TA. 2007. Lesion of the lateral parabrachial nucleus attenuates the anorectic effect of peripheral amylin and CCK. *Brain Research*. 1162:76–84
102. Nagai K, Ino H, Yamamoto H, Nakagawa H, Yamano M, et al. 1987. Lesions in the Lateral Part of the Dorsal Parabrachial Nucleus Caused Hyperphagia and Obesity. *Journal of Clinical Biochemistry and Nutrition*. 3(2):103–12
103. Wu Q, Clark MS, Palmiter RD. 2012. Deciphering a neuronal circuit that mediates appetite. *Nature*. 483(7391):594–97
104. D'Hanis W, Linke R, Yilmazer-Hanke DM. 2007. Topography of thalamic and parabrachial calcitonin gene-related peptide (CGRP) immunoreactive neurons projecting to subnuclei of the amygdala and extended amygdala. *J. Comp. Neurol.* 505(3):268–91
105. Schwaber JS, Sternini C, Brecha NC, Rogers WT, Card JP. 1988. Neurons containing calcitonin gene-related peptide in the parabrachial nucleus project to the central nucleus of the amygdala. *J. Comp. Neurol.* 270(3):416–26–398–9
106. Carter ME, Soden ME, Zweifel LS, Palmiter RD. 2013. Genetic identification of a neural circuit that suppresses appetite. *Nature*. 503(7474):111–14
107. Flak JN, Patterson CM, Garfield AS, D'Agostino G, Goforth PB, et al. 2014. Leptin-inhibited PBN neurons enhance responses to hypoglycemia in negative energy balance. *Nat. Neurosci.* 17(12):1744–50
108. Garfield AS, Shah BP, Madara JC, Burke LK, Patterson CM, et al. 2014. A parabrachial-hypothalamic cholecystokinin neurocircuit controls counterregulatory responses to hypoglycemia. *Cell Metab.* 20(6):1030–37
109. Sawchenko PE, Swanson LW. 1982. Immunohistochemical identification of neurons in the paraventricular nucleus of the hypothalamus that project to the medulla or to the spinal cord in the rat. *J. Comp. Neurol.* 205(3):260–72
110. Caverson MM, Ciriello J, Calaresu FR. 1984. Paraventricular nucleus of the hypothalamus: an electrophysiological investigation of neurons projecting directly to intermediolateral nucleus in the cat. *Brain Research*. 305(2):380–83
111. Elmquist JK, Bjørbaek C, Ahima RS, Flier JS, Saper CB. 1998. Distributions of leptin receptor mRNA isoforms in the rat brain. *J. Comp. Neurol.* 395(4):535–47
112. Bernardis LL, Bellinger LL. 1998. The dorsomedial hypothalamic nucleus revisited: 1998 update. *Experimental Biology and Medicine*

113. Swanson LW, Sawchenko PE. 1983. Hypothalamic integration: organization of the paraventricular and supraoptic nuclei. *Annu. Rev. Neurosci.* 6(1):269–324
114. Thompson RH, Canteras NS. 1996. Organization of projections from the dorsomedial nucleus of the hypothalamus: a PHA-L study in the rat. *The Journal of …*
115. Horst ter GJ, Luiten PG. 1986. The projections of the dorsomedial hypothalamic nucleus in the rat. *Brain Res. Bull.* 16(2):231–48
116. Elmquist JK, Ahima RS, Elias CF, Flier JS, Saper CB. 1998. Leptin activates distinct projections from the dorsomedial and ventromedial hypothalamic nuclei. *Proceedings of the National Academy of Sciences*. 95(2):741–46
117. Enriori PJ, Sinnayah P, Simonds SE, Garcia Rudaz C, Cowley MA. 2011. Leptin action in the dorsomedial hypothalamus increases sympathetic tone to brown adipose tissue in spite of systemic leptin resistance. *J. Neurosci.* 31(34):12189–97
118. Levin BE, Becker TC, Eiki J, Zhang BB. 2008. Ventromedial hypothalamic glucokinase is an important mediator of the counterregulatory response to insulin-induced hypoglycemia. *Diabetes*
119. Dhillon H, Zigman JM, Ye C, Lee CE, McGovern RA, et al. 2006. Leptin directly activates SF1 neurons in the VMH, and this action by leptin is required for normal body-weight homeostasis. *Neuron*. 49(2):191–203
120. Majdic G, Young M, Gomez-Sanchez E, Anderson P, Szczepaniak LS, et al. 2002. Knockout mice lacking steroidogenic factor 1 are a novel genetic model of hypothalamic obesity. *Endocrinology*. 143(2):607–14
121. Tong Q, Ye C, McCrimmon RJ, Dhillon H, Choi B, et al. 2007. Synaptic glutamate release by ventromedial hypothalamic neurons is part of the neurocircuitry that prevents hypoglycemia. *Cell Metab.* 5(5):383–93
122. Ulrich-Lai YM, Jones KR, Ziegler DR, Cullinan WE, Herman JP. 2011. Forebrain origins of glutamatergic innervation to the rat paraventricular nucleus of the hypothalamus: differential inputs to the anterior versus posterior subregions. *J. Comp. Neurol.* 519(7):1301–19
123. Vander Tuig JG, Knehans AW, Romsos DR. 1982. Reduced sympathetic nervous system activity in rats with ventromedial hypothalamic lesions. *Life Sci.* 30(11):913–20
124. Niijima A, Rohner-Jeanrenaud F, Jeanrenaud B. 1984. Role of ventromedial hypothalamus on sympathetic efferents of brown adipose tissue. *Am. J. Physiol.* 247(4 Pt 2):R650–54
125. Betley JN, Cao ZFH, Ritola KD, Sternson SM. 2013. Parallel, redundant circuit organization for homeostatic control of feeding behavior. *Cell*. 155(6):1337–50
126. Delgado JMR, Anand BK. 1953. Increase of food intake induced by electrical stimulation of the lateral hypothalamus. *Am. J. Physiol.* 172(1):162–68
127. Jennings JH, Rizzi G, Stamatakis AM, Ung RL, Stuber GD. 2013. The inhibitory circuit architecture of the lateral hypothalamus orchestrates feeding. *Science*. 341(6153):1517–21
128. Jennings JH, Ung RL, Resendez SL, Stamatakis AM, Taylor JG, et al. 2015. Visualizing hypothalamic network dynamics for appetitive and consummatory behaviors. *Cell*. 160(3):516–27

129. Hagan JJ, Leslie RA, Patel S, Evans ML, Wattam TA, et al. 1999. Orexin A activates locus coeruleus cell firing and increases arousal in the rat. *Proceedings of the National Academy of Sciences*. 96(19):10911–16
130. Leinninger GM, Jo YH, Leshan RL, Louis GW, Yang H, et al. 2009. Leptin acts via leptin receptor-expressing lateral hypothalamic neurons to modulate the mesolimbic dopamine system and suppress feeding. *Cell Metab.* 10(2):89–98
131. Leinninger GM, Opland DM, Jo YH, Faouzi M, Christensen L, et al. 2011. Leptin action via neurotensin neurons controls orexin, the mesolimbic dopamine system and energy balance. *Cell Metab.* 14(3):313–23
132. Patterson CM, Wong J-MT, Leinninger GM, Allison MB, Mabrouk OS, et al. 2015. Ventral tegmental area neurotensin signaling links the lateral hypothalamus to locomotor activity and striatal dopamine efflux in male mice. *Endocrinology*. 156(5):1692–1700
133. Sakurai T, Amemiya A, Ishii M, Matsuzaki I, Chemelli RM, et al. 1998. Orexins and orexin receptors: a family of hypothalamic neuropeptides and G protein-coupled receptors that regulate feeding behavior. *Cell*. 92(4):573–85
134. Kiwaki K, Kotz CM, Wang C, Lanningham-Foster L, Levine JA. 2004. Orexin A (hypocretin 1) injected into hypothalamic paraventricular nucleus and spontaneous physical activity in rats. *Am. J. Physiol. Endocrinol. Metab.* 286(4):E551–59
135. Kash TL, Pleil KE, Marcinkiewcz CA, Lowery-Gionta EG, Crowley N, et al. 2015. Neuropeptide regulation of signaling and behavior in the BNST. *Mol. Cells*. 38(1):1–13
136. Jennings JH, Sparta DR, Stamatakis AM, Ung RL, Pleil KE, et al. 2013. Distinct extended amygdala circuits for divergent motivational states. *Nature*. 496(7444):224–28
137. Betley JN, Xu S, Cao ZFH, Gong R, Magnus CJ, et al. 2015. Neurons for hunger and thirst transmit a negative-valence teaching signal. *Nature*. 521(7551):180–85
138. Berk ML, Finkelstein JA. 1981. Afferent projections to the preoptic area and hypothalamic regions in the rat brain. *Neuroscience*. 6(8):1601–24
139. Ziegler DR, Edwards MR, Ulrich-Lai YM, Herman JP, Cullinan WE. 2012. Brainstem origins of glutamatergic innervation of the rat hypothalamic paraventricular nucleus. *J. Comp. Neurol.* 520(11):2369–94
140. Wagner CK, Eaton MJ, Moore KE, Lookingland KJ. 1995. Efferent projections from the region of the medial zona incerta containing A13 dopaminergic neurons: a PHA-L anterograde tract-tracing study in the rat. *Brain Research*. 677(2):229–37
141. Alden M, Besson JM, Bernard JF. 1994. Organization of the efferent projections from the pontine parabrachial area to the bed nucleus of the stria terminalis and neighboring regions: a PHA-L study in the rat. *J. Comp. Neurol.* 341(3):289–314
142. Bester H, Besson JM, Bernard JF. 1997. Organization of efferent projections from the parabrachial area to the hypothalamus: a Phaseolus vulgaris-leucoagglutinin study in the rat. *J. Comp. Neurol.* 383(3):245–81
143. Cheung S, Ballew JR, Moore KE, Lookingland KJ. 1998. Contribution of dopamine neurons in the medial zona incerta to the innervation of the central

nucleus of the amygdala, horizontal diagonal band of Broca and hypothalamic paraventricular nucleus. *Brain Research*. 808(2):174–81
144. Behbehani MM. 1995. Functional characteristics of the midbrain periaqueductal gray. *Prog. Neurobiol.* 46(6):575–605
145. Cunningham ET, Sawchenko PE. 1988. Anatomical specificity of noradrenergic inputs to the paraventricular and supraoptic nuclei of the rat hypothalamus. *J. Comp. Neurol.* 274(1):60–76
146. Cunningham ET, Bohn MC, Sawchenko PE. 1990. Organization of adrenergic inputs to the paraventricular and supraoptic nuclei of the hypothalamus in the rat. *J. Comp. Neurol.* 292(4):651–67
147. Roland BL, Sawchenko PE. 1993. Local origins of some GABAergic projections to the paraventricular and supraoptic nuclei of the hypothalamus in the rat. *J. Comp. Neurol.* 332(1):123–43
148. Boudaba C, Szabó K, Tasker JG. 1996. Physiological mapping of local inhibitory inputs to the hypothalamic paraventricular nucleus. *Journal of Neuroscience*. 16(22):7151–60
149. Herman JP, Cullinan WE, Ziegler DR, Tasker JG. 2002. Role of the paraventricular nucleus microenvironment in stress integration. *Eur. J. Neurosci.* 16(3):381–85
150. Cullinan WE, Ziegler DR, Herman JP. 2008. Functional role of local GABAergic influences on the HPA axis. *Brain Struct Funct*. 213(1-2):63–72
151. Cole RL, Sawchenko PE. 2002. Neurotransmitter regulation of cellular activation and neuropeptide gene expression in the paraventricular nucleus of the hypothalamus. *J. Neurosci.* 22(3):959–69
152. Watkins ND, Cork SC, Pyner S. 2009. An immunohistochemical investigation of the relationship between neuronal nitric oxide synthase, GABA and presympathetic paraventricular neurons in the hypothalamus. *Neuroscience*. 159(3):1079–88

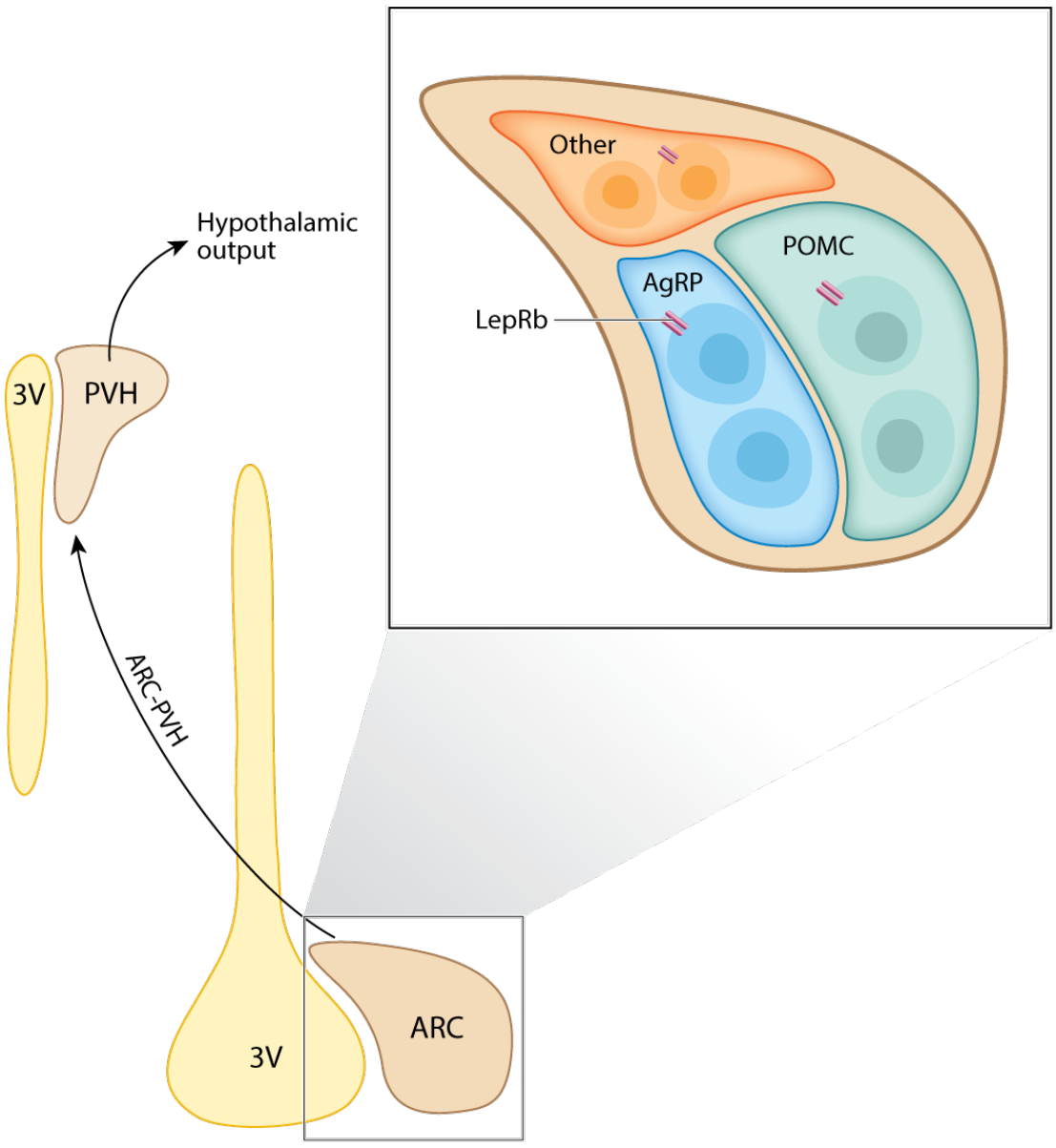
Other
POMC
AgRP
LepRb
Hypothalamic output
3V
PVH
ARC-PVH
3V
ARC

Figure 1.1 ARC-derived hypothalamic signals are integrated by the PVH. The arcuate nucleus (ARC) sits adjacent to the third ventricle (3V) and detects circulating signals of energy balance (including leptin via its receptor, LepRb). A variety of ARC populations express LepRb, including distinct energy balance neurons containing propiomelanocortin (POMC) or agouti-related peptide (AgRP). Leptin activates the anorexigenic POMC neurons while inhibiting the orexigenic AgRP neurons; both send dense projections to the PVH, where they mediate crucial signals to control feeding and energy balance. The ARC also contains other (non-AgRP, non-POMC) PVH-projecting neurons, some of which also express LepRb. The PVH integrates these ARC-derived signals with other information and represents the primary hypothalamic output to other brain regions for the control of energy balance.

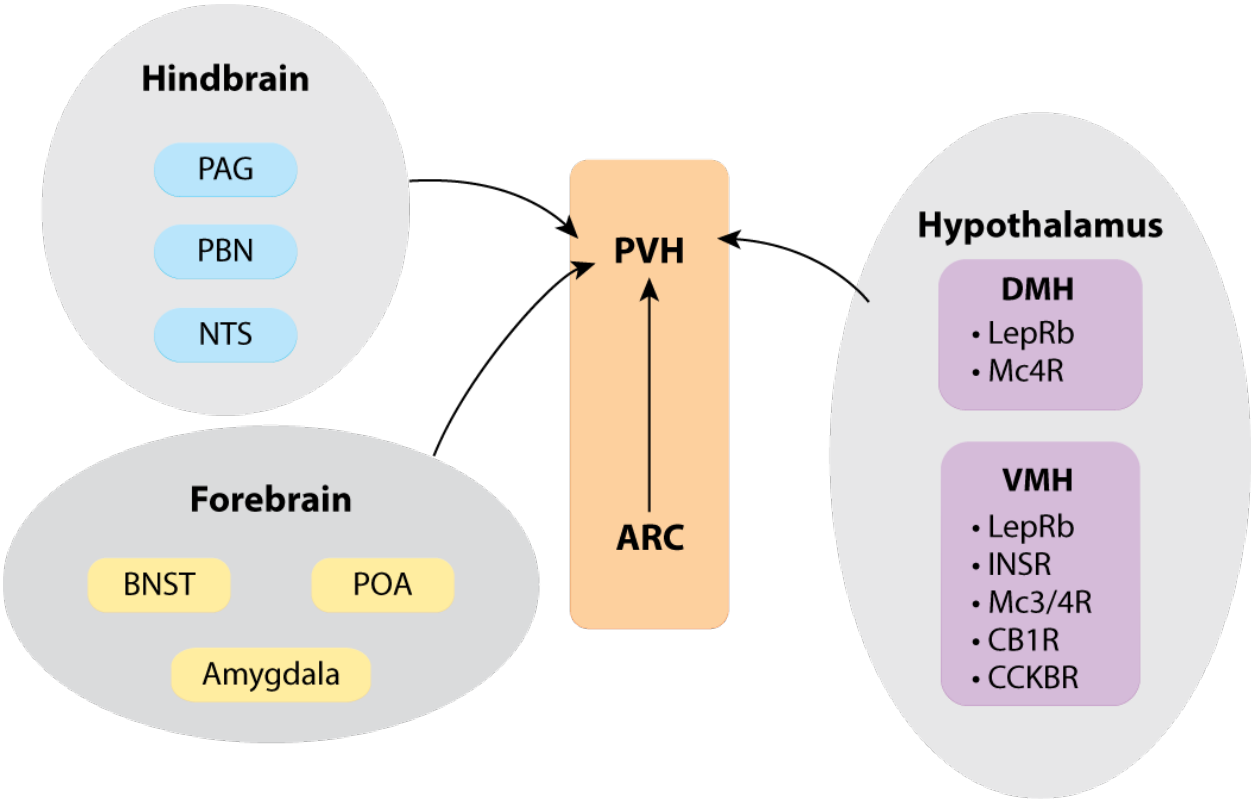
Hindbrain
PAG
PBN
NTS
Forebrain
BNST
POA
Amygdala
PVH
ARC
Hypothalamus
DMH
• LepRb
• Mc4R
VMH
• LepRb
• INSR
• Mc3/4R
• CB1R
• CCKBR

Figure 1.2. Upstream regulators of PVH circuits. The major hypothalamic input to the PVH originates in the arcuate nucleus (ARC). In addition to these inputs, PVH neurons receive information from other hypothalamic sites including the dorsomedial hypothalamus (DMH) and ventromedial hypothalamus (VMH). Both the DMH and VMH contain a variety of receptor populations for both central and peripheral signals and are therefore poised to relay a variety of information to the PVH to modulate parameters of energy balance. Consistent with the notion of the PVH as an integrating center, many nonhypothalamic regions project to the PVH, including sites in the forebrain [bed nucleus of the stria terminalis (BNST), preoptic area (POA), amygdala] and the hindbrain [periaqueductal gray (PAG), parabrachial nucleus (PBN), nucleus of the solitary tract (NTS)].

Chapter II

Control of food intake and energy expenditure by Nos1 neurons of the paraventricular hypothalamus[1]

Introduction

The paraventricular nucleus of the hypothalamus (PVH) is the major autonomic output area of the hypothalamus and is critical for energy homeostasis. Loss of one copy of *single-minded 1* (*Sim1*), a key transcription factor regulating PVH development, disrupts PVH maturation and function, resulting in hyperphagic obesity with associated glucose dysregulation in mammals (1, 2). Similar metabolic derangements also result from electrolytic destruction of the PVH (3, 4). In addition, the PVH serves as an important regulatory center for peptidergic signals and physiologic parameters known to modulate food intake, including leptin, melanocortins, and dehydration (5, 6). Indeed, the melanocortin pathway is essential for energy balance in mammals and is directly linked to PVH function. Leptin-responsive neurons in the arcuate nucleus (ARC) project to the PVH, a site of dense melanocortin receptor expression, and release melanocortin agonists and antagonists/inverse agonists to modulate PVH function (6, 7). Consistent with its role in feeding, the PVH sends dense projections to hindbrain regions such as

[1] Chapter II was previously published in the *Journal of Neuroscience*: **Sutton AK**, Pei H, Burnett KH, Myers MG Jr., Rhodes CJ, Olson DP. Control of food intake and energy expenditure by Nos1 neurons of the paraventricular hypothalamus. *Journal of Neuroscience*, 2014; 34(46):15306-18.

the nucleus of the solitary tract (NTS) and parabrachial nucleus (PBN) to modulate feeding behavior (8-10). Although PVH functions are understood in broad terms, the specific cell types within this heterogeneous structure that regulate feeding are not fully defined.

In addition to modulating feeding, a variety of data suggest that PVH neurons control energy expenditure. For example, infusion of the melanocortin receptor agonist MTII into the PVH increases energy expenditure (6), while ablation of Sim1 neurons throughout the central nervous system decreases metabolic rate (11). Furthermore, polysynaptic retrograde tracing links thermogenic brown adipose tissue to the PVH through the sympathetic nervous system via cholinergic, preganglionic neurons in the intermediolateral column of the thoracic spinal cord ($ChAT^{IML}$) (12). Similar to the PVH cells that control feeding, the neurochemical identity of the PVH neurons regulating energy expenditure via the sympathetic nervous system (SNS) has yet to be established.

Given the role of the PVH in energy balance, we sought to identify subsets of $Sim1^{PVH}$ neurons that contribute to energy homeostasis and reveal their roles in food intake or energy expenditure. We discovered that $Nos1^{PVH}$ neurons are a subset of $Sim1^{PVH}$ neurons and send dense projections to hindbrain regions important for feeding control and to the upper thoracic spinal cord that regulates sympathetic output. Moreover, $Nos1^{PVH}$ neuron activation regulates both feeding and energy expenditure, indicating the critical importance of $Nos1^{PVH}$ neurons in PVH-regulated energy balance. In addition, OXT^{PVH} neurons represent a subset of $Nos1^{PVH}$ neurons that project to and modulate $ChAT^{IML}$ neurons, yet make only a small contribution to energy balance.

These studies demonstrate discrete roles for $Nos1^{PVH}$ and OXT^{PVH} neurons in energy balance and position these neurons anatomically and functionally in the neural circuitry of energy balance.

Materials and Methods

Experimental Animals

Oxytocin-ires-Cre (*OXT-iCre*), *Nos1-ires-Cre* (*Nos1-iCre*) and *Sim1-Cre* mice were generated as described previously (13-15). Adult male mice (8-12 weeks old) were used for all studies. *OXT-iCre*, *Nos1-iCre* or *Sim1-iCre* mice were bred to a Cre-dependent GFP reporter line (16) to fluorescently label Cre-expressing PVH subpopulations. All animals were bred and housed within our colony according to guidelines approved by the University of Michigan Committee on the Care and Use of Animals. Unless otherwise noted, mice were provided *ad libitum* access to food and water.

Stereotaxic injections

OXT-iCre, *Nos1-iCre*, *Sim1-Cre* and non-transgenic (WT) mice were given pre-surgical analgesia and anesthetized with isofluorane. Mice were placed in a digital stereotaxic frame (Model 1900, Kopf Instruments) and the skull was exposed. Intracranial injection coordinates were determined from Bregma using the stereotaxic atlas of Paxinos and Franklin (17). Viral injections were performed using a pressurized picospritzer system coupled to a pulled glass micropipette (coordinates from bregma: A/P: -.500, M/L: +/-.220, D/V: -4.800). For tract tracing experiments, 50-150 nl of the adenoviral

synatophysin-mCherry terminal tracer (Ad-iN/syn-mCherry, (18)) was unilaterally injected in *Sim1-Cre*, *Nos1-iCre* or *OXT-iCre* mice. Additionally, stereotaxic injection of Red Retrobeads (RR) (Lumafluor) was performed in the NTS of *Sim1-Cre* and *Nos1-iCre* mice with a Cre-dependent GFP reporter (*lox-GFP*). Control mice also received unilateral injection of RR in order to determine PVH-NTS connections using OXT peptide staining. For NTS injections, mice were anesthetized and placed in the digital stereotax. The fourth ventricle was identified and used as a geographic landmark to determine the site of injection. A glass micropipette was lowered into the site (D/V: -.630) and ~25nl of RR was injected. For functional analysis of PVH neurons, bilateral PVH injections of AAV-hM3Dq-mCherry (AAV-hM3Dq, purchased from UNC Vector Core) were performed in *Sim1-Cre* (50nl/side), *Nos1-iCre* (50 nl/side) and *OXT-iCre* (75 nl/side) mice. To control for viral transduction, non-transgenic (WT) mice also received bilateral injections of AAV-hM3Dq (75 nl/side). Mice injected with the Ad-iN/syn-mCherry tracer were individually housed for five days following injection to allow for viral transduction and protein transport before perfusion, whereas mice injected with RR were perfused after seven days following injections. Mice injected with AAV-hM3Dq were allowed to recover for seven days following surgery before further experiments were performed.

Food Intake Measurements

Following recovery, *Nos1-iCre*, *OXT-iCre*, *Sim1-Cre*, and WT mice with bilateral PVH AAV-hM3Dq injections were given PBS (i.p.) for three consecutive days to allow for injection acclimatization. Prior to assessment, mice were fasted during the light cycle

(9:00-18:00) and had *ad libitum* access to water. Mice were then injected with vehicle (10% (2-Hydroxypropyl)-b-cyclodextrin, Sigma #C0926) at the onset of feeding (18:00) and food intake was measured at 2 hours, 4 hours, and 16 hours (overnight) post injection. The following day, mice were injected with CNO at the onset of feeding (0.3 mg/kg in 10% b-cyclodextrin) and food intake was measured at 2 hours, 4 hours, and 16 hours following injection.

Energy Expenditure Measurements

Energy expenditure was measured using the Comprehensive Laboratory Monitoring System (CLAMS, Columbus Instruments) in the University of Michigan's Small Animal Phenotyping Core to obtain multi-parameter analysis including open circuit calorimetry and activity via optical beam breaks. AAV-hM3Dq injected mice were acclimatized to the sealed chambers for two days with free access to food and water. The experimentation room had 12-12 hours dark-light cycles (18:00-6:00) and the temperature was maintained at 20-23°C. On experimental days (Day 3 and Day 4), food was removed at 9:00 and vehicle (Day 3) or CNO (Day 4, 0.3 mg/kg) was injected at 11:00. Food was then replaced at the onset of the dark cycle (18:00). Although measurements (oxygen consumption (VO_2), carbon dioxide production (VCO_2), and spontaneous motor activity) were carried out throughout the duration of the experiment, data shown is averaged VO_2 or activity over the four hours following injection of vehicle or CNO.

Intrascapular Temperature Measurements

University of Michigan's Small Animal Phenotyping Core placed temperature transponders (IPTT-300 model with corresponding DAS-7007R reader, Bio Medic Data Systems, Inc) in the intrascapular subcutaneous tissue directly above brown adipose tissue under isofluorane anesthesia. Mice were allowed to recover for 14 days before testing. On the day of testing, food was removed from the cages at 9:00 AM. Two hours later, mice with PVH-directed AAV-hM3Dq injections were injected with vehicle or CNO and temperatures were recorded prior to injection and at 15, 30, 60, and 120 minutes following injection.

Perfusion and Immunohistochemistry (IHC)

For tract tracing experiments, mice were perfused five days (Ad-iN/syn-mCherry) or seven days (RR) after intracranial injection. At the end of the neuronal activation studies, mice with bilateral AAV-hM3Dq injections were either treated with vehicle or CNO and perfused 90 minutes later as described previously (19). Briefly, mice were deeply anesthetized with an overdose of pentobarbital (150 mg/kg, IP) and transcardially perfused with sterile PBS followed by 10% neutral buffered formalin or 4% paraformaldehyde (for perfusions with spinal cord removal). Brains and spinal cords were removed, post-fixed, and dehydrated in 30% sucrose before sectioning into 30 µm slices on a freezing microtome (Leica). Coronal brain sections were collected in four representative sections whereas longitudinal thoracic spinal cord sections were collected in three representative sections and stored at -20°C. For Fos immunohistochemistry (IHC), free floating brain and spinal cord sections were pretreated with 30% H_2O_2 to remove endogenous peroxidase activity and then blocked

with normal goat or donkey serum and incubated in primary antibody overnight (rabbit anti-cFos 1:10,000, Calbiochem PC38). Detection of primary antibody was performed by avidin-biotin/diaminobenzidine (DAB) method (Biotin-SP-conjugated Donkey Anti-Rabbit, Jackson Immunoresearch, 1:200; ABC kit, Vector Labs; DAB reagents, Sigma). hM3Dq and choline acetyltransferase (ChAT) were detected using with primary antibodies for red fluorescent protein (RFP) (rat 1:2000, Allele Biotechnology) and ChAT (spinal cords only; goat, 1:500, Millipore AB144P) respectively followed by secondary immunofluorescence detection with donkey anti-rat-Alexa 568 or donkey anti-goat-Alexa 488 (1:200, Invitrogen). For PVH colocalization experiments, IHC immunostaining was performed using primary antibodies for GFP (rabbit 1:20,000, Invitrogen A6455, nNos1 (sheep 1:2500, (20), kindly provided by Dr. Vincent Prevot), or oxytocin (rabbit 1:2500, Peninsula Laboratories T-4084). For tract tracing experiments, immunostaining was performed using primary antibodies for RFP, GFP or oxytocin.

Immunoblotting of BAT UCP1 protein

Sim1-Cre, *OXT-iCre* and WT mice with bilateral PVH AAV-hM3Dq injections were given either vehicle or CNO and 90 minutes later mice were anesthetized with pentobarbital and BAT was removed, frozen on dry ice and stored in -80°C. Tissue was homogenized in protein lysis buffer (10% SDS, 1M Tris, pH 6.8, 12.7 mM EDTA) with metal beads in a Bullet blender for 30 minutes. Samples were clarified by centrifugation and protein concentration was quantified by BCA assay (Thermo Scientific, cat. #23225). Lysates were diluted to equal protein concentration in lysis buffer plus 1X NuPage SDS buffer (Invitrogen) with 2.5% 2-mercaptoethanol. Samples were boiled for

5 minutes and loaded on a SDS gradient polyacrylamide gel (Invitrogen) and separated by electrophoresis. Proteins were transferred to Immobilon PVDF membranes (Millipore) and Ponceau staining of membranes was used to confirm equal protein loading between lanes. Membranes were blocked in 5% milk for 1 hour at room temperature and then incubated with primary antibodies in 5% BSA (goat anti-UCP1, 1:2000, Santa Cruz Biotechnology #SC-6528); rat anti-α-Tubulin, 1:1000, Thermo Scientific MA1-80017), and appropriate HRP-conjugated secondary antibodies (1:5000 dilution in 5% milk, IgG peroxidase; GE Healthcare). Super Signal enhanced chemiluminescence (Pierce) was used for visualization by autoradiography and bands were quantified by densitometry.

Statistical Analysis

Paired t-tests, unpaired t-tests, or repeated measures two-way ANOVAs were calculated using GraphPad Prism. Significance was determined for $p<0.05$.

Results

nNos1 (Nos1) expression *defines a PVH subpopulation*

Nos1 in situ hybridization (Allen Brain Atlas) and *Nos1-iCre, lox-GFP* reporter mice demonstrate the existence of NOS1-containing neurons in the PVH. To determine if NOS1 peptide marks a neuronal subset of the entire PVH, we stained brains from *Sim1-Cre, lox-GFP* reporter mice for GFP and NOS1 immunoreactivity (-IR) and found that all $Nos1^{PVH}$ neurons express Sim1, but not all $Sim1^{PVH}$ neurons express NOS1 (Figure 2.1A, 1B). PVH cell counts in *Sim1-Cre, lox-GFP* brain slices immunostained for Nos1 peptide (n=5) revealed that $Nos1^{PVH}$ neurons account for ~21% of the $Sim1^{PVH}$ field. To

identify some potential $Nos1^{PVH}$ subtypes, we also investigated the overlap between $Nos1^{PVH}$ and oxytocin (OXT)-expressing PVH neurons. Using *Nos1-iCre, lox-GFP* sections, we found that almost all OXT^{PVH} neurons (~90%, n=3) contain GFP, whereas only 16% (n=3) of Nos1-$iCre^{PVH}$ neurons contain OXT peptide. This confirms that OXT^{PVH} neurons are a subset of $Nos1^{PVH}$ neurons (Figure 2.1C, 1D). This establishes that $Nos1^{PVH}$ neurons represent a discrete subset of $Sim1^{PVH}$ neurons and that most OXT^{PVH} neurons lie within the $Nos1^{PVH}$ field (Figure 2.1E). Given the importance of $Sim1^{PVH}$ neurons in energy balance regulation and the limited information regarding the roles of specific PVH subtypes in this regulation, we investigated the potential contributions of $Nos1^{PVH}$ and OXT^{PVH} neurons to the control of energy balance parameters.

$Nos1^{PVH}$ neurons send dense projections to hindbrain regions important for satiety

As hindbrain regions (eg., NTS/DMV, PBN and specifically PVH→NTS neuronal projections) have been implicated in feeding regulation, we characterized efferent projections from defined PVH subpopulations to the NTS/DMV and the PBN. We used $Sim1^{PVH}$ neurons as a reference group to establish projection targets for comparison with $Nos1^{PVH}$ and OXT^{PVH} subsets. *Sim1-Cre* mice were unilaterally injected with a Cre-dependent adenoviral synaptophysin-mCherry tracer (Ad-iN/syn-mCherry, Figure 2.2A), which traffics predominantly to synaptic terminals and preferentially identifies projection terminals as opposed to axons of passage. We observed dense $Sim1^{PVH}$ neuron-derived mCherry-IR (Figure 2.2B) in hindbrain regions important for satiety, including the medial and lateral PBN (mPBN and lPBN, respectively, Figure 2.2C) and the NTS

(Figure 2.2D). Similar mCherry-IR was observed in these hindbrain regions from Nos1^{PVH} neurons injected with Ad-iN/syn-mCherry (Figure 2.2F, 2G, 2H). In contrast, we detected very little OXT^{PVH}-derived syn-mCherry in the PBN (Figure 2.2K) or NTS (Figure 2.2L). Unilateral PVH injections of Ad-iN/syn-mCherry in *OXT-iCre* mice demonstrated syn-mCherry expression (red) only in OXT^{PVH} neurons (green; Figure 2.2J), confirming the fidelity of the Cre-dependent Ad-iN/syn-mCherry virus. As expected, Sim1^{PVH}, Nos1^{PVH}, and OXT^{PVH} neurons also sent dense projections to the median eminence, reflecting the parvocellular PVH subpopulation projections that influence pituitary function and the magnocellular projections that release their contents directly from the posterior pituitary into the systemic circulation (Figure 2.2E, 2I, 2M).

To better characterize the PVH neurons that project to the NTS/DMV and potentially affect feeding behaviors, we injected fluorescent latex microspheres (Lumafluor Red Retrobeads, RRs) unilaterally in the NTS of *Sim1-Cre, lox-GFP, Nos1-iCre, lox*-GFP and wildtype mice (Figure 2.3A, 3E, 3J, respectively). RRs are preferentially taken up by pre-synaptic terminals at the site of injection and undergo retrograde transportation back to the cell body, thus allowing neuron identification by autofluorescence. As might be expected, all RR-labeled PVH neurons from *Sim1-Cre, loxGFP* animals co-express GFP, suggesting that all PVH→NTS projections originate from Sim1^{PVH} neurons (Figure 2.3B-D). Retrograde labeling from the NTS/DMV in *Nos1-iCre, lox-GFP* mice also demonstrates extensive (but not complete) overlap between NTS-projecting RR labeled neurons and Nos1^{PVH} neurons (Figure 2.3F-H). Since previous reports suggest the presence of OXT^{PVH} projections to the NTS/DMV and essentially all OXT^{PVH} neurons are within the Nos1-iCre^{PVH} field, we co-stained

Nos1-iCre, lox-GFP mice with NTS RR injections for OXT peptide (Figure 2.3I^{I}- 3I^{IV}). As expected, OXT-IR is seen within Nos1^{PVH} neurons (Figure 2.3^{IV}, green, open arrowheads), however NTS-injected RR predominantly labeled Nos1^{PVH} neurons that do not contain OXT (white arrowheads). In agreement with these findings, very few OXT^{PVH} cell bodies were labeled with NTS-injected RRs (Figure 2.3J-M) in separate control mice, even though OXT peptide (green) was detectable in the NTS/DMV at the site of the RR injection (Figure 2.3J). This suggests that much of the OXT-IR in the NTS identifies fibers of passage, as opposed to synaptic terminals. Nevertheless, it is the non-OXT Nos1^{PVH} neurons that comprise the bulk of the NTS-projecting Nos1^{PVH} neurons.

Nos1^{PVH} and OXT^{PVH} neurons project to the spinal cord

Since sympathetic outflow promotes energy expenditure and the PVH is implicated in energy expenditure regulation, we also investigated whether Nos1^{PVH} and OXT^{PVH} neurons project to hindbrain and spinal cord regions important for sympathetic nervous system (SNS) control (6, 11). The raphe pallidus (RPa) is an important hindbrain region controlling brown adipose tissue (BAT) function and energy expenditure (12, 21, 22). We found few syn-mCherry terminals originating from Sim1^{PVH} (Figure 2.4A), Nos1^{PVH} (Figure 2.4B) or OXT^{PVH} (Figure 2.4C) neurons in the RPa. To determine if Sim1^{PVH}, Nos1^{PVH} and OXT^{PVH} neurons project to the preganglionic, sympathetic output neurons of the thoracic spinal cord, we also examined longitudinal spinal cord sections from *Sim1-Cre*, *Nos1-iCre* or *OXT-iCre* mice following unilateral PVH Ad-iN/syn-mCherry

injections. We identified robust syn-mCherry tracer in thoracic spinal cord regions originating from $Sim1^{PVH}$ (Figure 2.4D), $Nos1^{PVH}$ (Figure 2.4E), and OXT^{PVH} neurons (Figure 2.4F). Syn-mCherry-IR is localized in close proximity to neurons expressing choline acetyltransferase (ChAT) in the intermediolateral column of the thoracic spinal cord ($ChAT^{IML}$), suggesting potential $Sim1^{PVH}$, $Nos1^{PVH}$ and OXT^{PVH} neuronal connections with and regulation of IML pre-ganglionic sympathetic neurons (Figure 2.4D', 4E', 4F').

Temporal control of PVH neuronal subpopulations

Having established the anterograde projection targets for $Sim1^{PVH}$, $Nos1^{PVH}$ and OXT^{PVH} neurons, we tested the physiologic effects of acute activation of these PVH neurons on feeding and energy expenditure. To selectively activate these PVH subsets, we employed Designer Receptors Exclusively Activated by Designer Drugs (DREADDs) technology (23). The hM3Dq DREADD is a modified human muscarinic receptor designed to couple with stimulatory Gq-proteins. Binding of an otherwise inert, synthetic ligand CNO (clozapine N-oxide) activates neurons expressing hM3Dq. This system has been engineered to be Cre recombinase-dependent in order to achieve cell-specific control (Figure 2.5A). Thus, site-specific injection of a Cre-dependent adeno-associated virus (AAV)-hM3Dq allows for remote and temporal activation only of neurons that express Cre recombinase. As for our tracing studies, we used *Sim1-Cre* mice to target the majority of PVH neurons and establish an upper threshold of PVH "output capacity" upon DREADDs activation followed by $Nos1^{PVH}$ and OXT^{PVH} subset

activation. As a control for DREADD injection, bilateral PVH injections of AAV-hM3Dq into wildtype (WT) mice were also performed.

Although AAV-hM3Dq was primarily limited to the PVH of *Sim1-Cre* injected mice, there was a small amount of AAV-hM3Dq expression in Sim1-Cre^{+} areas in the anterior hypothalamus (Figure 2.5B). Similarly, while injections in *Nos1-iCre* mice were targeted for the PVH, some *Nos1-iCre*$^{+}$ neurons in the thalamus also expressed hM3Dq (Figure 2.5C). Importantly, any injected *Nos1-iCre* animals that expressed hM3Dq in peri-PVH areas implicated in feeding (i.e., DMH) were excluded from the analysis. PVH injections of AAV-hM3Dq were restricted to OXT^{PVH} neurons, as Cre expression in *OXT-iCre* mice is limited to the PVH and SON (Figure 2.5D). Using nuclear Fos staining as an indicator of neuronal activation, vehicle injection caused little PVH activation in *Sim1-Cre* (Figure 2.5E), *Nos1-iCre* (Figure 2.5F), or *OXT-iCre* (Figure 2.5G) mice with bilateral PVH AAV-hM3Dq injections. In contrast, hM3Dq-injected mice treated with CNO prior to perfusion demonstrated a marked increase in nuclear Fos staining in transduced PVH neurons (Figure 2.5H-J). Specifically CNO-stimulated PVH nuclear Fos expression in Sim1-Cre + AAV-hM3Dq mice (176.5 ± 6.5 vs. 51.0 ± 6.0 (vehicle); n=2 each, unpaired t-test, $t(2)=14.2$, $p=0.005$), Nos1-iCre + AAV-hM3Dq mice (200.7 ± 39.0 vs. 36.0 ± 5.0 (vehicle); vehicle n=2, CNO n=3, unpaired t-test, $t(3)=3.3$, $p=0.047$) and OXT-iCre + AAV-hM3Dq mice (130 ± 14 vs. 63.0 ± 5.1 (vehicle); n=4 each, unpaired t-test, $t(6)=4.4$, $p=0.005$). This demonstrates that cell-specific DREADD expression allows for temporal control of PVH neuron activity. Nuclear Fos was also apparent in non-Cre expressing cells suggesting that PVH subtypes can activate neighboring PVH cells via local connections (Figure 2.5J inset) (24, 25). We detected

no hM3Dq expression or CNO-dependent activation in the PVH of wild type control mice (data not shown).

Direct activation of PVH neurons alters food intake

Based on our anterograde tracing of PVH subsets, we hypothesized that activation of $Sim1^{PVH}$ and $Nos1^{PVH}$ neurons would alter feeding (via projections to hindbrain regions). To test this hypothesis, we injected AAV-hM3Dq bilaterally into the PVH of *Sim1-Cre*, *Nos1-iCre* and *OXT-iCre* mice and treated these animals with CNO (0.3 mg/kg) at the onset of dark cycle feeding. Body weights of the animals used in these studies are as follows (BW ± SEM): *Sim1-Cre* 22.6g ± 1.6g (n=4), *Nos1-iCre* 25.6g ± 0.7g (n=8), *OXT-iCre* 22.8g ± 0.8g (n=10), WT 24.1g ± 0.8g (n=4). Wild type controls with bilateral PVH AAV-hM3Dq injections showed no change in feeding behavior in response to CNO compared to vehicle injections, demonstrating that neither viral transduction nor CNO alone altered food intake (Figure 2.6A, first panel). Activation of $Sim1^{PVH}$ neurons robustly suppressed feeding as compared to vehicle control (Figure 2.6A, second panel, paired t-test, $t(3)=5.0$, $p=0.015$). As hypothesized, *Nos1-iCre* mice with bilateral AAV-hM3Dq injections also ate significantly less following CNO-activation of $Nos1^{PVH}$ neurons as compared to vehicle (Figure 2.6A third panel, paired t-test, $t(7)=7.9$, $p<0.0001$). Interestingly, the suppression of two hour food intake following activation of $Sim1^{PVH}$ and $Nos1^{PVH}$ neurons is comparable ($t(10)=1.0$, $p=0.35$, unpaired t-test), suggesting that the anorexia associated with $Sim1^{PVH}$ activation is mediated largely via $Nos1^{PVH}$ neurons. The anorectic effect of $Nos1^{PVH}$ activation persists through four hours of re-feeding (paired t-test, $t(7)=11.2$, $p<0.0001$) (there is a similar trend for

Sim1^{PVH} neuron activation, Figure 2.6B), although total overnight food intake (16 hours) approximates controls (Figure 2.6C). In contrast to Sim1^{PVH} and Nos1^{PVH} neurons, activation of OXT^{PVH} neurons had little effect on two or four-hour food intake (Figure 2.6A, 6B, fourth panel). Thus Nos1^{PVH} neuron activation suppresses feeding to a similar extent as Sim1^{PVH} neurons, suggesting a major role for Nos1^{PVH} neurons in the control of food intake. Furthermore, since activation of the OXT-containing subset of Nos1^{PVH} neurons fails to blunt feeding, the activation of non-OXT Nos1^{PVH} neurons must be required for this effect.

Activation of PVH neurons increases Fos expression in sympathetic output neurons and promotes energy expenditure

The role of the PVH in modulating energy expenditure has received less attention than its contribution to feeding regulation. Given the robust spinal cord projections from Sim1^{PVH}, Nos1^{PVH} and OXT^{PVH} neurons, we determined the effect of DREADD-mediated activation of these PVH neural subsets on nuclear Fos expression in preganglionic, sympathetic output neurons and overall oxygen consumption. First, we treated *Sim1-Cre* +AAV-hM3Dq, *Nos1-iCre* +AAV-hM3Dq or *OXT-iCre* +AAV-hM3Dq mice with vehicle (Figure 2.7A, 7C, 7E) or CNO (Figure 2.7B, 7D, 7F) and analyzed thoracic spinal cord sections for nuclear Fos accumulation in ChAT^{IML} neurons. Acute activation of Sim1^{PVH}, Nos1^{PVH} and OXT^{PVH} neurons all appeared to increase nuclear Fos expression in ChAT^{IML} neurons relative to vehicle control. To estimate this effect, we determined the percentage of ChAT^{IML} neurons containing nuclear Fos immunoreactivity in thoracic spinal cord sections from Sim1-Cre + AAV-hM3Dq mice in

response to CNO vs. vehicle. Activation of $Sim1^{PVH}$ neurons showed a trend towards increased nuclear Fos expression in $ChAT^{IML}$ neurons with 42.6 $\pm$ 7.2 % (CNO-treated) vs. 16.1 $\pm$ 5.4% (vehicle treated) $ChAT^{IML}$ neurons counted (n=2 each; unpaired t-test, $t(2)=2.9$, $p=0.099$). These data thereby suggest a potential neuroanatomical pathway for the regulation of sympathetic output and energy expenditure.

To determine the ability of each PVH subset to modulate energy expenditure, we used metabolic cages to measure oxygen consumption (VO_2) and locomotor activity in animals expressing hM3Dq in $Sim1^{PVH}$, $Nos1^{PVH}$ and OXT^{PVH} neurons. Activation of $Sim1^{PVH}$ neurons and $Nos1^{PVH}$ neurons increased average oxygen consumption in the absence of food (Figure 2.8A, 8B, second and third panels) (Sim1: paired t-test, average 4hr VO_2 $t(3)=8.8$, $p=0.003$, average 4hr VO_2 LBM $t(3)=11.0$, $p=0.002$; Nos1: average 4hr VO_2 $t(3)=3.2$, $p=0.05$, average 4hr VO_2 LBM $t(3)=3.6$ $p=0.038$). Acute activation of OXT^{PVH} neurons also significantly increased oxygen consumption (Figure 2.8A, 8B, fourth panel) (average 4hr VO_2 $t(9)=2.4$, $p=0.042$, average 4hr VO_2 LBM $t(9)=2.3$, $p=0.05$), albeit not to the extent seen with activation of $Nos1^{PVH}$ neurons (unpaired t-test of average change in 4hr VO_2, $t(13)=2.5$, $p=0.029$). Baseline oxygen consumption was elevated in the initial cohort of *OXT-iCre* +AAV-hM3Dq mice in comparison to other groups (One-way ANOVA of average change in 4hr VO_2, $F(3,19)=7.3$, $p=0.002$). To exclude the possibility that this elevated baseline O_2 consumption was a property of the *OXT-iCre* transgenic line as opposed to a cohort effect, oxygen consumption experiments were repeated in a second cohort of mice naïve to CNO (Figure 2.8C, 8D). Indeed, *OXT-iCre +3Dq* mice treated with vehicle had the same baseline oxygen consumption as WT and *OXT-iCre* mice without 3Dq (One-

way ANOVA of average change in 4hr VO_2, F(2,9)=1.0, p=0.4), indicating that *OXT-iCre* mice are not metabolically compromised. Interestingly, activation of any of the PVH subpopulations increased average total activity, although not equally (Figure 2.8E; paired t-test Sim1+3Dq: t(3)=4.7, p=0.019; Nos1+3Dq: t(3)=26.8, p=0.0001; OXT+3Dq: t(9)=4.3, p=0.002). As expected, WT+AAV-hM3Dq mice showed no change in oxygen consumption or activity in response to CNO (Figure 2.8A-E). Body weights of the animals used in these studies are as follows (BW ± SEM): *Sim1-Cre* 30.5g ± 2.1g (n=4), *Nos1-iCre* 29.4g ± 0.9g (n=4), *OXT-iCre +3Dq cohort 1* 23.9g ± 0.6g (n=10), *WT cohort 1* 26.3g ± 1.3g (n=4), *OXT-iCre +3Dq cohort 2* 28.9g ± 1.3g (n=4), *OXT-iCre (no 3Dq)* 28.1g ± 1.8g (n=4), *WT cohort 2* 30.4g ± 1.6g (n=4). Therefore, $Nos1^{PVH}$ or OXT^{PVH} neuron activation promotes locomotor activity and overall energy expenditure, although to a lesser extent than that seen with pan-PVH activation. Unlike the feeding effects observed with $Nos1^{PVH}$ activation, $Nos1^{PVH}$-driven increases in VO_2 and activity were significantly smaller than those seen with $Sim1^{PVH}$ activation (unpaired t-test of average 4hr VO_2, F(3,3)=1.062, p=0.009; unpaired t-test of average 4hr activity, F(3,3)=274.3, p=0.023), suggesting that both $Nos1^{PVH}$ and non-$Nos1^{PVH}$ subsets of Sim1 neurons contribute to the control of energy expenditure. As increased locomotor activity may contribute to overall energy expenditure and oxygen consumption (VO_2), we analyzed VO_2 in *Sim1-Cre + AAV-hM3Dq* and *Nos1-iCre + AAV-hM3Dq* mice for at timepoints when locomotor activity was approximately matched before and after CNO treatment (Figure 2.8F). While this analysis revealed a trend towards increased VO_2 for both *Sim1-Cre + AAV-hM3Dq* and *Nos1-iCre + AAV-hM3Dq* animals when matched for activity (Sim1-Cre, paired t-test, t(3)=2.4, p=0.093; Nos1-iCre, paired t-test, t(3)=2.9,

p=0.064), the magnitude of the effect was small relative to the overall increase in VO_2. This suggests that increased locomotor activity contributes significantly to the increased oxygen consumption observed with PVH stimulation, but that changes independent of locomotor activity may also play a role.

Acute Sim1^{PVH} activation increases intrascapular BAT temperature

Since the activation of PVH neurons tends to increase energy expenditure in mice matched for locomotor activity and Sim1^{PVH}, Nos1^{PVH} and OXT^{PVH} neurons send dense projections to pre-ganglionic sympathetic ChAT neurons in the thoracic spinal cord, we hypothesized that activation of these PVH subpopulations might promote thermogenesis in addition to potentially playing a role in locomotor activation. To test this, temperature transponders were placed in the subcutaneous tissue directly above intrascapular BAT in *Sim1-Cre +hM3Dq*, *OXT-iCre +hM3Dq* and *WT +hM3Dq* mice and intrascapular temperatures (T_{IS}) were measured before and after PVH neuron activation. Body weights of the animals used in these studies are as follows (BW ± SEM): *Sim1-Cre* 27.4g ± 1.6g (n=3), *OXT-iCre* 28.5g ± 0.8g (n=4), WT 31.5g ± 1.2g (n=5). Activation of Sim1^{PVH} neurons increased T_{IS} when compared to baseline T_{IS} before injection of vehicle or CNO (Figure 2.9A, 9B; Repeated measures two-way ANOVA of change in baseline T_{IS} $F(1,2)=102.9$, $p=0.010$ with Sidak multiple comparisons post-hoc test 15-min $t(8)=4.2$, $p=0.016$; 30-min $t(8)=8.3$, $p=<0.001$; 60-min $t(8)=6.5$, $p=0.001$; 120-min $t(8)=5.3$, $p=0.004$). Additionally, activation of OXT^{PVH} neurons display a trend of increased T_{IS}, though this did not reach statistical

significance. T_{IS} in WT +hM3Dq mice were not altered in response to CNO administration.

Since acute PVH activation increased T_{IS}, we determined if this was mediated by increased BAT uncoupling protein 1 (UCP1), the primary facilitator of BAT thermogenesis (26). We examined UCP1 protein levels in BAT from *Sim1-Cre +AAV-hM3Dq*, *OXT-iCre +AAV-hM3Dq*, or *WT+AAV-hM3Dq* mice treated with either vehicle or CNO. UCP1 protein levels did not change in response to $Sim1^{PVH}$ or OXT^{PVH} neuronal activation when normalized to the loading control (Figure 2.10). Therefore, increases in T_{IS} following PVH activation may be via mechanisms that increase UCP1 activity rather than protein levels (27, 28).

Discussion

The importance of the PVH in feeding regulation, energy balance and endocrine and autonomic function is well established (6, 8, 15). However, a detailed understanding of the cellular and neural pathways used by the PVH to regulate these physiologic functions has been complicated by the heterogeneity of this nucleus and the inability to investigate specific PVH cell populations independently. To tackle these issues, we combined Cre-dependent viral vectors with PVH cell-specific Cre drivers to probe the function of discrete PVH neuron subsets and explore their connectivity with brain regions known to be involved in energy homeostasis.

The hypothalamic transcription factor *Sim1* marks PVH neurons involved in feeding regulation. Sim1-restricted melanocortin-4 receptor (Mc4R) expression in an otherwise Mc4R-null background corrects the associated hyperphagia of Mc4R-null

mice and targeted ablation of Sim1 neurons in the CNS results in hyperphagia and altered energy expenditure (11, 15). Sim1 neurons lie in other brain areas, but most if not all PVH neurons express *Sim1* (1). We now show that acute activation of $Sim1^{PVH}$ neurons suppresses feeding and increases energy expenditure and activity, highlighting the ability of PVH neurons to regulate both energy balance parameters and validating our experimental system. To clarify the neurochemical identity and neural circuitry of the PVH neurons mediating these effects, we identified and utilized *Nos1* expression to mark a specific $Sim1^{PVH}$ subset. Our tracing studies revealed dense $Nos1^{PVH}$ projections to hindbrain and spinal cord structures involved in energy balance regulation. Using a pharmacogenetic approach, we showed that activation of $Nos1^{PVH}$ neurons suppressed food intake at the onset of feeding to an extent that is comparable to that observed upon activation of the entire $Sim1^{PVH}$ field. These experiments therefore establish $Nos1^{PVH}$ neurons as an important $Sim1^{PVH}$ subset in feeding regulation.

OXT^{PVH} neurons are a subset of $Nos1^{PVH}$ neurons and pharmacologic evidence has demonstrated the ability of hindbrain OXT action to suppress feeding, suggesting a role for OXT^{PVH} neurons in anorectic signaling by the PVH (9, 29, 30). In contrast, however, genetic inactivation of OXT or its receptors minimally impacts feeding, and ablation of OXT neurons in adult mice neither alters feeding nor the anorexic response to a melanocortin agonist (13, 31, 32). In order to determine the contribution of OXT^{PVH} neurons to $Nos1^{PVH}$-regulated feeding, we subjected OXT^{PVH} neurons to Cre-dependent synaptic tracing and pharmacogenetic analysis. DREADD-mediated activation of OXT^{PVH} neurons failed to suppress feeding under normal conditions. Therefore, while

$Nos1^{PVH}$ neurons mediate a powerful anorectic signal, the OXT-expressing subset of $Nos1^{PVH}$ neurons cannot account for this effect, thus revealing a requisite role for non-OXT $Nos1^{PVH}$ neurons in food intake control.

The role of the PVH in energy expenditure regulation has received less attention than its role in food intake control. *Sim1* haploinsufficiency or manipulation of Mc4R expression in *Sim1* neurons alters feeding, but minimally affects energy expenditure (15, 33). Selective ablation of *Sim1* neurons in the CNS, however, lowers oxygen consumption, suggesting a role for *Sim1* neurons in the regulation of both food intake and energy expenditure (11). Indeed, recent data reveal that glutamatergic signaling in *Sim1* neurons contributes to energy expenditure regulation (34). In this study, we show that direct activation of $Sim1^{PVH}$ neurons increases energy expenditure and that both $Nos1^{PVH}$ and OXT^{PVH} neurons contribute to this physiologic response. Using a novel anterograde viral tracing tool, we did not find significant projections to the RPa. However, we did identify dense terminals from $Sim1^{PVH}$, $Nos1^{PVH}$ and OXT^{PVH} neurons in close proximity to $ChAT^{IML}$ neurons of the thoracic spinal cord, a cholinergic preganglionic structure that regulates sympathetic output. Importantly, direct activation of $Nos1^{PVH}$ and OXT^{PVH} neurons appears to stimulate $ChAT^{IML}$ cells concomitant with increases in metabolic rate, locomotor activity, and thermogenesis. This physical connection between PVH neuron subsets and $ChAT^{IML}$ neurons provides a potential neuroanatomical mechanism by which sympathetic output may be increased to promote energy expenditure following activation of these PVH neurons. Indeed, activation of $Sim1^{PVH}$ neurons increases intrascapular temperature overlying BAT. As thermogenesis requires BAT UCP1 (35) and there is no change in UCP1 protein

expression following $Sim1^{PVH}$ stimulation, this effect is likely dependent on a change in UCP1 activity.

The increase in oxygen consumption upon $Sim1^{PVH}$ activation is more robust than that seen with activation of either $Nos1^{PVH}$ or OXT^{PVH} neurons alone. Interestingly, the extent of $ChAT^{IML}$ activation is relatively similar, suggesting that additional CNS pathways are engaged to regulate energy expenditure acutely. Only an estimated 25% of hindbrain and spinal cord-projecting PVH neurons have been neurochemically-defined (8). Therefore, other, unidentified PVH neurons likely play important roles in modulating energy expenditure. Additional studies directed at identifying and manipulating chemically-defined populations of PVH neurons will be critical in understanding the cellular and neuroanatomical pathways used by the PVH to modulate energy expenditure and achieve energy homeostasis.

The neurotransmitters by which $Nos1^{PVH}$ and OXT^{PVH} neurons regulate feeding and energy expenditure remain undefined. It is likely that both neuropeptides and fast-acting neurotransmitters such as glutamate, the predominant PVH neurotransmitter, contribute to PVH-mediated energy balance. Indeed, Sim1 glutamate signaling is important for overall control of energy balance (34). Our DREADD activation studies suggest the possibility that PVH neurons regulate adjacent cells. Given the presence of local, intra-PVH glutamatergic connections, it is conceivable that PVH neuronal subsets can recruit certain neighboring cell types to affect functional outputs (24).

Overall, our dissection of PVH neuron subpopulations reveals that specific subsets of PVH neurons play distinct roles in energy balance regulation. Specifically, we reveal a role for $Nos1^{PVH}$ neurons in the control of feeding, and that this function

requires the participation of non-OXT Nos1^{PVH} neurons. Moreover, both Nos1^{PVH} and the OXT^{PVH} neurons project to sympathetic output areas of the thoracic spinal cord and are capable of increasing energy expenditure (although to a lesser extent than Sim1^{PVH} neurons, suggesting roles for non-*Nos1* Sim1^{PVH} cells). The identification and analysis of other PVH subpopulations will be crucial to determining the molecular mechanisms by which the PVH regulates energy homeostasis.

References

1. Michaud JL, Rosenquist T, May NR, Fan CM. 1998. Development of neuroendocrine lineages requires the bHLH-PAS transcription factor SIM1. *Genes Dev.* 12(20):3264–75
2. Holder JL, Butte NF, Zinn AR. 2000. Profound obesity associated with a balanced translocation that disrupts the SIM1 gene. *Hum. Mol. Genet.* 9(1):101–8
3. Gold RM. 1973. Hypothalamic obesity: the myth of the ventromedial nucleus. *Science*. 182(4111):488–90
4. Effect of paraventricular nucleus lesions on body weight, food intake and insulin levels. 1986. Effect of paraventricular nucleus lesions on body weight, food intake and insulin levels. 22(3):265–81
5. McKinley MJ, Johnson AK. 2004. The physiological regulation of thirst and fluid intake. *News Physiol. Sci.* 19:1–6
6. Cowley MA, Pronchuk N, Fan W, Dinulescu DM, Colmers WF, Cone RD. 1999. Integration of NPY, AGRP, and melanocortin signals in the hypothalamic paraventricular nucleus: evidence of a cellular basis for the adipostat. *Neuron*. 24(1):155–63
7. Kishi T, Aschkenasi CJ, Lee CE, Mountjoy KG, Saper CB, Elmquist JK. 2003. Expression of melanocortin 4 receptor mRNA in the central nervous system of the rat. *J. Comp. Neurol.* 457(3):213–35
8. Sawchenko PE, Swanson LW. 1982. The organization of noradrenergic pathways from the brainstem to the paraventricular and supraoptic nuclei in the rat. *Brain Research*. 257(3):275–325
9. Blevins JE, Schwartz MW, Baskin DG. 2004. Evidence that paraventricular nucleus oxytocin neurons link hypothalamic leptin action to caudal brain stem nuclei controlling meal size. *Am. J. Physiol. Regul. Integr. Comp. Physiol.* 287(1):R87–R96
10. Fulwiler CE, Saper CB. 1985. Cholecystokinin-immunoreactive innervation of the ventromedial hypothalamus in the rat: possible substrate for autonomic regulation of feeding. *Neurosci. Lett.* 53(3):289–96
11. Xi D, Gandhi N, Lai M, Kublaoui BM. 2012. Ablation of Sim1 neurons causes obesity through hyperphagia and reduced energy expenditure. *PLoS ONE*. 7(4):e36453
12. Bamshad M, Song CK, Bartness TJ. 1999. CNS origins of the sympathetic nervous system outflow to brown adipose tissue. *Am. J. Physiol.* 276(6 Pt 2):R1569–78
13. Wu Z, Xu Y, Zhu Y, Sutton AK, Zhao R, et al. 2012. An obligate role of oxytocin neurons in diet induced energy expenditure. *PLoS ONE*. 7(9):e45167
14. Leshan RL, Greenwald-Yarnell M, Patterson CM, Gonzalez IE, Myers MG. 2012. Leptin action through hypothalamic nitric oxide synthase-1-expressing neurons controls energy balance. *Nat. Med.* 18(5):820–23
15. Balthasar N, Dalgaard LT, Lee CE, Yu J, Funahashi H, et al. 2005. Divergence of melanocortin pathways in the control of food intake and energy expenditure. *Cell*. 123(3):493–505
16. Bergner AJ, Stamp LA, Gonsalvez DG, Allison MB, Olson DP, et al. 2014. Birthdating of myenteric neuron subtypes in the small intestine of the mouse. *J.*

Comp. Neurol. 522(3):514–27
17. Paxinos G, Franklin K. 2001. *The Mouse Brain in Stereotaxic Coordinates*. San Diego, CA: Academic Press. 1 p. Second ed.
18. Opland D, Sutton A, Woodworth H, Brown J, Bugescu R, et al. 2013. Loss of neurotensin receptor-1 disrupts the control of the mesolimbic dopamine system by leptin and promotes hedonic feeding and obesity. *Mol Metab*. 2(4):423–34
19. Münzberg H, Jobst EE, Bates SH, Jones J, Villanueva E, et al. 2007. Appropriate inhibition of orexigenic hypothalamic arcuate nucleus neurons independently of leptin receptor/STAT3 signaling. *J. Neurosci.* 27(1):69–74
20. Herbison AE, Simonian SX, Norris PJ, Emson PC. 1996. Relationship of neuronal nitric oxide synthase immunoreactivity to GnRH neurons in the ovariectomized and intact female rat. *J. Neuroendocrinol.* 8(1):73–82
21. Cano G, Passerin AM, Schiltz JC, Card JP, Morrison SF, Sved AF. 2003. Anatomical substrates for the central control of sympathetic outflow to interscapular adipose tissue during cold exposure. *J. Comp. Neurol.* 460(3):303–26
22. Morrison SF. 1999. RVLM and raphe differentially regulate sympathetic outflows to splanchnic and brown adipose tissue. *Am. J. Physiol.* 276(4 Pt 2):R962–73
23. Alexander GM, Rogan SC, Abbas AI, Armbruster BN, Pei Y, et al. 2009. Remote control of neuronal activity in transgenic mice expressing evolved G protein-coupled receptors. *Neuron*. 63(1):27–39
24. Ziegler DR, Herman JP. 2000. Local integration of glutamate signaling in the hypothalamic paraventricular region: regulation of glucocorticoid stress responses. 141(12):4801–4
25. Boudaba C, Szabó K, Tasker JG. 1996. Physiological mapping of local inhibitory inputs to the hypothalamic paraventricular nucleus. *Journal of Neuroscience*. 16(22):7151–60
26. Matthias A, Ohlson KBE, Fredriksson JM, Jacobsson A, Nedergaard J, Cannon B. 2000. Thermogenic responses in brown fat cells are fully UCP1-dependent. UCP2 or UCP3 do not substitute for UCP1 in adrenergically or fatty scid-induced thermogenesis. 275(33):25073–81
27. Divakaruni AS, Humphrey DM, Brand MD. 2012. Fatty acids change the conformation of uncoupling protein 1 (UCP1). *J. Biol. Chem.* 287(44):36845–53
28. Richard D, Monge-Roffarello B, Chechi K, Labbé SM, Turcotte EE. 2012. Control and physiological determinants of sympathetically mediated brown adipose tissue thermogenesis. *Front Endocrinol (Lausanne)*. 3:36
29. Kublaoui BM, Gemelli T, Tolson KP, Wang Y, Zinn AR. 2008. Oxytocin deficiency mediates hyperphagic obesity of Sim1 haploinsufficient mice. *Mol. Endocrinol.* 22(7):1723–34
30. Tolson KP, Gemelli T, Gautron L, Elmquist JK, Zinn AR, Kublaoui BM. 2010. Postnatal Sim1 deficiency causes hyperphagic obesity and reduced Mc4r and oxytocin expression. *J. Neurosci.* 30(10):3803–12
31. Takayanagi Y, Kasahara Y, Onaka T, Takahashi N, Kawada T, Nishimori K. 2008. Oxytocin receptor-deficient mice developed late-onset obesity. *Neuroreport*. 19(9):951–55
32. Camerino C. 2009. Low sympathetic tone and obese phenotype in oxytocin-

deficient mice. *Obesity (Silver Spring)*. 17(5):980–84
33. Michaud JL, Boucher F, Melnyk A, Gauthier F, Goshu E, et al. 2001. Sim1 haploinsufficiency causes hyperphagia, obesity and reduction of the paraventricular nucleus of the hypothalamus. *Hum. Mol. Genet.* 10(14):1465–73
34. Xu Y, Wu Z, Sun H, Zhu Y, Kim ER, et al. 2013. Glutamate mediates the function of melanocortin receptor 4 on sim1 neurons in body weight regulation. *Cell Metab.* 18(6):860–70
35. Cannon B, Nedergaard J. 2004. Brown adipose tissue: function and physiological significance. *Physiol. Rev.* 84(1):277–359

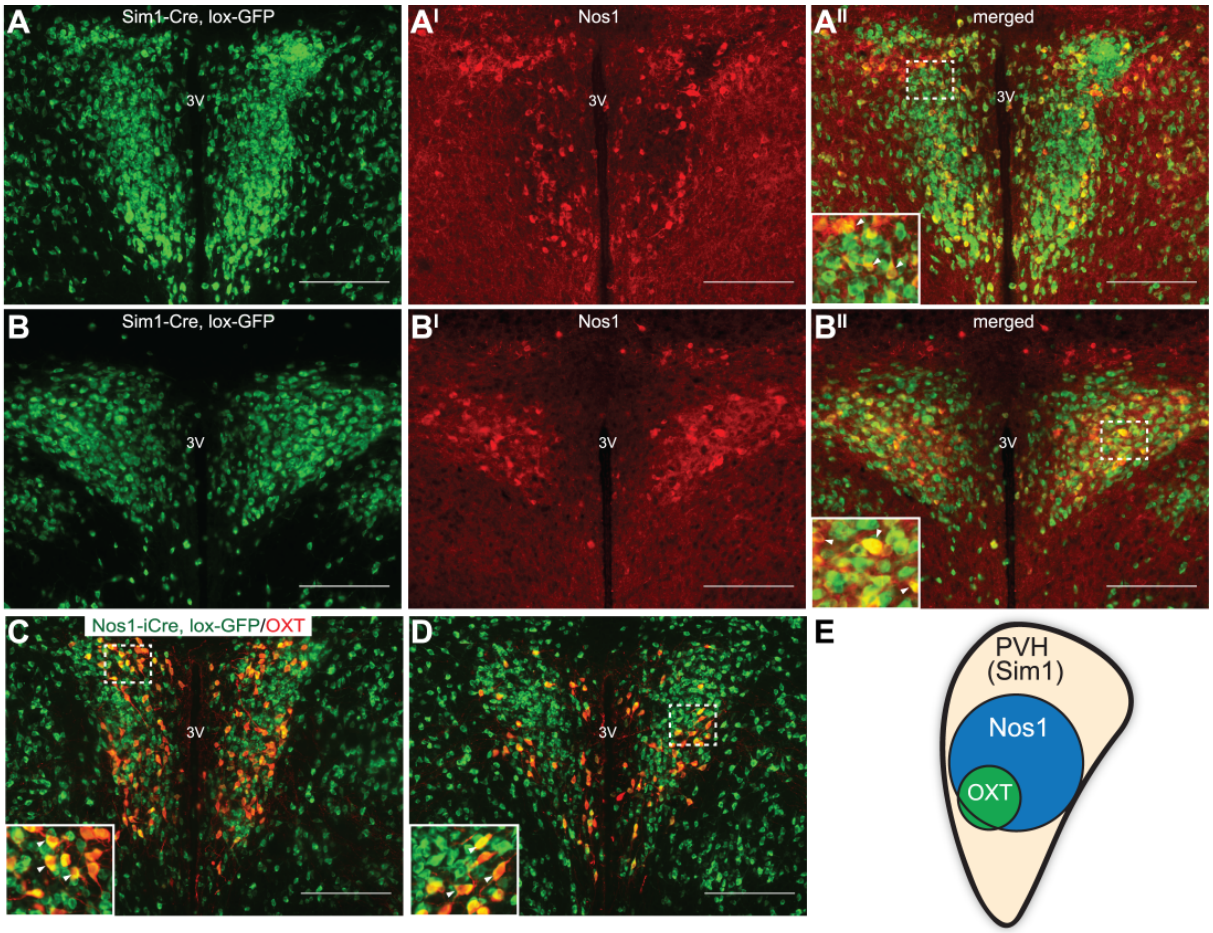
A
Sim1-Cre, lox-GFP
3V
A'
Nos1
3V
A''
merged
3V
B
Sim1-Cre, lox-GFP
3V
B'
Nos1
3V
B''
merged
3V
C
Nos1-iCre, lox-GFP/OXT
3V
D
3V
E
PVH
(Sim1)
Nos1
OXT

Figure 2.1. Neuronal nitric oxide synthase 1 (*Nos1*) marks a subset of PVH neurons. A, B) Immunohistochemistry (IHC) for NOS1 peptide (red) in the PVH of *Sim1-Cre*, *lox-GFP* reporter mice (*lox-GFP*, green) identifies $Nos1^{PVH}$ neurons as a $Sim1^{PVH}$ neuronal subset. C, D) OXT^{PVH} neurons are contained within the $Nos1^{PVH}$ population (green), as shown by expression of OXT (red) in sections from *Nos1-iCre, lox-GFP* mice. (E) A model of neurochemically-defined cell types within the PVH. Dashed boxes indicate regions that are digitally enlarged and shown as insets. Arrowheads indicate representative overlapped cell-bodies. Scale bar =200 μm, 3V=third ventricle.

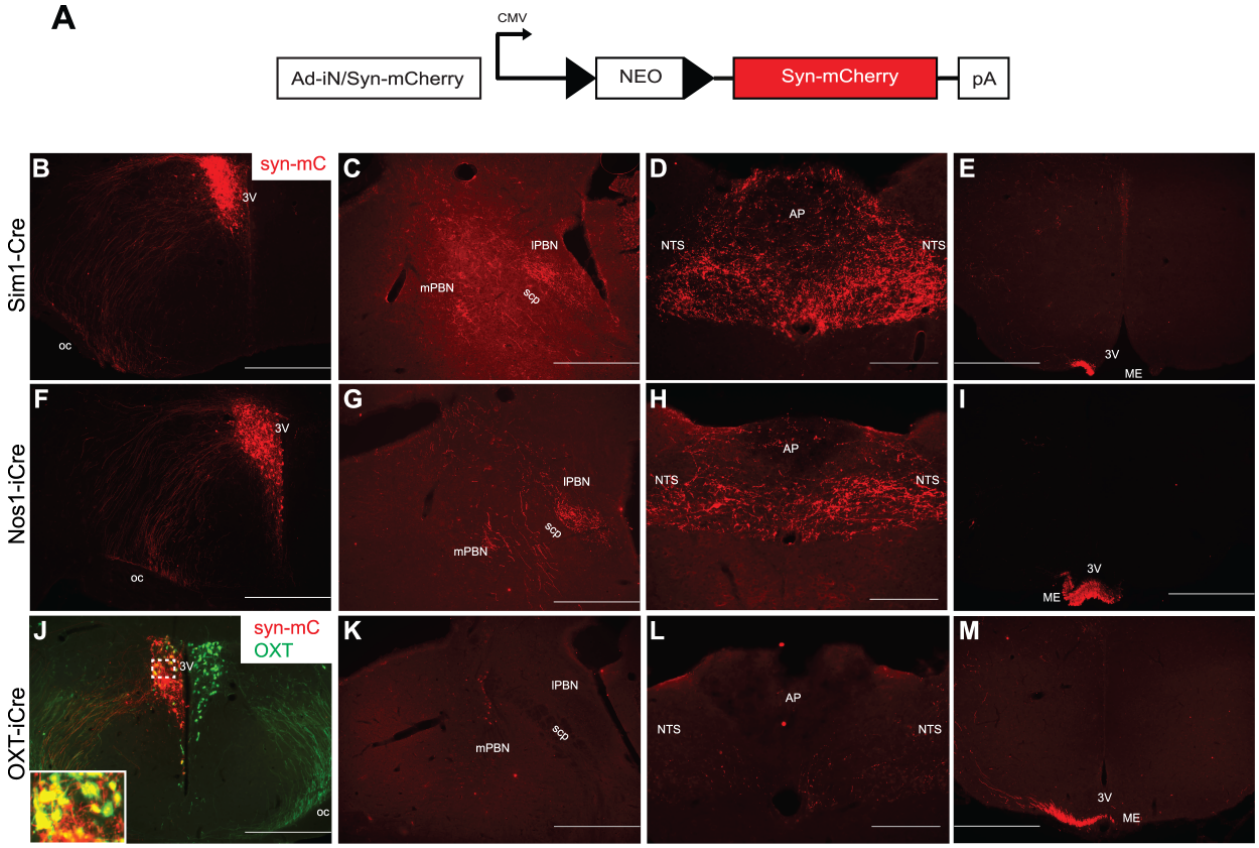
A
CMV
Ad-iN/Syn-mCherry
NEO
Syn-mCherry
pA
Sim1-Cre
Nos1-iCre
OXT-iCre
B
syn-mC
3V
oc
C
lPBN
mPBN
scp
D
AP
NTS
NTS
E
3V
ME
F
3V
oc
G
lPBN
scp
mPBN
H
AP
NTS
NTS
I
3V
ME
J
syn-mC
OXT
3V
oc
K
lPBN
scp
mPBN
L
AP
NTS
NTS
M
3V
ME

Figure 2.2. $Nos1^{PVH}$ neurons project to hindbrain regions important for satiety. A) A Cre-dependent synaptophysin-mCherry viral vector allows for anterograde-tracing of projections in the CNS. B) Unilateral PVH-specific injections of Ad-iN/syn-mCherry in *Sim1-Cre* mice identify projections to the parabrachial nucleus (C), nucleus of the solitary tract (D), and the median eminence (ME) (E). F) Stereotaxic injection of Ad-iN/syn-mCherry in the PVH of *Nos1-iCre* mice demonstrates similar projections to the PBN (G), NTS (H), or ME (I). In contrast, injection of Ad-iN/syn-mCherry in the PVH of *OXT-iCre* mice (J) reveals few projections to either the PBN (K) or NTS (L), though projections to the ME are readily apparent (M). Sections were co-stained for OXT peptide (green) to show the fidelity of the Cre-dependent virus (J). Dashed boxes indicate regions that are digitally enlarged and shown as insets. Scale bar in D, H, L=200 μm, scale bar in all others=500 μm. 3V=third ventricle, mPBN, lPBN=medial, lateral parabrachial nucleus, respectively, scp=superior cerebellar peduncle, AP=area postrema, NTS=nucleus of solitary tract, cc=central canal, ME=median eminence.

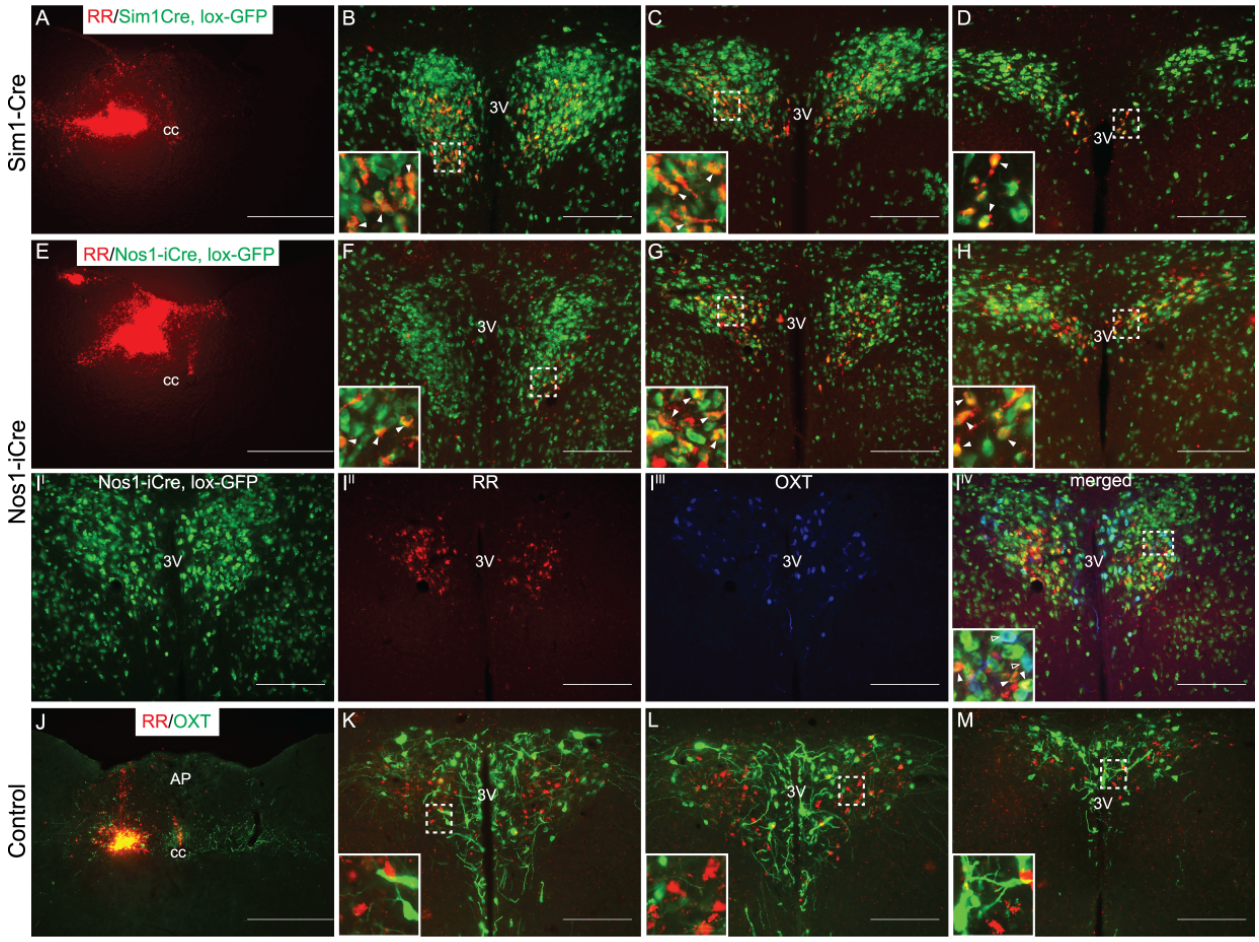
Sim1-Cre
Nos1-iCre
Control
A
RR/Sim1Cre, lox-GFP
cc
B
3V
C
3V
D
3V
E
RR/Nos1-iCre, lox-GFP
cc
F
3V
G
3V
H
3V
I
Nos1-iCre, lox-GFP
3V
II
RR
3V
III
OXT
3V
IV
merged
3V
J
RR/OXT
AP
cc
K
3V
L
3V
M
3V

Figure 2.3. Retrograde labeling of PVH neurons from the NTS. Red Retrobeads (RR) were injected in the hindbrains of in *Sim1-Cre, lox-GFP* (A) or *Nos1-iCre, lox-GFP* (E) mice to identify NTS projecting $Sim1^{PVH}$ (B, C, D) and $Nos1^{PVH}$ (F, G, H) neurons. Additional sections from *Nos1-iCre, lox-GFP* mice with hindbrain RR injections (same injection shown in E) were stained for OXT peptide (Fig. $3I^{III}$) and show RR-labeled Nos1 neurons do not contain OXT peptide (Fig. $3I^{IV}$ white arrowheads). OXT neurons only co-localize with Nos1, but not RR (Fig. $3I^{IV}$, open arrowheads). Furthermore, RR injected in the NTS of control mice (J) do not colocalize with OXT peptide (green) in the PVH (J-M). At the site of injection, beads appear in both green and red channels due to bead intensity (note yellow injection site). Immunohistochemistry identifies OXT peptide (green) expression near injection site (J). Dashed boxes indicate regions that are digitally enlarged and shown as insets. Arrowheads indicate representative overlapped cell-bodies. Scale bar in A, E, J=500 μm, all other scale bars=200 μm. AP=area postrema, cc=central canal, 3V=third ventricle.

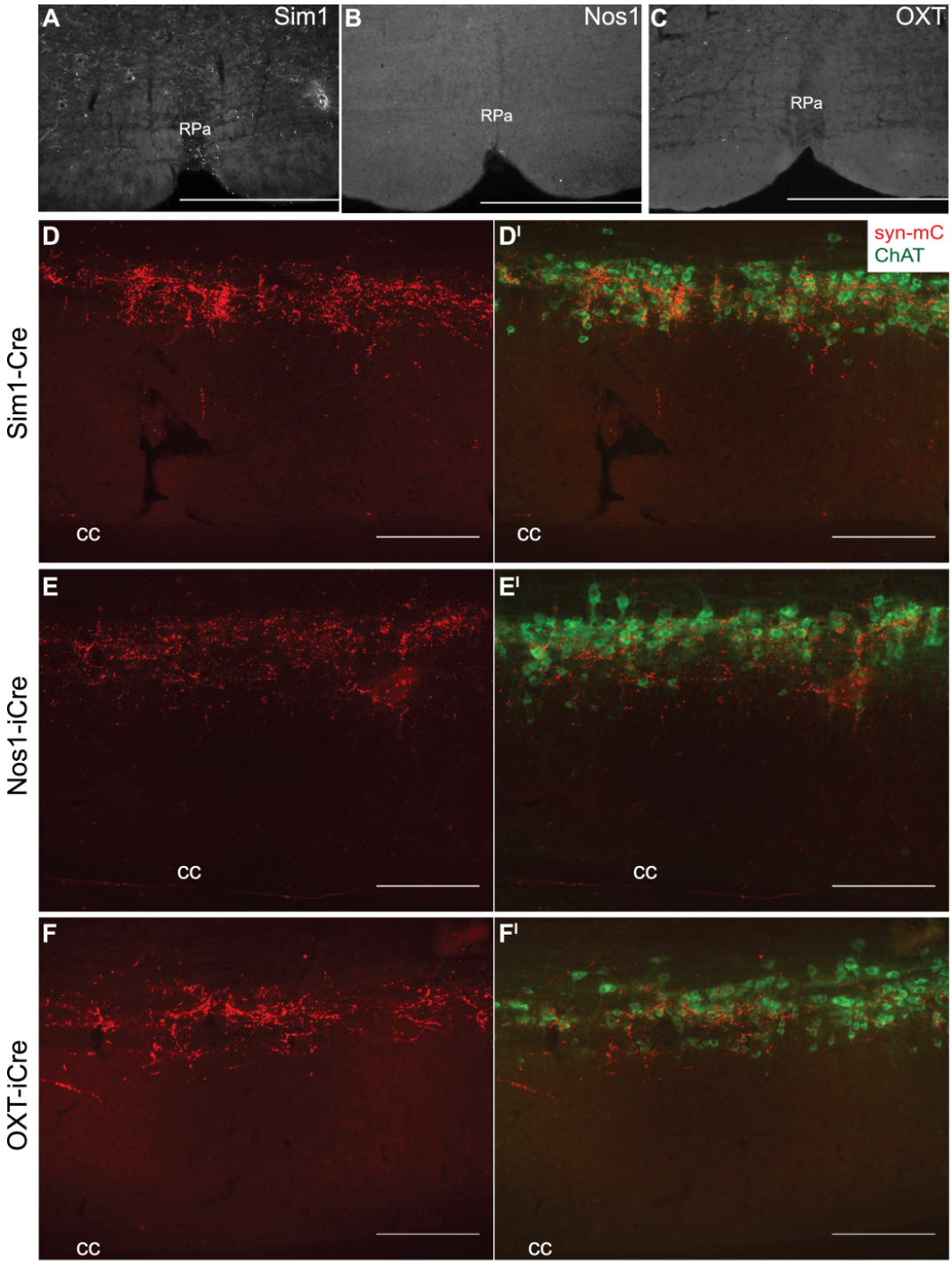
A
Sim1
RPa
B
Nos1
RPa
C
OXT
RPa
Sim1-Cre
D
CC
D'
syn-mC
ChAT
CC
Nos1-iCre
E
CC
E'
CC
OXT-iCre
F
CC
F'
CC

Figure 2.4. Nos1^{PVH} and OXT^{PVH} neurons project to pre-ganglionic neurons in the spinal cord. A) *Sim1-Cre*, B) *Nos1-iCre,* or C) *OXT-iCre* mice with unilateral Ad-iN/syn-mCherry injections (red) show few projections to the raphe pallidus (RPa). In contrast, Sim1^{PVH} (D), Nos1^{PVH} (E) and OXT^{PVH} (F) all innervate thoracic spinal cord regions in close proximity to cholinergic neurons of the intermediolateral column expressing choline acetyltransferase (ChAT, green, D', E', F'). Scale bars in A-C=500 μm, scale bars in D-F=200 μm. cc=central canal, RPa=raphe pallidus.

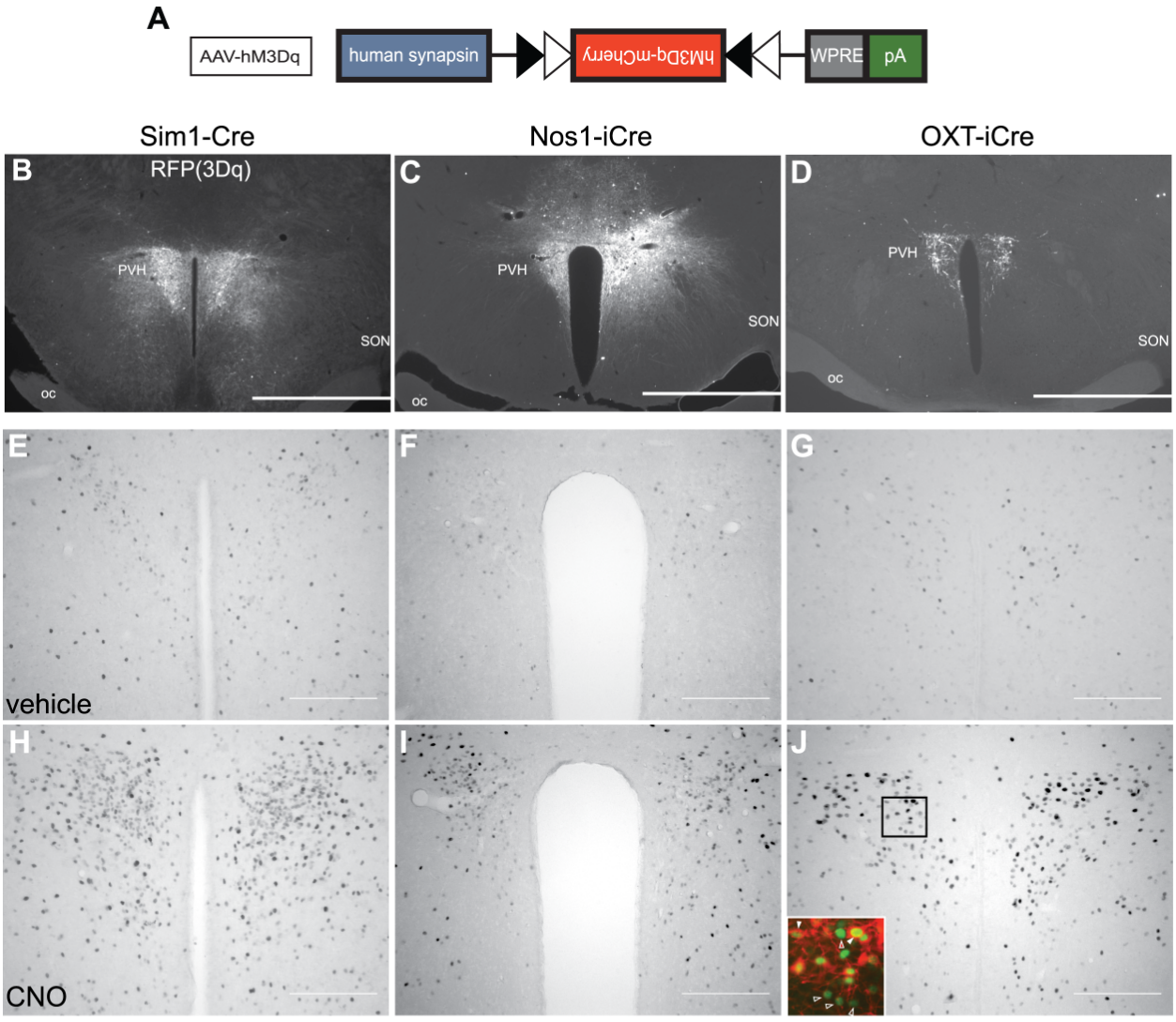
A
AAV-hM3Dq
human synapsin
hM3Dq-mCherry
WPRE
pA
Sim1-Cre
Nos1-iCre
OXT-iCre
B
RFP(3Dq)
C
D
PVH
SON
oc
E
F
G
vehicle
H
I
J
CNO

Figure 2.5. DREADDs allow for remote and temporal control of PVH neuronal activity. A) Diagram of the Cre-dependent hM3Dq Designer Receptor Exclusively Activated by Designer Drugs (DREADDs) expression vector. Expression of AAV-hM3Dq-mCherry in the PVH of *Sim1-Cre* (B), *Nos1-iCre* (C), or *OXT-iCre* (D) mice is detected by immunohistochemistry (IHC). *Sim1-Cre* (E), *Nos1-iCre* (F), or *OXT-iCre* (G) mice with bilateral AAV-hM3Dq injections demonstrate little nuclear Fos immunoreactivity after treatment with vehicle. In contrast, PVH neurons expressing hM3Dq are activated following injection of CNO (H, I, J). OXT^{PVH} neuronal activation leads to nuclear Fos expression (J, inset, green) not only in hM3Dq-expressing OXT^{PVH} neurons (J inset, red, closed arrowheads), but also in neighboring non-OXT^{PVH} neurons (open arrowheads). Scale bar in B-D=1 mm, scale bar in E-J=200 μm. oc=optic chiasm, PVH=paraventricular nucleus, SON=supraoptic nucleus.

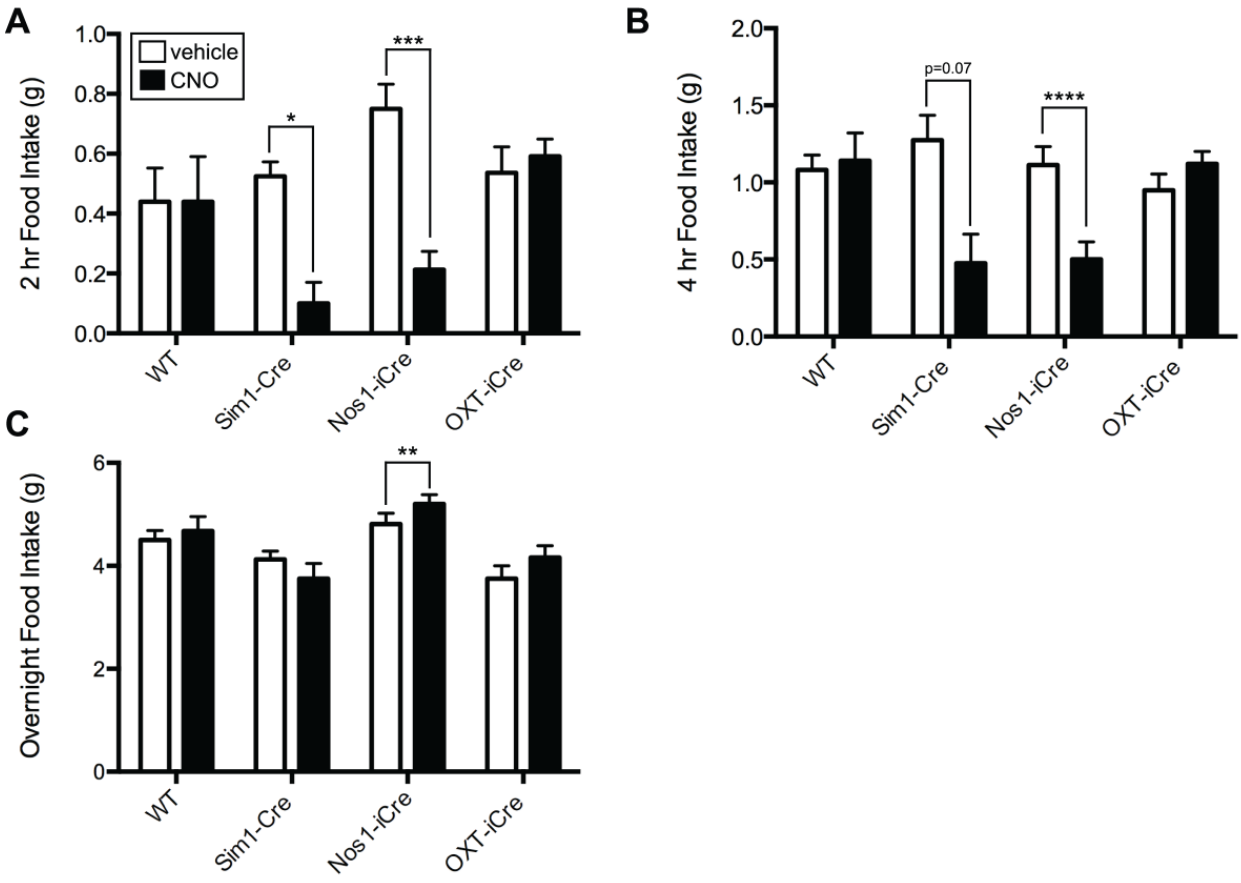
A
2 hr Food Intake (g)
vehicle
CNO
*
***
WT
Sim1-Cre
Nos1-iCre
OXT-iCre
B
4 hr Food Intake (g)
p=0.07
****
C
Overnight Food Intake (g)
**

Figure 2.6. Acute activation of Nos1^{PVH} neurons suppresses feeding. WT +AAV-hM3Dq, *Sim1-Cre* +AAV-hM3Dq, *Nos1-iCre* or *OXT-iCre* +AAV-hM3Dq mice were injected with vehicle (white bars) or CNO (black bars). Activation of Sim1^{PVH} or Nos1^{PVH} neurons decreases A) 2-hour food intake whereas activation of OXT^{PVH} neurons had no effect on food intake. Activation of Nos1^{PVH} neurons also significantly decrease 4-hour food intake (B), and Sim1^{PVH} neuronal activation shows a similar trend, though this is not significant. Cumulative overnight food intake (16hr) is not altered by activation of PVH neuronal subsets (C). Average values ± SEM are shown, *p<0.05, ***p<0.01, ****p<0.0001 compared to vehicle values (WT n=5, *Sim1-Cre* n=4, *Nos1-iCre* n=8, *OXT-iCre* n=10). Significance was determined using two-tailed paired t-test.

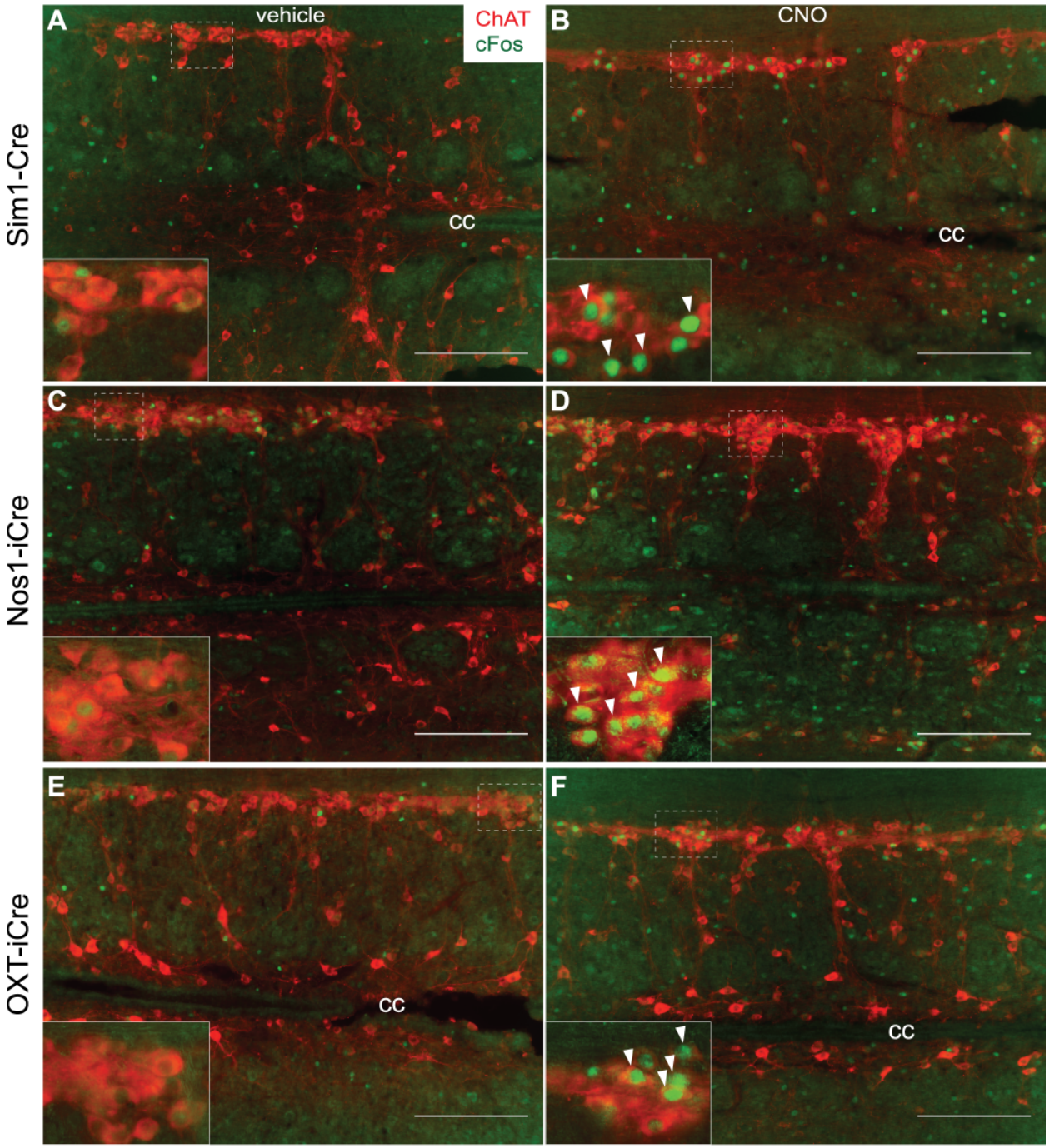
A
vehicle
ChAT
cFos
B
CNO
Sim1-Cre
cc
cc
C
D
Nos1-iCre
E
F
OXT-iCre
cc
cc

Figure 2.7. Nos1^{PVH} and OXT^{PVH} neurons can activate ChAT^{IML} neurons. While basal neuronal activity of ChAT^{IML} neurons is minimal in *Sim1-Cre* +AAV-hM3Dq (A), *Nos1-iCre* +AAV-hM3Dq (C) or *OXT-iCre* +AAV-hM3Dq (E) mice injected with vehicle, CNO-mediated activation of Sim1^{PVH} (B), Nos1^{PVH} (D) or OXT^{PVH} (F) neurons increases nuclear Fos (green) in IML ChAT neurons (red). All scale bars=200 μm. Dashed white boxes identify regions where 40X inset images were taken. Arrowheads indicate representative overlapped cell-bodies and Fos-IR nuclei upon treatment with CNO. All scale bars=200 μm. cc=central canal.

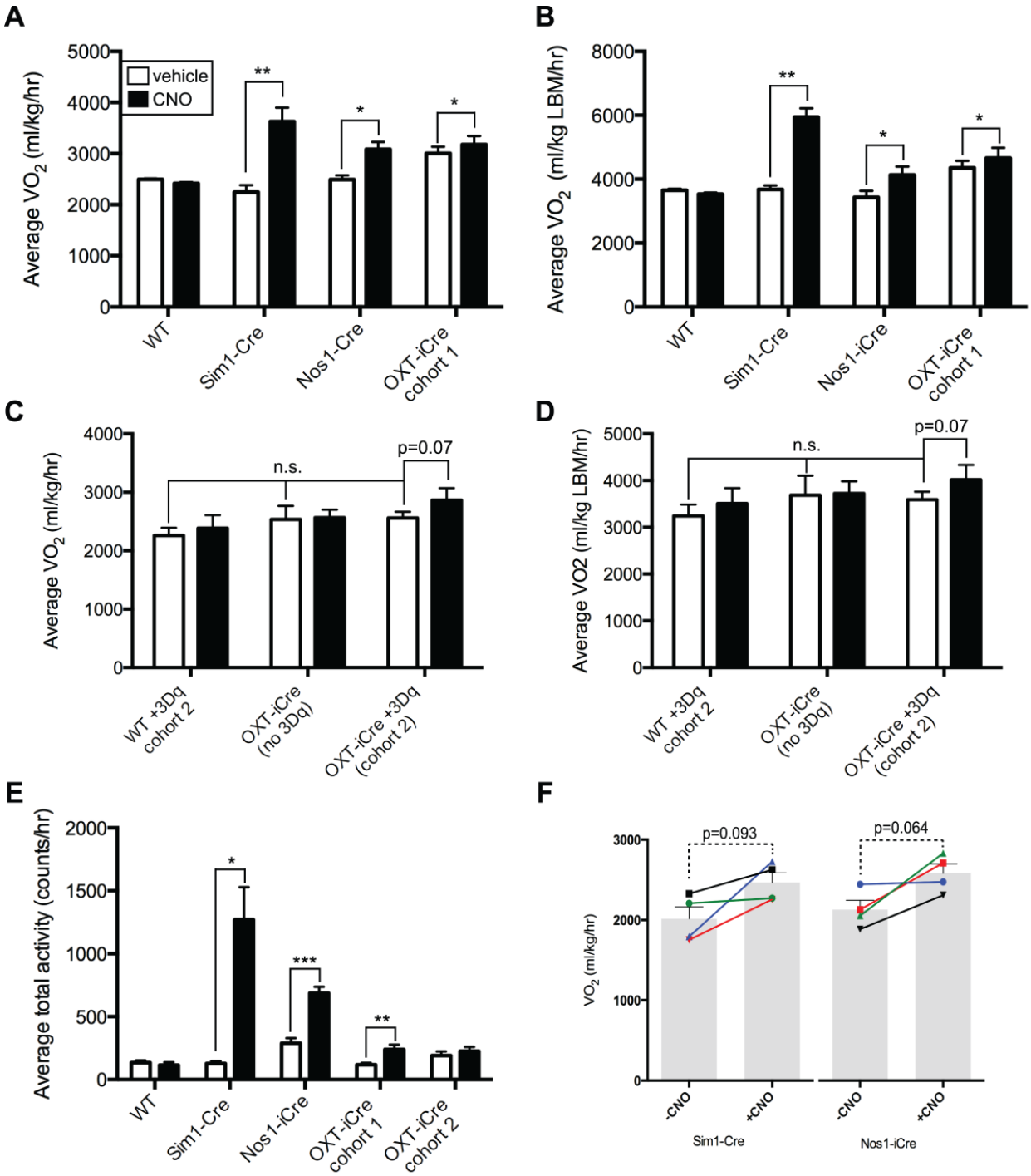
A
Average VO2 (ml/kg/hr)
vehicle
CNO
WT
Sim1-Cre
Nos1-Cre
OXT-iCre cohort 1
B
Average VO2 (ml/kg LBM/hr)
C
Average VO2 (ml/kg/hr)
n.s.
p=0.07
WT +3Dq cohort 2
OXT-iCre (no 3Dq)
OXT-iCre +3Dq (cohort 2)
D
Average VO2 (ml/kg LBM/hr)
E
Average total activity (counts/hr)
OXT-iCre cohort 2
F
p=0.093
p=0.064
VO2 (ml/kg/hr)
-CNO
+CNO
Sim1-Cre
Nos1-iCre

Figure 2.8. Acute activation of Nos1^{PVH} neurons increases energy expenditure. WT +AAV-hM3Dq, *Sim1-Cre* +AAV-hM3Dq, *Nos1-iCre* or *OXT-iCre* +AAV-hM3Dq mice were injected with vehicle (white bars) or CNO (black bars). Activation of Sim1^{PVH}, Nos1^{PVH} or OXT^{PVH} neurons increases average oxygen consumption (A, B) and total activity (E) over four hours following injection. A second cohort of CNO-naïve mice also shows a trend towards increased 4-hour average VO_2 in response to activation of OXT^{PVH} neurons, while baseline VO_2 is unchanged in comparison to WT+3Dq or *OXT-iCre* mice without 3Dq injections (C, D) (WT n=5, *Sim1-Cre* n=4, *Nos1-iCre* n=4, *OXT-iCre cohort 1* n=10, WT cohort 2 n=4, *OXT-iCre +3Dq cohort 2* n=4, *OXT-iCre* n=4). To determine potential activity-independent changes in VO_2, VO_2 was determined in *Sim1-Cre +3Dq* and *Nos1-iCre +3Dq* (F) mice before and after CNO treatment, at time points when locomotor activity was approximately matched at activity levels below a threshold value of 300 counts/hr (bars indicate average values ± SEM, line segments indicate individual mice; Sim1 n=4, Nos1 n=4). Average values ± SEM are shown, *p<0.05, **p<0.01, ***p<0.001 compared to vehicle values. Significance was determined using two-tailed paired t-test within groups or unpaired t-test between groups.

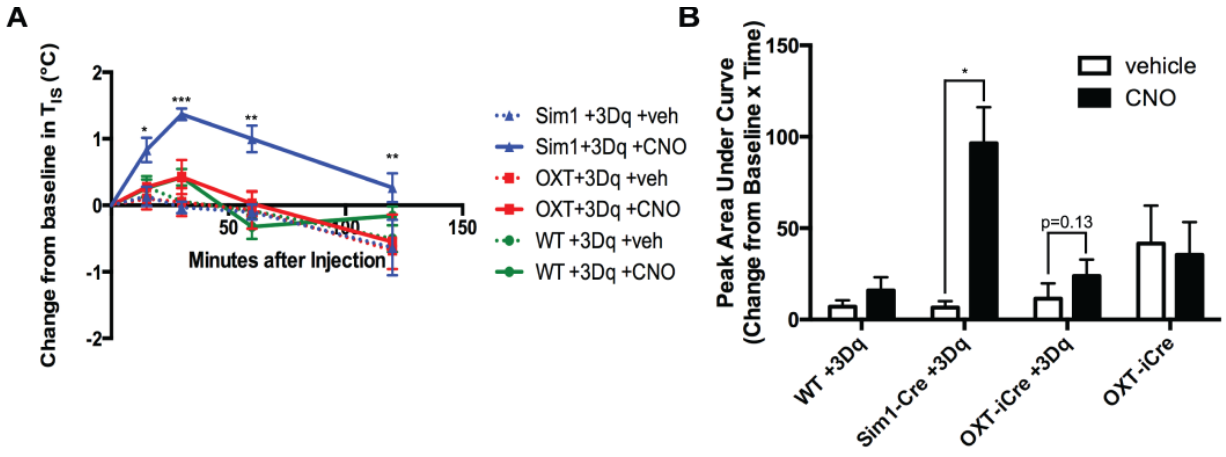
A
Change from baseline in T_{IS} (°C)
2
1
0
-1
-2
50
100
150
Minutes after Injection
*
***
**
**
Sim1 +3Dq +veh
Sim1+3Dq +CNO
OXT+3Dq +veh
OXT+3Dq +CNO
WT +3Dq +veh
WT +3Dq +CNO
B
Peak Area Under Curve
(Change from Baseline x Time)
150
100
50
0
vehicle
CNO
*
p=0.13
WT +3Dq
Sim1-Cre +3Dq
OXT-iCre +3Dq
OXT-iCre

Figure 2.9. Acute activation of Sim1^{PVH} neurons increases subcutaneous intrascapular temperature. *Sim1-Cre +3Dq*, *OXT-iCre +3Dq* and WT+3Dq mice received temperature transponders in the subcutaneous intrascapular tissue directly above brown adipose tissue (BAT). Intrascapular temperature (T_{IS}) was measured before and after vehicle or CNO administration. T_{IS} is shown relative to baseline T_{IS} before and after injection of vehicle or CNO (A, dashed and solid lines, respectively) and also represented as peak area under the curve (B). Average values ± SEM are shown, *p<0.05, **p<0.01, ***p<0.001 compared to vehicle values (WT n=5, *Sim1-Cre* n=3, *OXT-iCre* n=4). Significance was determined using repeated measures two-way ANOVA with Sidak multiple comparisons post-hoc test.

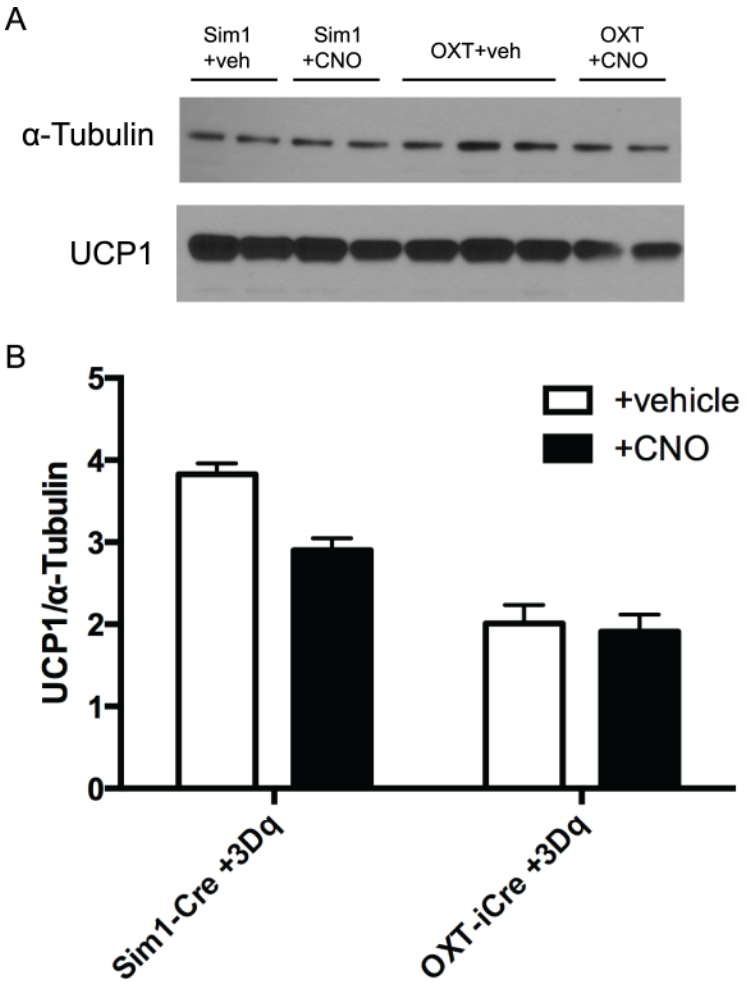
A
Sim1 +veh
Sim1 +CNO
OXT+veh
OXT +CNO
α-Tubulin
UCP1
B
+vehicle
+CNO
UCP1/α-Tubulin
0
1
2
3
4
5
Sim1-Cre +3Dq
OXT-iCre +3Dq

Figure 2.10. Acute activation of PVH neurons does not alter BAT UCP1 protein expression. BAT protein lysates were prepared from *Sim1-Cre +3Dq* and *OXT-iCre +3Dq* mice treated with either vehicle or CNO for 90 minutes. UCP1 protein levels are no different following $Sim1^{PVH}$ (A, left) or OXT^{PVH} (A, right) activation with CNO in comparison to vehicle. B) Quantification of BAT UCP1 protein levels relative to the loading control, α -tubulin. (Sim1 +vehicle (veh), n=2; Sim1 +CNO, n=2; OXT +veh, n=3; OXT +CNO n=2).

Chapter III

Paraventricular hypothalamic IRS4 neuronal activity is required for energy homeostasis

Introduction

As information increases regarding the genetic variability associated with common obesity, it is clear that genetic polymorphisms affecting neural function and architecture in the central nervous system (CNS) are disproportionately correlated with obesity (1). Within the brain, the paraventricular nucleus of the hypothalamus (PVH) is a primary hypothalamic node essential for relaying information to non-hypothalamic structures in the hindbrain and spinal cord that control satiety and energy expenditure (2-4). Critical signals of overall energy balance to the PVH originate in the arcuate nucleus (ARC) from neurons that produce melanocortin agonists (α-MSH) or antagonists (AgRP) that ultimately act on melanocortin 4 receptors (Mc4R) in the PVH (5-9). Dysregulation of the entire PVH with site-directed lesions or inhibition of PVH Mc4R action using genetic mouse models both lead to similar levels of obesity (10-12). However, while obesity resulting from the disruption of PVH^{Mc4R} activity is entirely due to hyperphagia, lesions of the entire PVH result in dysregulation of both feeding and energy expenditure (12-14). Moreover, the genetic identity of the Mc4R-containing PVH population remains elusive, since it is clear that Mc4R action in the PVH cannot be ascribed to neural populations expressing oxytocin (OXT), vasopressin (AVP), or corticotropin-releasing hormone (CRH)(12).

While significant research has examined the role of $Mc4R^{PVH}$ neurons in the control of feeding behavior, it is clear that the role of the PVH in energy balance regulation is more complex than originally understood. PVH neurons are predominantly glutamatergic and highly interconnected, partly by PVH interneurons that may coordinate neural activity between PVH subpopulations, including OXT and AVP (15-17). The genetic identity of these connections and their significance in the functional control of PVH neuron populations is largely unknown. We have previously shown the capacity of a PVH population containing neuronal nitric oxide synthase 1 ($Nos1^{PVH}$) to reduce feeding upon chemogenetic activation (chapter II). The $Nos1^{PVH}$ population represents a relatively large percentage of PVH neurons as determined by Cre-dependent reporter labeling (~70%), and therefore may likely include both interneurons and parvocellular PVH populations projecting to hindbrain and spinal cord sites. The OXT^{PVH} neuronal population is almost entirely contained within the $Nos1^{PVH}$ field; it is capable of driving small changes in energy expenditure, but is not a component of the PVH's ability to suppress feeding. While this uncovers a role for non-OXT $Nos1^{PVH}$ neurons in the control of feeding, it is imperative to characterize the connectivity and role of smaller PVH subsets on the control of both feeding and energy expenditure in order to identify and understand potential targets for obesity. With this in mind, we characterized a non-OXT, non-$Nos1^{PVH}$, population expressing insulin receptor substrate 4 (IRS4) in the PVH that projects to both hindbrain and spinal cord regions. Surprisingly, $IRS4^{PVH}$ neuronal activity is necessary for normal feeding and bodyweight, but not energy expenditure, suggesting a functional role for multiple PVH populations in

the control of feeding behavior and energy expenditure. Additionally, we discovered that NTS-projecting and PBN-projecting IRS4^{PVH} neurons both receive dense innervation from local, non-IRS4, PVH neurons, supporting a role for an interconnected PVH network in the regulation of energy balance. Overall, our study proposes a novel framework for the regulation of bodyweight through multiple interconnected PVH populations that are, perhaps, independently capable of controlling distinct energy balance parameters including feeding and energy expenditure.

Materials and Methods

Experimental Animals

IRS4-ires-Cre (*IRS4-iCre*) mice were generated using methods previously described (18). Briefly, genomic DNA including the 3' UTR of the murine *Irs4* gene was PCR amplified from R1 ES cells and cloned into a plasmid for insertion of an Frt-flanked neomycin selection cassette followed by an internal ribosomal entry sequence fused to a Cre recombinase transgene (iCre) between the STOP codon and the polyadenylation site. Constructs were linearized and electroporated into R1 ES cells by the University of Michigan Transgenic Animal Model Core. Correctly targeted ES cells were identified by quantitative real-time PCR and Southern blots and then injected into C57Bl/6J blastocysts to generate chimeric animals. Chimeras were then bred to C57Bl/6J females to confirm germline transmission and generate the *IRS4-neo-iCre* mice. To remove the frt-flanked neo cassette, *IRS4-neo-iCre* mice were then bred to Flp deleter mice (Jax 012 930).

Adult male mice (8-12 weeks old) were used for all studies. *IRS4-iCre* mice bred to a Cre-dependent GFP reporter line to fluorescently label Cre-expressing IRS4 neurons resulted in germline recombination of loxP sites and subsequent ectopic GFP expression (19). When mice still containing the neo selection cassette (*IRS4-neo-iCre*) were crossed to *lox-GFP* mice germline recombination was not detected and IRS4^{PVH} neurons could be visualized. All animals were bred and housed within our colony according to guidelines approved by the University of Michigan Committee on the Care and Use of Animals. Unless otherwise noted, mice were provided *ad libitum* access to food and water. All mice were acclimatized to intraperitoneal (i.p.) injections three days prior to any experimental i.p. injection.

Generation of Cre-dependent rabies helper virus

TVA-2A-B19G was PCR amplified from the pAAV-EF1-TVA-B19G-GFP plasmid (Addgene #26197) and cloned into the TOPO cloning vector. SpeI and SacI restriction sites were added to the PCR product via TOPO and used to insert the product into the pAAV-hSyn-Flex vector (20) .

Generation of modified rabies virus

EnvA- ΔG-mCherry and EnvA- ΔG-GFP were generated in the University of Michigan viral vector core using conditions previously described (21, 22).

Stereotaxic injections

Stereotaxic injections were performed in *IRS4-iCre* and non-transgenic (WT) mice as previously described (Chapter II). Briefly, mice were placed in a digital stereotaxic frame (Model 1900, Kopf Instruments) under isofluorane and provided with pre-surgical analgesia. Viral injections were performed using a pressurized picospritzer system coupled to a pulled glass micropipette (coordinates from bregma: PVH: A/P= -.500, M/L= +/- .220, D/V= -4.800). For tract tracing experiments, 50 nl of the adenoviral synatophysin-mCherry terminal tracer (Ad-iN/syn-mCherry, (23)) was unilaterally injected in *IRS4-iCre* mice. For functional analysis of $IRS4^{PVH}$ neurons, bilateral PVH injections of AAV-Flex-hM3Dq-mCherry (AAV-Flex-hM3Dq, purchased from UNC Vector Core), AAV-DTA (Patrick Fuller, Harvard Medical School), AAV-Flex-TetTox (purchased from the Stanford Viral Vector core) or control injections of AAV-Flex-GFP were performed in *IRS4-iCre* or WT mice (50 nl/side). For analysis of monosynaptic upstream inputs to $IRS4^{PVH}$ neurons, *IRS4-iCre* mice were unilaterally injected with AAV-Flex-TVA-B19G in the PVH and allowed to recover for at least 21 days to ensure adequate helper virus expression throughout both cell bodies and terminals. Mice then underwent a second surgery with dual stereotaxic injections into ipsilateral PVH projection targets with rabies-GFP in the PBN (A/P=-4.770, M/L=+/- 1.35, D/V=-2.8) and rabies-mCherry injected into the NTS. NTS injections were performed as previously described, whereby the fourth ventricle was identified and used as a geographic landmark to determine the site of injection (Sutton AK). A glass micropipette was lowered into the site (D/V: -.550) and ~25nl of virus was injected. Mice injected with the Ad-iN/syn-mCherry tracer were individually housed for five days following injection to allow for viral transduction and protein transport before perfusion, whereas mice

injected with modified rabies virus were perfused seven days following rabies virus injections. Mice injected with AAV-Flex-hM3Dq were allowed to recover for fourteen days following surgery before further experiments were performed, whereas bodyweight and food intake analysis on mice injected with AAV-Flex-TetTox began seven days following surgery.

Longitudinal bodyweight, food intake, and calorimetry measurements

Mice injected with AAV-DTA, AAV-Flex-TetTox, or control viruses were allowed to recover for 7 days before weekly body weight and food intake measurements began. Two weeks after surgery, blood glucose was measured following a four-hour fast (AAV-DTA only). Energy expenditure was monitored using the Comprehensive Laboratory Monitoring System (CLAMS, Columbus Instruments) in the University of Michigan's Small Animal Phenotyping Core to obtain multi-parameter analysis including open circuit calorimetry and activity via optical beam breaks 11 (AAV-Flex-TetTox) or 25 (AAV-DTA) days post injection. Mice were allowed to acclimatize to the chambers for two days, followed by VO_2 and locomotor activity data collection for three consecutive days. Body composition analysis (EchoMRI) was performed prior to CLAMS measurements, as well as 7 weeks following injection (AAV-Flex-TetTox only).

MT-II-induced feeding suppression

Five weeks following viral injection, *IRS4-iCre* mice injected with AAV-Flex-TetTox and appropriate controls were fasted during the light cycle (9:00-18:00). At the onset of the dark cycle, mice received an i.p. injection of PBS or melanotan-II (MT-II, 150 ug/mouse,

Bachem) and *ad libitum* access to food. Food intake was measured two and four hours post injection. The following week, injections were counterbalanced and corresponding food intake measured.

Effect of PVH^{IRS4} neuronal activation on feeding and energy expenditure

Following recovery, *IRS4-iCre* +AAV-Flex-hM3Dq mice underwent feeding and energy expenditure assays as previously described. Briefly, to measure changes in energy expenditure, *IRS4-iCre* +AAV-Flex-hM3Dq mice were acclimatized to CLAMS units for two consecutive days. Importantly, energy expenditure measurements were performed in mice naïve to CNO, since previous results suggest CNO-induced increases in baseline VO_2 (Chapter II). Following acclimatization, food was removed from metabolic cages during the light cycle on experimental days beginning two hours prior to experiments. Mice received an i.p. injection of vehicle (10% β-cyclodextrin, Sigma) and CLAMS measurements analyzed for the following four hours. Mice remained in the chambers with food access at the onset of the dark cycle and the experiment repeated at the same time the following day instead with i.p. injection of CNO (0.3 mg/kg in 10% B-cyclodextrin). In experiments aimed to identify satiety induced by $IRS4^{PVH}$ neuronal activation, mice were fasted during the day and received an i.p. injection of vehicle at the onset of the dark cycle with the presentation of food. Food intake was measured at two and four hours after injection and the experiment repeated the following day upon injection of CNO at the onset of the dark cycle. With the exception of two mice, the majority of *IRS4-iCre +AAV-Flex-hM3Dq* mice used for CLAMS were also used for feeding suppression assays, and therefore feeding suppression was not performed in

CNO-naïve mice. No statistical changes were identified between the two groups in either baseline feeding or CNO-mediated feeding suppression (unpaired t-test, vehicle: p=0.71; CNO: p=0.47). Data collected in Chapter II was used to compare AAV-Flex-hM3Dq results to the physiologic outcomes following activation of other PVH subsets.

Perfusion and Immunohistochemistry (IHC)

At the end of all experiments, mice were perfused to verify viral injection sites. Briefly, mice were deeply anesthetized with an overdose of pentobarbital (150 mg/kg, IP) and transcardially perfused with sterile PBS followed by 10% neutral buffered formalin or 4% paraformaldehyde (for perfusions with spinal cord removal). Epididymal and perirenal fat pad weights were dissected and weighed following perfusion in mice injected with AAV-DTA or AAV-Flex-TetTox. Brains and spinal cords (syn-mCherry injections only) were removed, post-fixed, and dehydrated in 30% sucrose before sectioning into 30 µm slices on a freezing microtome (Leica). Coronal brain sections were collected in four representative sections whereas longitudinal thoracic spinal cord sections were collected in three representative sections and stored at -20°C. For 2A peptide immunohistochemistry (IHC), free floating brain and spinal cord sections were pretreated with 30% H_2O_2 to remove endogenous peroxidase activity and then blocked with normal goat or donkey serum and incubated in primary antibody overnight (rabbit anti-2A 1:1,000, Millipore). Detection of primary antibody was performed by avidin-biotin/diaminobenzidine (DAB) method (Biotin-SP-conjugated Donkey Anti-Rabbit, Jackson Immunoresearch, 1:200; ABC kit, Vector Labs; DAB reagents, Sigma). mCherry and choline acetyltransferase (ChAT) were detected using with primary

antibodies for dsRed (rabbit 1:1000, Clontech, 632496) and ChAT (spinal cords only; goat, 1:500, Millipore AB144P) respectively followed by secondary immunofluorescence detection with donkey anti-rabbit-Alexa 568 or donkey anti-goat-Alexa 488 (1:200, Invitrogen). For PVH colocalization and rabies experiments, IHC immunostaining was performed using primary antibodies for GFP (rabbit 1:20,000, Invitrogen A6455), nNos1 (sheep 1:1500, (24), kindly provided by Dr. Vincent Prevot), neurophysin (goat, 1:1000, Santa Cruz Biotechnology, sc-7810) and copeptin (goat 1:1000, Santa Cruz Biotechnology, sc-7812). For all AAV-DTA and AAV-hM3Dq injections, bilateral PVH hit sites were verified and misses eliminated from data analysis. Imaging was performed using an Olympus BX-51 upright microscope with DP30BW camera (Olympus, Figures 3.1B-C, 3.2, 3.4, Figure 3.2D-E,), Nikon 90i upright microscope (Nikon) with CoolSNAP HQ2 CD camera (Photometrics, Figures 3.1K-N, 6), or an Olympus BX-53 upright microscope (Olympus) with G6000 camera (Q imaging, Figures 3.1D, 3.3, Figure 3.2B-C, Figure 3.5-3).

Statistical Analysis

Paired t-tests, one-way ANOVAs or two-way ANOVAs followed by Tukey or Sidak's post-hoc tests were calculated using GraphPad Prism 6 as appropriate. Significance was determined for $p<0.05$.

Results

IRS4 neurons are distinct from other PVH populations

Recent reports indicate the necessity of IRS4 and IRS2 synergy in neurons lacking the leptin receptor (LepRb) in obesity prevention (25). Since *in situ* hybridization results (Allen Brain Atlas) reveal dense *Irs4* expression in the PVH, a site lacking significant LepRb production, we sought to determine the role of IRS4^{PVH} neurons on energy homeostasis using Cre-dependent technology in combination with an *IRS4-iCre* mouse model. The *Irs4* gene is located on the X chromosome leading to random X inactivation of Cre activity in female mice, therefore male mice were used exclusively in all studies. Initial studies aimed at determining the overlap of PVH populations with IRS4^{PVH} neurons using a Cre-dependent GFP reporter (*lox-GFP*) led to germline recombination and systemic GFP expression. Therefore, Cre-activity driven by *Irs4* expression was instead identified using injection of a Cre-dependent GFP reporter virus in the PVH of *IRS4-iCre* mice (Figure 3.1A). Of note, this approach eliminates the possibility of overrepresentation of the IRS4^{PVH} population due to developmental *Irs4* expression and more accurately aligns with the Cre-dependent viral technology used throughout this study. Brains stained for GFP (indicating *IRS4-iCre* activity) and neurophysin I, the carrier protein for oxytocin, indicate that adult IRS4^{PVH} neurons do not substantially overlap with OXT^{PVH} neurons (Figure 3.1B). Since our previous work revealed that non-OXT Nos1^{PVH} neurons are capable of controlling feeding, we hypothesized that IRS4^{PVH} neurons might be contained within the Nos1^{PVH} field. Immunoreactivity for Nos1 peptide and GFP in *IRS4-iCre* mice injected with AAV-Flex-GFP demonstrates that IRS4^{PVH} neurons are in fact a separate population from Nos1 as well (Figure 3.1C). Lastly, since AVP^{PVH} neurons are also able to modestly control feeding, we determined if IRS4^{PVH} neurons are distinct from the AVP^{PVH} population. Indeed, GFP-identified PVH neurons

representing *IRS4-iCre* activity do not overlap substantially with immunoreactivity for copeptin, the carrier molecule for AVP (Figure 3.1D). To corroborate these results, mice still harboring the neo selection cassette upstream of *ires-Cre* were crossed to *lox-GFP* mice in an attempt to eliminate the ectopic, germline GFP expression (Figure 3.2A). Indeed, GFP expression, indicating *IRS4-neo-iCre* activity, is identified in the PVH (Figure 3.2B). Using this approach, IRS4^{PVH} neurons do not show significant overlap with OXT^{PVH}, AVP^{PVH}, or Nos1^{PVH} neurons (Figure 3.2C-E, respectively). Taken together, these data suggest that IRS4^{PVH} neurons represent a novel PVH subpopulation.

IRS4^{PVH} neurons project to hindbrain and spinal cord regions

To determine the neural circuits engaged by IRS4^{PVH} neurons, we identified their synaptic targets using PVH-directed injection of a Cre-dependent adenovirus, synaptophysin-mCherry (syn-mCherry), capable of highlighting neuronal synaptic terminals in *IRS4-iCre* mice. Unilateral injection of syn-mCherry identifies robust IRS4^{PVH} projections to hindbrain projection targets including the parabrachial nucleus (PBN), nucleus of the solitary tract (NTS), and the dorsal motor nucleus of the vagus (DMV) (Figure 3.3A-C). IRS4^{PVH} neurons also send projections to the median eminence, a site important for endocrine control through the pituitary (Figure 3.3D). In addition to hindbrain regions, syn-mCherry projections were identified in the intermediolateral column (IML) of the thoracic spinal cord in close proximity to choline acetyltransferase (ChAT)-producing neurons, suggesting potential control of sympathetic activity via IRS4^{PVH} neurons (Figure 3.3E). Of note, these results are

strikingly similar to projections originating from Nos1^{PVH} neurons, as previously shown (Figure 2.2F-I).

Modified rabies virus identifies projection-specific regulation of IRS4^{PVH} neurons

Since IRS4^{PVH} neurons are separate from Nos1^{PVH} neurons, yet also project to hindbrain and spinal cord sites important for feeding and energy expenditure, we sought to determine the neuroanatomical regulation of IRS4^{PVH} neurons by sites throughout the brain. We hypothesized that regulation of distinct IRS4^{PVH} circuits might differ based on IRS4^{PVH} neuronal projection site, and therefore identified monosynaptic inputs to either NTS-projecting or PBN-projecting IRS4^{PVH} neurons in the same brain. We employed a modified rabies virus approach that requires Cre-dependent helper virus (AAV-Flex-TVA-B19G) expression. Due to limited efficacy with previously used helper virus reagents, we generated a Cre-dependent helper virus that co-expresses both the TVA receptor and B19 glycoprotein (B19G) using a 2A peptide linker (Figure 3.4A). Modified rabies virus (EnvA-ΔG-mCherry (rabies-mCherry) or EnvA-ΔG-GFP (rabies-GFP)) cannot enter cells without the TVA receptor; it is also modified to express a fluorescent protein (mCherry or GFP) instead of B19G (21, 22). Therefore, infection of the modified rabies virus requires prior helper virus expression of the TVA receptor. Furthermore, B19G (expressed by the helper virus) is required for retrograde transport of rabies-mCherry or rabies-GFP (Figure 3.4B,C). This is demonstrated by a lack of rabies-mCherry expression in the brain of *Sim1-Cre* mice in which the helper virus injection missed the PVH (determined by a lack of 2A staining in the PVH), despite rabies-mCherry injection into the NTS (Figure 3.5A). With this approach, non-Cre expressing

neurons upstream of primary infected neurons do not have B19G, thereby identifying monosynaptic inputs to IRS4^{PVH} neurons with rabies-mCherry or rabies-GFP.

TVA receptor is expressed throughout the cell body and at synaptic terminals, thereby allowing terminal-specific rabies infection (26). In order to characterize inputs to projection-specified IRS4^{PVH} neurons, we performed dual rabies virus injections at disparate projection targets in the same mouse. Specifically, three weeks following helper virus injection, rabies-mCherry was injected in the NTS whereas rabies-GFP was injected into the PBN. Moderate neuronal gliosis at the site of rabies virus injection occurs and therefore allows for injection site verification (Figure 3.4K-L). While IRS4^{PVH} neurons that project to the NTS or PBN are largely distinct, some neuronal co-localization between GFP and mCherry identifies neurons that regulate both the NTS and PBN (Figure 3.4E-G).

With this technique, it cannot be determined whether these overlapping PVH populations are non-IRS4 afferents to NTS-projecting and PBN-projecting neurons, or whether IRS4^{PVH} neurons send collateral projections to both targets. To verify results, both versions of rabies virus (rabies-mCherry + rabies-GFP) were mixed and injected in the PBN of *Sim1-Cre* mice previously injected with helper virus in the PVH. While PVH neurons co-labeled GFP and mCherry, rabies-GFP expression was markedly reduced in comparison to rabies-mCherry, suggesting attenuated efficacy of rabies-GFP (Figure 3.5C-D). Therefore, results obtained using dual-rabies virus injection in the same mouse likely underreport neuronal regulators of PBN-projecting IRS4^{PVH} populations. Moreover, these control injections indicate that very few neurons upstream of PVH populations are capable of co-expressing rabies-GFP and rabies-mCherry (Figure 3.5E-

F). Therefore, although it appears that regulators of PBN-projecting or NTS-projecting IRS4^{PVH} neurons are predominantly distinct, it is still possible that some of the same neuronal inputs are regulating both populations. Nonetheless, our findings are consistent with previous literature evaluating PVH circuitry, demonstrating that the arcuate nucleus (ARC) is the main region upstream of NTS-projecting IRS4^{PVH} neurons (Figure 3.4G). Additional hypothalamic sites regulating NTS-projecting IRS4^{PVH} neurons include the lateral hypothalamic area (LHA) and the dorsomedial hypothalamus (DMH), whereas sites upstream of PBN-projecting IRS4^{PVH} neurons largely include the ventromedial hypothalamus (VMH) and LHA. Some LHA neurons co-express GFP and mCherry, suggesting dual-regulation of the IRS4^{PVH}-PBN and IRS4^{PVH}-NTS circuits. Forebrain sites including the preoptic area (POA) and bed nucleus of the stria terminalis (BNST) include largely non-overlapping populations upstream of both IRS4^{PVH} circuits, suggesting distinct forebrain circuits capable of regulating IRS4^{PVH} neuronal function. Although few midbrain or hindbrain regions express rabies-mCherry or rabies-GFP, rabies-mCherry identifies lateral PBN neurons upstream of NTS-projecting IRS4^{PVH} neurons, thereby connecting multiple PVH projection targets to one another via IRS4^{PVH} neurons.

IRS4^{PVH} neurons are capable of regulating both feeding and energy expenditure

Since IRS4^{PVH} neuronal populations receive dense input from other hypothalamic regions important for relaying information regarding an organism's energy status, we aimed to determine the sufficiency of these neurons in regulating distinct aspects of energy balance. Thus, we used Cre-dependent DREADD (Designer Receptors

Exclusively Activated by Designer Drugs) viruses that enable acute modulation of neuronal activity using a modified G-protein coupled receptor in response to peripheral injection of an otherwise inert compound, clozapine N-oxide (CNO). In this way, bilateral injection of the Cre-dependent G_q-coupled DREADD (AAV-Flex-hM3Dq) allows for remote neuronal activation in response to CNO administration (Figure 2.5). To achieve remote activation of IRS4^{PVH} neurons, we performed bilateral PVH injection of AAV-Flex-hM3Dq in *IRS4-iCre* mice (Figure 3.6A-C). Following recovery, mice were fasted during the day and injected with either vehicle or CNO at the onset of the dark cycle, when feeding normally occurs. Activation of IRS4^{PVH} neurons results in robust suppression of feeding (Figure 3.6D). In an attempt to compare the ability of the IRS4^{PVH} subpopulation to regulate feeding to other PVH populations previously studied, the change in feeding resulting from PVH neuronal activation detailed in Chapter II using the same experimental parameters was grossly compared to IRS4^{PVH} neuronal activation results. Indeed, activation of IRS4^{PVH} neurons is capable of suppressing feeding to a similar degree as activation of the entire PVH (using *Sim1-Cre*) or Nos1^{PVH} neurons (Figure 3.6E). To test the ability of IRS4^{PVH} neurons to regulate energy expenditure, the same mice were placed in metabolic chambers where oxygen consumption (VO_2) and locomotor activity were measured. In the absence of food, activation of IRS4^{PVH} neurons increases both VO_2 and total activity (Figure 3.6F, H, J). As with feeding data, a similar comparison was performed to other PVH populations previously studied, suggesting that IRS4^{PVH} neuronal activation does not increase VO_2 to the same degree as total PVH activation, even though it is likely more than that achieved with Nos1^{PVH} or OXT^{PVH} neuronal activation (Figure 3.6I). Some of these

changes in VO_2 appear to be independent of locomotor activity, since the change in activity achieved by IRS4^{PVH} neuronal activation is less than that achieved by total PVH activation (Figure 3.6G).

IRS4^{PVH} neurons are necessary for normal feeding and energy balance

To test the necessity of IRS4^{PVH} neurons for body weight regulation, we used bilateral injection of a Cre-dependent diphtheria toxin virus (AAV-DTA) in *IRS4-iCre* mice, to ablate neurons in adult mice (Figure 3.7A). In comparison to control Cre-dependent viral injections into the PVH, mice with IRS4^{PVH} neuronal ablation show robust obesity driven by hyperphagia within three weeks following viral injection (Figure 3.7B-E). This is demonstrated by analyzing 7 day food intake prior to the onset of significant obesity, from 14-21 days following injection, in which AAV-DTA injected mice eat significantly more than controls (Figure 3.7G). In contrast, AAV-DTA mice did not show any difference in energy expenditure as measured by oxygen consumption and total X activity when measured days 25-28 days following injection, despite elevated lean body mass (Figure 3.7I-L). Analysis of fat pad weights at the end of the study indicates that both epididymal and perirenal fat pad weights are increased after IRS4^{PVH} neuronal ablation. Importantly, bilateral injection of AAV-DTA in the PVH of wildtype mice not expressing Cre recombinase does not change bodyweight or feeding (Figure 3.8A-D).

Although IRS4^{PVH} neuronal ablation showed robust changes in energy balance, post-study immunohistochemical verification of PVH hit sites identified alteration in PVH architecture and decreased expression of non-IRS4^{PVH} neuronal populations in comparison to control injections (Figure 3.8E, 2F). Since AAV-DTA injections in control

animals did not show any expression (data not shown), it is possible that DTA-mediated IRS4^{PVH} neuronal ablation is inherently hazardous to surrounding neurons and therefore PVH architecture changes in response to varying degrees of PVH cell death. As this potentially confounds results obtained from IRS4^{PVH} neuronal ablation, we sought to permanently silence IRS4^{PVH} neurons using a Cre-dependent tetanus toxin virus (AAV-Flex-TetTox) that cleaves the SNARE protein, synaptobrevin, and inhibits synaptic vesicle release (27). This construct has been modified to express the A subunit and therefore does not travel retrogradely, limiting neuronal silencing to IRS4^{PVH} neurons (28) (Figure 3.9A). Similar to IRS4^{PVH} neuronal ablation, IRS4^{PVH} neuronal silencing in adult mice results in rapid hyperphagia and corresponding obesity in comparison to *IRS4-iCre* mice injected with a control virus or WT mice injected with AAV-Flex-TetTox (Figure 3.9B-D), with no changes in energy expenditure or body composition measured prior to the onset of obesity (Figure 3.9E-I). Given the important role of the PVH in mediating melanocortin-induced satiety, and the identification of numerous ARC inputs to IRS4^{PVH} neurons, we tested the ability of the melanocortin agonist MTII to drive changes in dark cycle feeding in mice without the ability to transmit information from IRS4^{PVH} neurons. Although MTII injection (150 ug/mouse) was able to suppress both two and four hour feeding in both control cohorts, this response was greatly diminished in mice with IRS4^{PVH} neuronal silencing suggesting that IRS4^{PVH} neuron activity is required for the melanocortin response (Figure 3.9J). Post-hoc IHC analysis of *IRS4-iCre +AAV-Flex-TetTox* injections is ongoing to validate PVH hit sites. Since preliminary results suggest that only 1/4 *IRS4-iCre* mice display appropriate bilateral AAV-Flex-

TetTox expression, additional cohorts will likely be required to further analyze the effect of IRS4^{PVH} neuronal silencing.

Discussion

Recent advances in genetic mouse models used in combination with chemogenetic and optogenetic tools have greatly advanced our understanding of the role of the PVH in controlling energy balance through feeding and/or energy expenditure. Nonetheless, few studies have genetically identified specific PVH populations crucial for these functions. It is now well established that Mc4R^{PVH} neurons are critical for feeding but seem dispensable for energy expenditure regulation (12, 13, 29, 30). The role of other PVH populations in the control of feeding behavior and energy balance has not been well characterized. Our previous work suggests the importance of non-OXT Nos1^{PVH} population in feeding regulation (Chapter II). Here, we identify a smaller, non-OXT, and non-Nos1^{PVH} population expressing *insulin receptor substrate 4* that is necessary for normal feeding and bodyweight maintenance.

While our previous studies narrowed down the PVH population capable of controlling feeding, it was pressing to determine if there is a unifying genetic identity for PVH "feeding" neurons. We have found that multiple PVH populations (Sim1, Nos1, and now IRS4) are capable of coordinating feeding behavior. Interestingly IRS4^{PVH} neurons do not express Nos1 peptide, yet are both necessary and sufficient in the regulation of feeding and bodyweight maintenance. To test necessity, multiple experimental methods were taken to achieve either ablation or silencing of IRS4^{PVH} neurons, with similar resultant phenotypes. Our initial attempt at IRS4^{PVH} neuronal

ablation appears to alter PVH architecture and therefore confounds our interpretation of the resulting effects on energy balance parameters. Given that the PVH is overwhelmingly glutamatergic, it is possible that DTA-induced IRS4^{PVH} neuronal cell death results in significant glutamate release within the PVH causing local excitotoxicity in non-Cre (and therefore non-DTA-expressing) neurons (17, 31). Still, preliminary studies suggest that permanent inhibition of IRS4^{PVH}-specific synaptic release also resulted in robust obesity due to altered feeding, but not energy expenditure. In contrast, chemogenetic activation using AAV-Flex-hM3Dq indicates IRS4^{PVH} neurons are capable of controlling both feeding behavior and energy expenditure. While changes in oxygen consumption are seemingly larger than results obtained from total PVH activation from previous studies, this could be partially due to non-activity induced changes in energy expenditure since total activity changes in response to IRS4^{PVH} neuronal activation are less than that obtained when activating all PVH neurons. Additionally, the sufficiency of IRS4^{PVH} neurons to change energy expenditure in an acute setting, despite not being necessary for normal energy expenditure, is interesting. A plausible explanation for this phenomenon could be the likely connection of IRS4^{PVH} neurons with local PVH circuits, causing large-scale activation of other PVH neurons resulting in an “indirect” energy expenditure effect (15, 17).

The circuitry used by IRS4^{PVH} neurons to regulate feeding and energy expenditure are similar to those investigated for Nos1^{PVH} neurons, since IRS4^{PVH} neurons also project densely to hindbrain sites including the PBN and NTS, as well as sending sparse projections to the spinal cord. While our studies do not indicate which projection site is relevant for controlling these distinct physiologic responses, it is likely

that IRS4^{PVH} neurons projecting to the PBN control feeding behavior since the PBN is the relevant output in Mc4R-mediated feeding suppression (29). Further investigation will be required to determine whether IRS4^{PVH} neurons are part of this Mc4R^{PVH} population that controls feeding through the PBN, or whether distinct PVH populations control feeding and energy expenditure via disparate projection sites (e.g. PBN vs. NTS vs. IML). Although it is possible that some IRS4^{PVH} neurons express Mc4R, it is likely that many do not, since IRS4^{PVH} neurons can control energy expenditure whereas Mc4R^{PVH} neurons do not (29). Moreover, it is unclear if Mc4R^{PVH} neurons are capable of suppressing feeding to the same extent as the entire PVH, suggesting the potential for non-Mc4R dependent control of feeding behavior by the PVH.

Since IRS4^{PVH} and Nos1^{PVH} neuronal populations are distinct and both capable of driving increased energy expenditure, it is not surprising that IRS4^{PVH} neurons are dispensable in the control of energy expenditure. However, whether this reflects redundancy in the PVH in energy expenditure regulation is unknown. It is certainly possible that non-IRS4^{PVH} neuronal populations (i.e. Nos1) are necessary for energy expenditure control, despite the ability for IRS4^{PVH} neurons to drive energy expenditure changes. Certainly, this is the case for PVH circuits driving satiety since the necessity of IRS4^{PVH} neurons in the control of feeding indicate that the Nos1^{PVH} circuit requires additional PVH populations to achieve feeding suppression upon chemogenetic activation. This finding raises the possibility that PVH interconnectivity is functionally relevant in feeding control, and potentially energy expenditure. Certainly, connections between separate PVH populations are well documented (17, 32-34). Moreover, monosynaptic retrograde tracing from hindbrain-projecting IRS4^{PVH} neurons suggest

dense PVH interconnectivity; this finding suggests that PVH populations have the potential to function as a large unit and coordinately regulate hindbrain structures.

The PVH has been well documented as a hypothalamic relay station, situated to receive dense innervation from sites critical for feeding and energy expenditure regulation and transmit this information to hindbrain sites to achieve corresponding physiologic and behavioral responses (5, 35-37). Yet, studies to date have not been able to piece together multiple components engaging projection-specific PVH circuits. Here, we identify unique regulators of NTS-projecting and PBN-projecting IRS4^{PVH} neurons. We demonstrate that NTS-projecting IRS4^{PVH} neurons receive dense innervation from the ARC, confirming this approach in a well-defined circuit. Moreover, the relevance of this circuit is illustrated by the inability of melanocortin agonists to reduce feeding in mice in which IRS4^{PVH} neurons have been silenced. Although these studies were unable to fully characterize ARC inputs to IRS4^{PVH} populations due to technical limitations, it is possible that POMC^{ARC} neurons are directly upstream of the IRS4^{PVH} population. Additionally, PBN-projecting IRS4^{PVH} neurons receive innervation from the VMH. Given the role for direct PVH connections to the PBN in mediating Mc4R-induced satiety, it is possible that the VMH-IRS4^{PVH}-PBN circuit is relevant in feeding control, though future studies will be necessary to determine this (29). Results obtained from retrograde tracing indicate that inputs to IRS4^{PVH} neurons projecting to the hindbrain are largely hypothalamic, further validating the role for the PVH as a hypothalamic relay station.

Taken together, our results demonstrate that IRS4^{PVH} neurons are a unique population capable of controlling feeding behavior and overall energy balance,

presumably through projections to hindbrain and spinal cord regions. Moreover, synaptic release from PVH neurons containing IRS4 is essential in preventing hyperphagia and obesity. Furthermore, we identify the potential for an interconnected PVH in the regulation of hindbrain structures previously shown to control energy balance parameters. While the significance of this communication between PVH subpopulations in the control of distinct aspects of energy balance remains to be elucidated, it is apparent that further characterization of the composition and circuitry of individual PVH populations is necessary to fully understand the control of feeding and energy expenditure by an essential hypothalamic output center.

References

1. Locke AE, Kahali B, Berndt SI, Justice AE, Pers TH, et al. 2015. Genetic studies of body mass index yield new insights for obesity biology. *Nature*. 518(7538):197–206
2. Sawchenko PE, Swanson LW. 1982. Immunohistochemical identification of neurons in the paraventricular nucleus of the hypothalamus that project to the medulla or to the spinal cord in the rat. *J. Comp. Neurol.* 205(3):260–72
3. Schwartz MW, Woods SC, Porte D, Seeley RJ, Baskin DG. 2000. Central nervous system control of food intake. *Nature*. 404(6778):661–71
4. Caverson MM, Ciriello J, Calaresu FR. 1984. Paraventricular nucleus of the hypothalamus: an electrophysiological investigation of neurons projecting directly to intermediolateral nucleus in the cat. *Brain Research*. 305(2):380–83
5. Cowley MA, Pronchuk N, Fan W, Dinulescu DM, Colmers WF, Cone RD. 1999. Integration of NPY, AGRP, and melanocortin signals in the hypothalamic paraventricular nucleus: evidence of a cellular basis for the adipostat. *Neuron*. 24(1):155–63
6. Kishi T, Aschkenasi CJ, Lee CE, Mountjoy KG, Saper CB, Elmquist JK. 2003. Expression of melanocortin 4 receptor mRNA in the central nervous system of the rat. *J. Comp. Neurol.* 457(3):213–35
7. Ollmann MM, Wilson BD, Yang YK, Kerns JA, Chen Y, et al. 1997. Antagonism of central melanocortin receptors in vitro and in vivo by agouti-related protein. *Science*. 278(5335):135–38
8. Rossi M, Kim MS, Morgan DG, Small CJ, Edwards CM, et al. 1998. A C-terminal fragment of Agouti-related protein increases feeding and antagonizes the effect of alpha-melanocyte stimulating hormone in vivo. *Endocrinology*. 139(10):4428–31
9. Hruby VJ, Lu D, Sharma SD, Castrucci AL, Kesterson RA, et al. 1995. Cyclic lactam alpha-melanotropin analogues of Ac-Nle4-cyclo[Asp5, D-Phe7,Lys10] alpha-melanocyte-stimulating hormone-(4-10)-NH2 with bulky aromatic amino acids at position 7 show high antagonist potency and selectivity at specific melanocortin receptors. *J. Med. Chem.* 38(18):3454–61
10. Gold RM. 1973. Hypothalamic obesity: the myth of the ventromedial nucleus. *Science*. 182(4111):488–90
11. Sims JS, Lorden JF. 1986. Effect of paraventricular nucleus lesions on body weight, food intake and insulin levels. *Behav. Brain Res.*
12. Shah BP, Vong L, Olson DP, Koda S, Krashes MJ, et al. 2014. MC4R-expressing glutamatergic neurons in the paraventricular hypothalamus regulate feeding and are synaptically connected to the parabrachial nucleus. *Proc. Natl. Acad. Sci. U.S.A.* 111(36):13193–98
13. Balthasar N, Dalgaard LT, Lee CE, Yu J, Funahashi H, et al. 2005. Divergence of melanocortin pathways in the control of food intake and energy expenditure. *Cell*. 123(3):493–505
14. Xi D, Gandhi N, Lai M, Kublaoui BM. 2012. Ablation of Sim1 neurons causes obesity through hyperphagia and reduced energy expenditure. *PLoS ONE*. 7(4):e36453
15. Daftary SS, Boudaba C, Szabó K, Tasker JG. 1998. Noradrenergic excitation of magnocellular neurons in the rat hypothalamic paraventricular nucleus via

intranuclear glutamatergic circuits. *Journal of Neuroscience*. 18(24):10619–28
16. Latchford KJ, Ferguson AV. 2004. ANG II-induced excitation of paraventricular nucleus magnocellular neurons: a role for glutamate interneurons. *Am. J. Physiol. Regul. Integr. Comp. Physiol.* 286(5):R894–902
17. Csáki A, Kocsis K, Halász B, Kiss J. 2000. Localization of glutamatergic/aspartatergic neurons projecting to the hypothalamic paraventricular nucleus studied by retrograde transport of [3H]D-aspartate autoradiography. *Neuroscience*. 101(3):637–55
18. Greenwald-Yarnell ML, Marsh C, Allison MB, Patterson CM, Kasper C, et al. 2016. ERα in Tac2 neurons regulates puberty onset in female mice. *Endocrinology*, p. en20151928
19. Bergner AJ, Stamp LA, Gonsalvez DG, Allison MB, Olson DP, et al. 2014. Birthdating of myenteric neuron subtypes in the small intestine of the mouse. *J. Comp. Neurol.* 522(3):514–27
20. Krashes MJ, Shah BP, Madara JC, Olson DP, Strochlic DE, et al. 2014. An excitatory paraventricular nucleus to AgRP neuron circuit that drives hunger. *Nature*. 507(7491):238–42
21. Wickersham IR, Lyon DC, Barnard RJO, Mori T, Finke S, et al. 2007. Monosynaptic restriction of transsynaptic tracing from single, genetically targeted neurons. *Neuron*. 53(5):639–47
22. Wall NR, Wickersham IR, Cetin A, La Parra De M, Callaway EM. 2010. Monosynaptic circuit tracing in vivo through Cre-dependent targeting and complementation of modified rabies virus. *Proc. Natl. Acad. Sci. U.S.A.* 107(50):21848–53
23. Opland D, Sutton A, Woodworth H, Brown J, Bugescu R, et al. 2013. Loss of neurotensin receptor-1 disrupts the control of the mesolimbic dopamine system by leptin and promotes hedonic feeding and obesity. *Mol Metab*. 2(4):423–34
24. Herbison AE, Simonian SX, Norris PJ, Emson PC. 1996. Relationship of neuronal nitric oxide synthase immunoreactivity to GnRH neurons in the ovariectomized and intact female rat. *J. Neuroendocrinol.* 8(1):73–82
25. Sadagurski M, Dong XC, Myers MG, White MF. 2014. Irs2 and Irs4 synergize in non-LepRb neurons to control energy balance and glucose homeostasis. *Mol Metab*. 3(1):55–63
26. Betley JN, Cao ZFH, Ritola KD, Sternson SM. 2013. Parallel, redundant circuit organization for homeostatic control of feeding behavior. *Cell*. 155(6):1337–50
27. Verderio C, Coco S, Bacci A, Rossetto O. 1999. Tetanus toxin blocks the exocytosis of synaptic vesicles clustered at synapses but not of synaptic vesicles in isolated axons. *The Journal of …*
28. McMahon HT, Foran P, Dolly JO, Verhage M, Wiegant VM, Nicholls DG. 1992. Tetanus toxin and botulinum toxins type A and B inhibit glutamate, gamma-aminobutyric acid, aspartate, and met-enkephalin release from synaptosomes. Clues to the locus of action. *J. Biol. Chem.* 267(30):21338–43
29. Garfield AS, Li C, Madara JC, Shah BP, Webber E, et al. 2015. A neural basis for melanocortin-4 receptor-regulated appetite. *Nat. Neurosci.* 18(6):863–71
30. Xu Y, Wu Z, Sun H, Zhu Y, Kim ER, et al. 2013. Glutamate mediates the function of melanocortin receptor 4 on sim1 neurons in body weight regulation. *Cell Metab.*

18(6):860–70
31. Vong L, Ye C, Yang Z, Choi B, Chua S, Lowell BB. 2011. Leptin action on GABAergic neurons prevents obesity and reduces inhibitory tone to POMC neurons. *Neuron*. 71(1):142–54
32. van den Pol AN. 1982. The magnocellular and parvocellular paraventricular nucleus of rat: intrinsic organization. *J. Comp. Neurol.* 206(4):317–45
33. Liposits Z, Paull WK, Sétáló G, Vigh S. 1985. Evidence for local corticotropin releasing factor (CRF)-immunoreactive neuronal circuits in the paraventricular nucleus of the rat hypothalamus. An electron microscopic immunohistochemical analysis. *Histochemistry*. 83(1):5–16
34. Herman JP, Cullinan WE, Ziegler DR, Tasker JG. 2002. Role of the paraventricular nucleus microenvironment in stress integration. *Eur. J. Neurosci.* 16(3):381–85
35. Saper CB, Loewy AD, Swanson LW, Cowan WM. 1976. Direct hypothalamo-autonomic connections. *Brain Research*. 117(2):305–12
36. Swanson LW, Kuypers HG. 1980. The paraventricular nucleus of the hypothalamus: cytoarchitectonic subdivisions and organization of projections to the pituitary, dorsal vagal complex, and spinal cord as demonstrated by retrograde fluorescence double-labeling methods. *J. Comp. Neurol.* 194(3):555–70
37. Marsh DJ, Hollopeter G, Huszar D, Laufer R, Yagaloff KA, et al. 1999. Response of melanocortin-4 receptor-deficient mice to anorectic and orexigenic peptides. *Nat. Genet.* 21(1):119–22

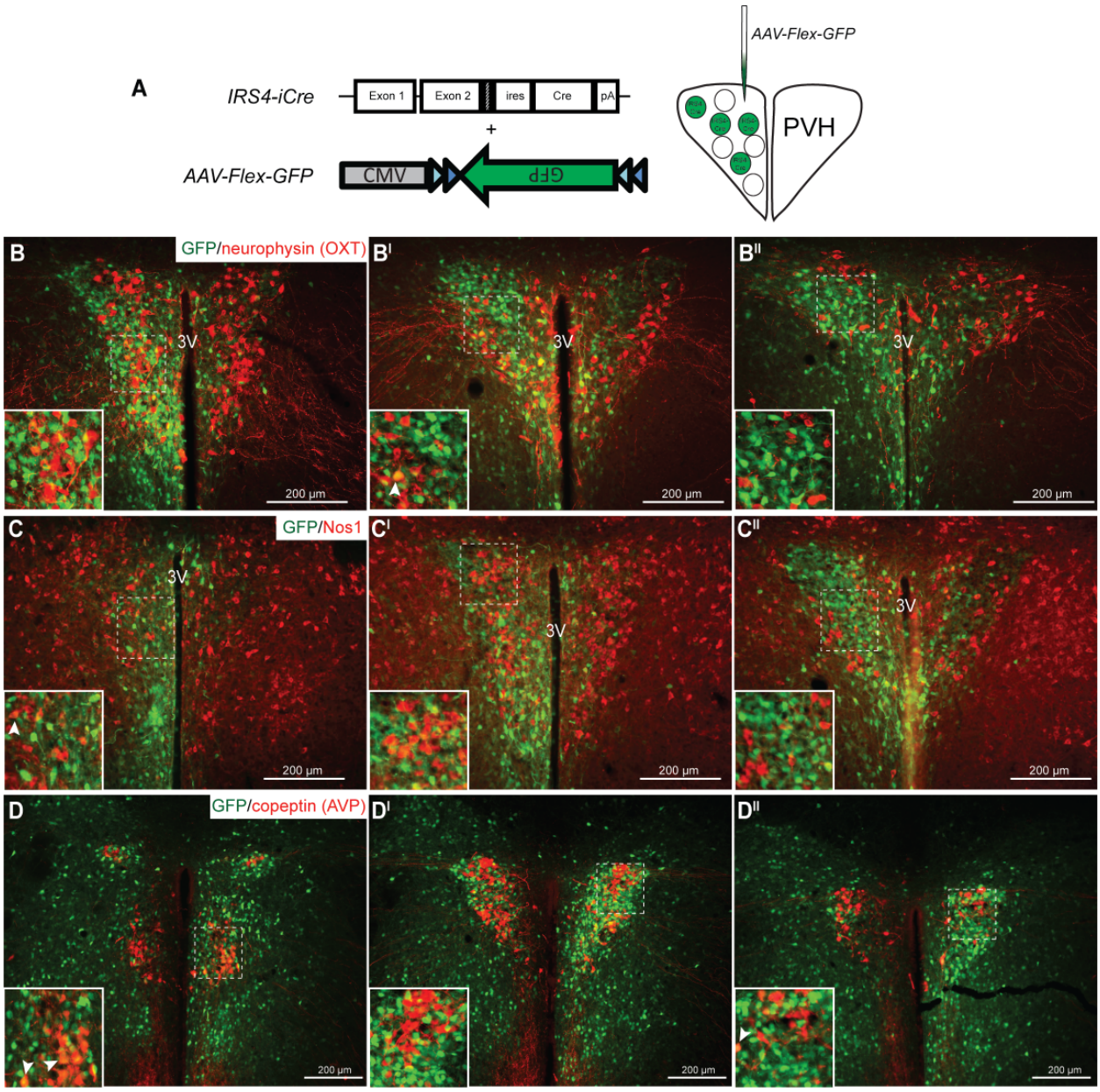
A
IRS4-iCre
Exon 1
Exon 2
ires
Cre
pA
+
AAV-Flex-GFP
CMV
GFP
AAV-Flex-GFP
PVH
B
GFP/neurophysin (OXT)
BI
BII
C
GFP/Nos1
CI
CII
D
GFP/copeptin (AVP)
DI
DII
3V
200 µm

Figure 3.1. IRS4 neurons comprise a unique PVH population. A) Adult *IRS4-iCre* mice were stereotaxically injected with a Cre-dependent GFP reporter virus (AAV-Flex-GFP) in the PVH to visualize Cre-expressing neurons in the adult mouse. B) Immunohistochemistry (IHC) in the PVH demonstrates limited co-localization between $IRS4^{PVH}$ neurons (green) and oxytocin (OXT, red) neurons (identified with the OXT carrier molecule, neurophysin). C-D) IHC for GFP (green) and Nos1 (C, red) or copeptin (D, red) indicates that few $IRS4^{PVH}$ neurons overlap with Nos1 or AVP neurons in the PVH. Dashed boxes indicate regions that are digitally enlarged and shown as insets. White arrowheads indicate the few overlapping $IRS4^{PVH}$ neurons with respective PVH populations. 3V=third ventricle.

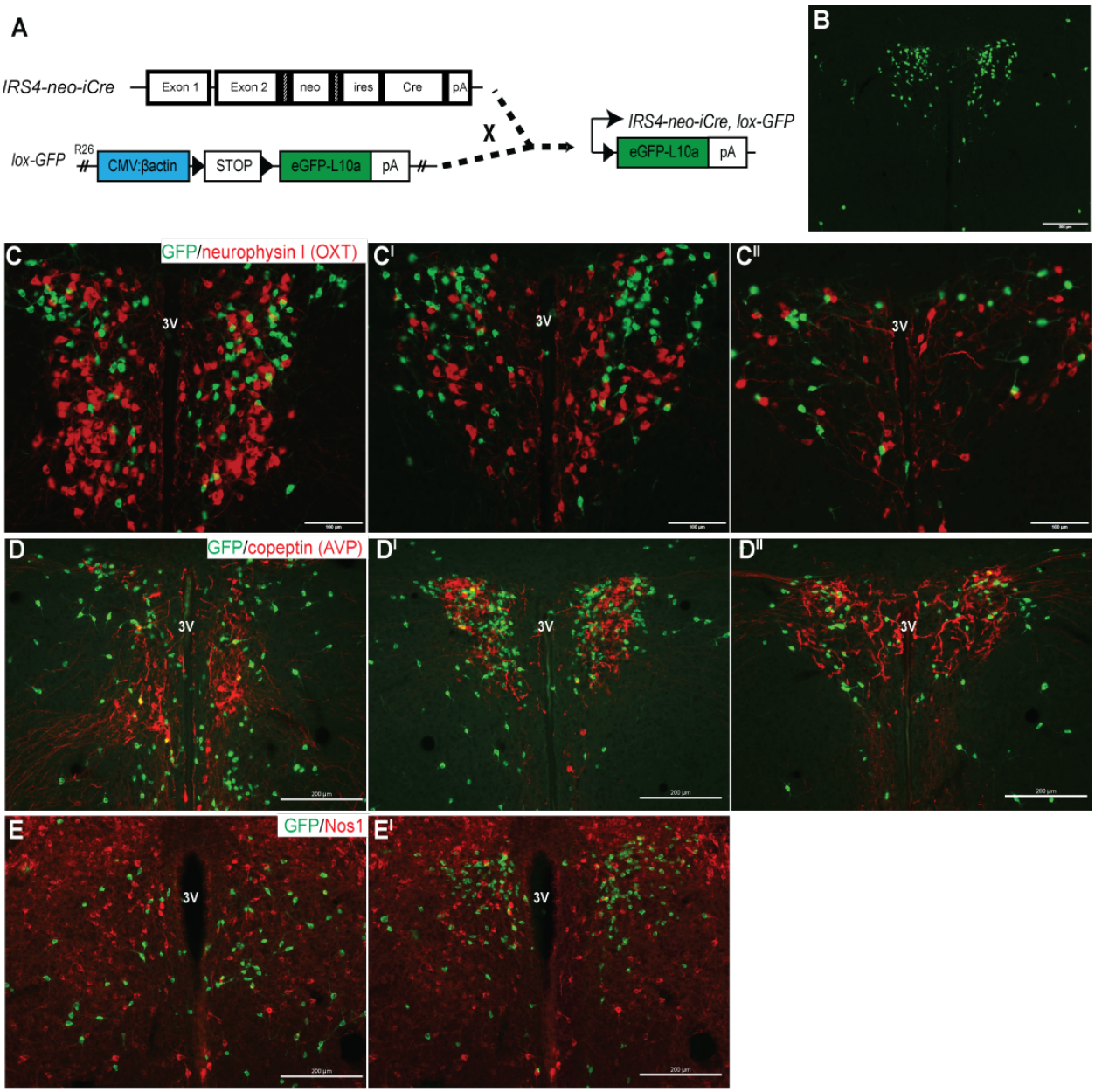
A
IRS4-neo-iCre
Exon 1
Exon 2
neo
ires
Cre
pA
lox-GFP
R26
CMV:βactin
STOP
eGFP-L10a
pA
X
IRS4-neo-iCre, lox-GFP
eGFP-L10a
pA
B
C
GFP/neurophysin I (OXT)
3V
C'
3V
C''
3V
D
GFP/copeptin (AVP)
3V
D'
3V
D''
3V
E
GFP/Nos1
3V
E'
3V

Figure 3.2. Cre-dependent GFP reporter mice allow for further characterization of IRS4^{PVH} neurons. A) *IRS4-iCre* mice still expressing the neo selection cassette (*IRS4-neo-iCre*) were used to avoid systemic GFP expression resulting from germline recombination of Cre-dependent reporter alleles during development. Upon crossing to the Cre-dependent *lox-GFP* mouse line, IRS4neo^{PVH} neurons can be visualized in the PVH (B). C-E) IHC for neurophysin (C), copeptin (D), and Nos1 (E), demonstrates little overlap between IRS4neo^{PVH} neurons and OXT, AVP, or Nos1 respectively. 3V=third ventricle.

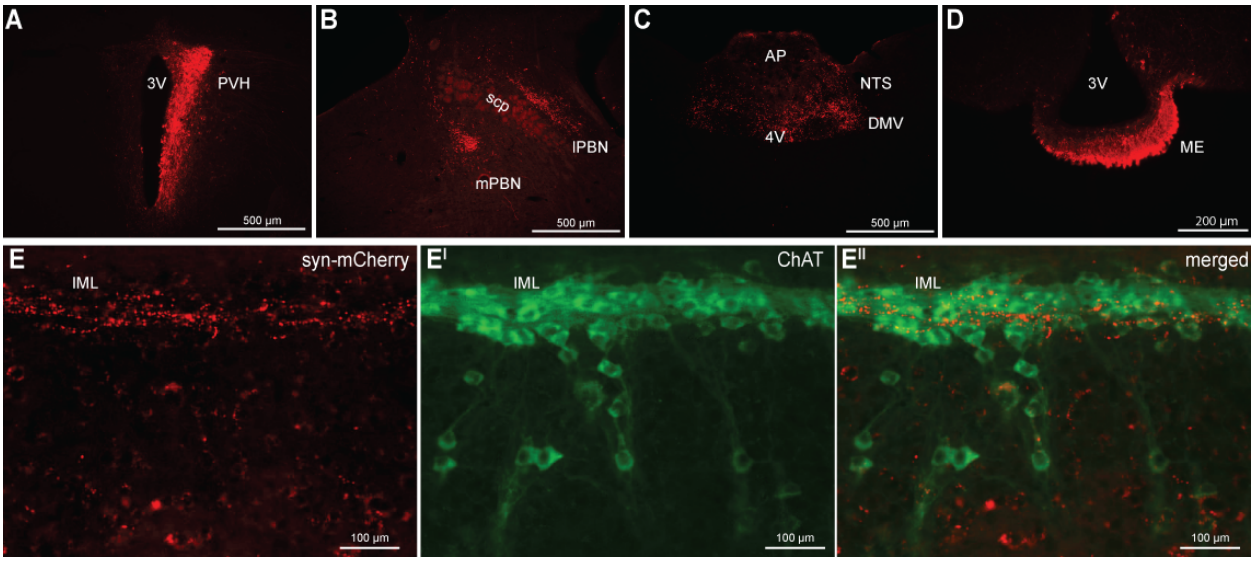
A
3V
PVH
500 µm
B
scp
lPBN
mPBN
500 µm
C
AP
NTS
DMV
4V
500 µm
D
3V
ME
200 µm
E
syn-mCherry
IML
100 µm
E^I
ChAT
IML
100 µm
E^II
merged
IML
100 µm

Figure 3.3. IRS4^{PVH} neurons send direct projections to hindbrain and spinal cord regions. A) A Cre-dependent synaptophysin-mCherry adenovirus (syn-mCherry) was unilaterally injected in the PVH of *IRS4-iCre* mice to trace synaptic terminals throughout the brain. B-C) IHC identification of syn-mCherry terminals is observed in hindbrain regions including the medial and lateral parabrachial nucleus (mPBN, lPBN, respectively, B), as well as the dorsal motor nucleus of the vagus (DMV) and nucleus of the solitary tract (NTS, C). D) IRS4^{PVH} neurons also project to the median eminence (ME). E) Syn-mCherry (red) identifies synaptic terminals in the intermediolateral column of the spinal cord (IML) in close proximity to neurons expressing choline acetyltransferase (ChAT, green). scp= superior cerebellar peduncle, 4V=fourth ventricle, 3V=third ventricle, AP=area postrema

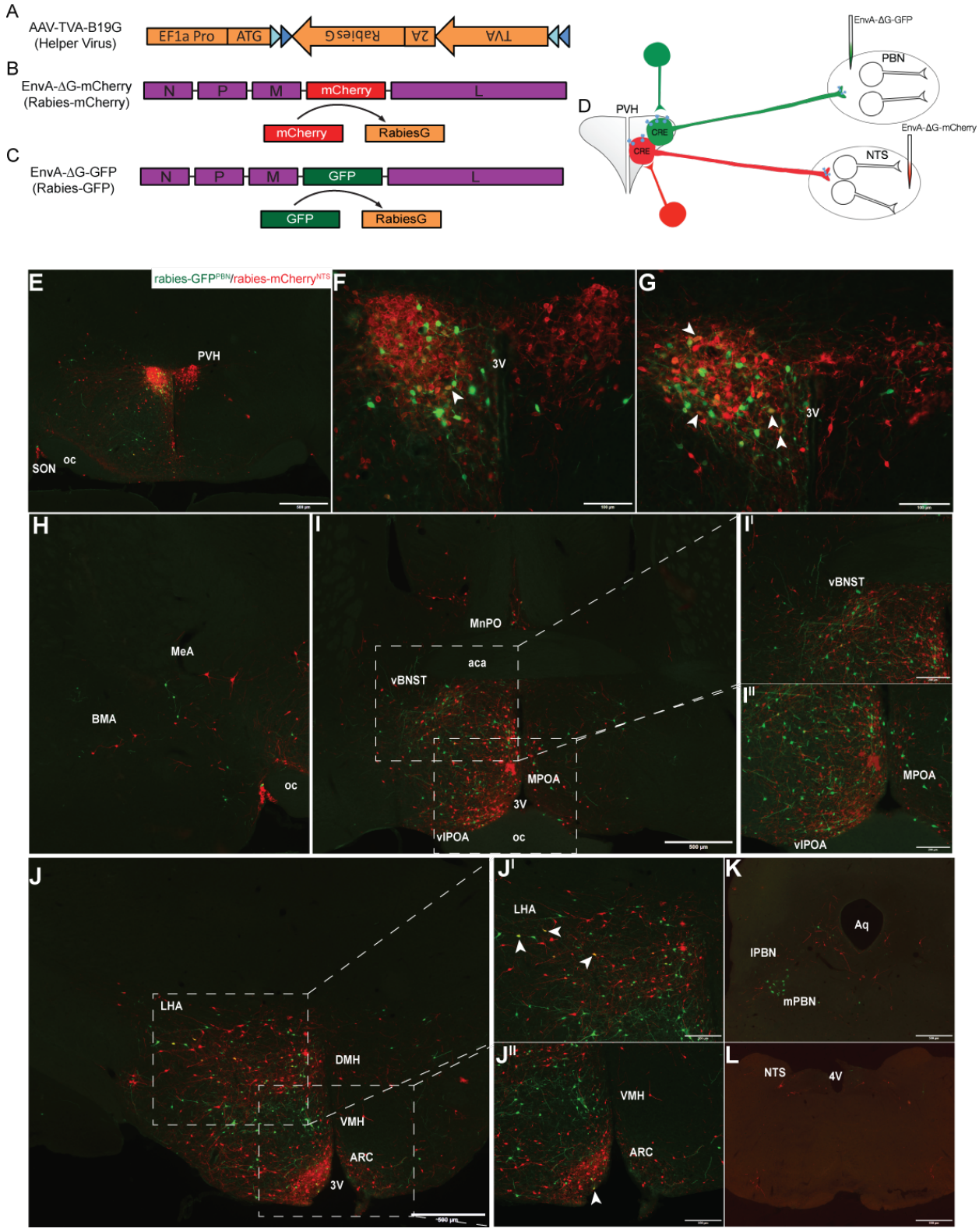
A
AAV-TVA-B19G
(Helper Virus)
EF1a Pro
ATG
RabiesG
2A
TVA
B
EnvA-ΔG-mCherry
(Rabies-mCherry)
N
P
M
mCherry
L
mCherry
RabiesG
C
EnvA-ΔG-GFP
(Rabies-GFP)
N
P
M
GFP
L
GFP
RabiesG
D
PVH
CRE
CRE
EnvA-ΔG-GFP
PBN
EnvA-ΔG-mCherry
NTS
E
rabies-GFPPBN/rabies-mCherryNTS
PVH
SON
oc
F
3V
G
3V
H
MeA
BMA
oc
I
MnPO
aca
vBNST
MPOA
3V
vlPOA
oc
I'
vBNST
I''
MPOA
vlPOA
J
LHA
DMH
VMH
ARC
3V
J'
LHA
J''
VMH
ARC
K
Aq
lPBN
mPBN
L
NTS
4V

Figure 3.4. Identification of monosynaptic inputs to NTS-projecting or PBN-projecting IRS4^{PVH} neurons using modified rabies virus. A) A Cre-dependent helper virus construct is used to insert rabies B19 glycoprotein (B19G) and the TVA receptor (blue receptor, D) in IRS4^{PVH} cell bodies and terminals. Modified rabies virus expresses a fluorescent tag (mCherry, B; GFP, C) instead of B19G. After initial infection with helper virus, rabies-mCherry is injected at one projection site (NTS), whereas rabies-GFP is injected at another (PBN) in the same mouse. E-G) IHC for mCherry and GFP identify largely non-overlapping NTS-projecting and PBN-projecting IRS4^{PVH} neurons, respectively. Sites upstream of both NTS and PBN-projecting IRS4^{PVH} neurons include the supraoptic nucleus (SON), amygdala (H), bed nucleus of the stria terminalis (BNST, I), preoptic area (POA, I), and lateral hypothalamic area (LHA, J). The ventromedial hypothalamus (VMH) is upstream of PBN-projecting IRS4^{PVH} neurons (J^{II}, green), whereas both the arcuate nucleus (ARC, J^{II}, red) and PBN (K, red) are upstream of IRS4^{PVH} neurons projecting to the NTS. Glial damage represents injection site in the PBN (K, green) and NTS (L, red). 3V=third ventricle, oc=optic chiasm, MeA=medial amygdala, BMA=basomedial amygdala, vBNST=ventral BNST, vlPOA=ventral lateral POA, MPOA=medial POA, MnPO=median preoptic nucleus, aca=anterior part of anterior commissure, DMH=dorsomedial hypothalamus, aq=aqueduct, 4V=fourth ventricle

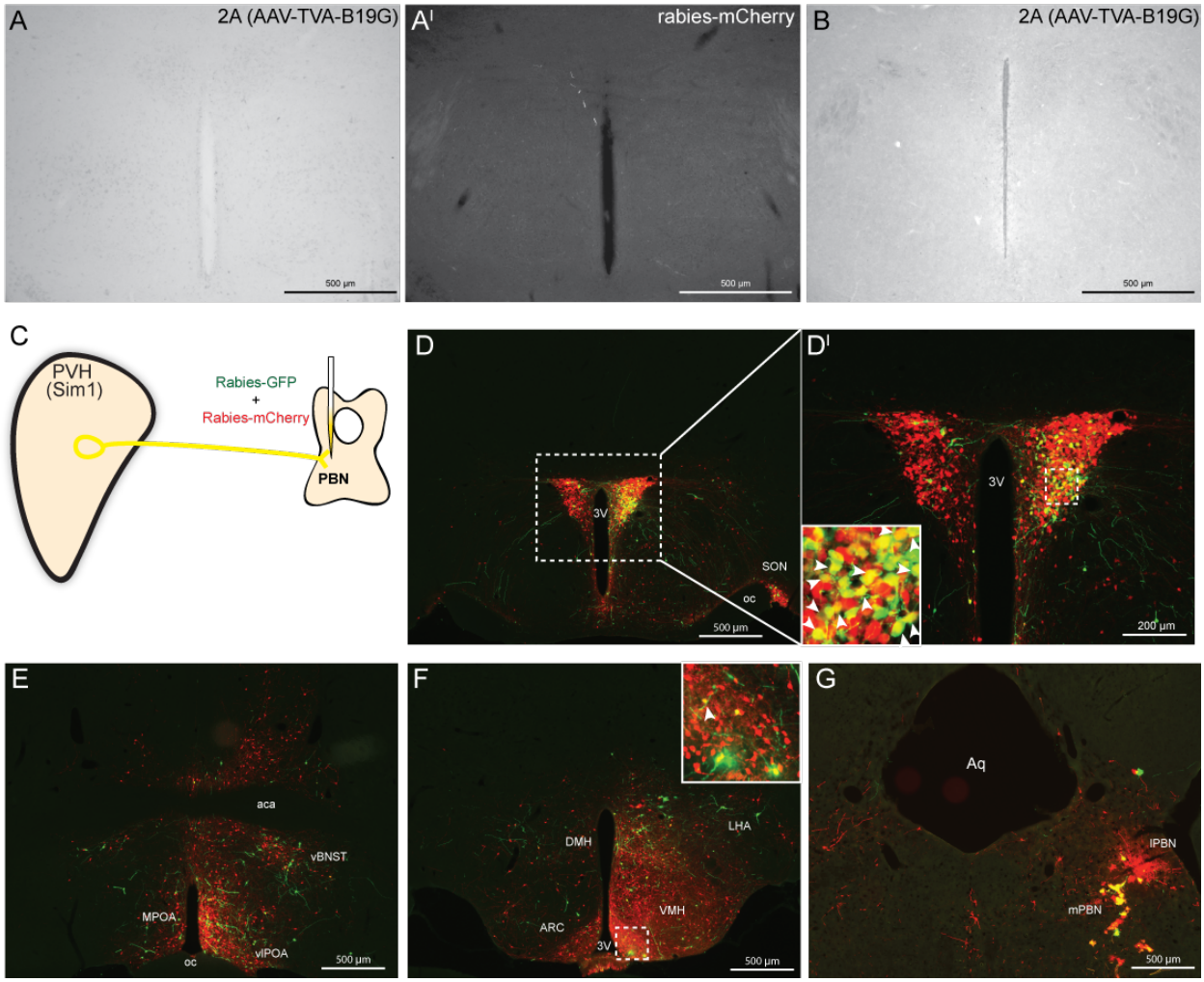
A
2A (AAV-TVA-B19G)
500 μm
A'
rabies-mCherry
500 μm
B
2A (AAV-TVA-B19G)
500 μm
C
PVH
(Sim1)
Rabies-GFP
+
Rabies-mCherry
PBN
D
3V
SON
oc
500 μm
D'
3V
200 μm
E
aca
vBNST
MPOA
oc
vlPOA
500 μm
F
DMH
LHA
VMH
ARC
3V
500 μm
G
Aq
lPBN
mPBN
500 μm

Figure 3.5. Dual rabies virus infection is limited in efficacy. A) IHC in the PVH of *Sim1-Cre +AAV-Flex-TVA-B19G* mice validates a "miss" since 2A staining is not detected. Still, NTS-directed rabies-mCherry injection in the same mouse displays limited mCherry expression in the PVH, therefore confirming the requirement of AAV-Flex-TVA-B19G expression for modified rabies virus expression. B) 2A expression in wildtype mice injected with AAV-Flex-TVA-B19G demonstrates that Cre recombinase is required for helper virus expression. C) Injection of both rabies-mCherry and rabies-GFP in the same PBN projection target in *Sim1-Cre +AAV-Flex-TVA-B19G* mice illustrates that both rabies viruses can be expressed in PBN-projecting PVH neurons (D), though sites upstream including the bed nucleus of the stria terminalis (BNST, E), preoptic area (POA), arcuate nucleus (ARC, F) and VMH (F) show limited co-labeling. G) Gliosis in the PBN due to rabies-mCherry/rabies-GFP injection demonstrates that both rabies-GFP and rabies-mCherry were mixed and injected at the same site. Dashed boxes indicate regions that are digitally enlarged and shown as insets. White arrowheads indicate co-localization in neurons with both rabies-GFP and rabies-mCherry. 3V=third ventricle, aca= anterior part of anterior commissure, DMH=dorsomedial hypothalamus, oc=optic chiasm, LHA=lateral hypothalamic area.

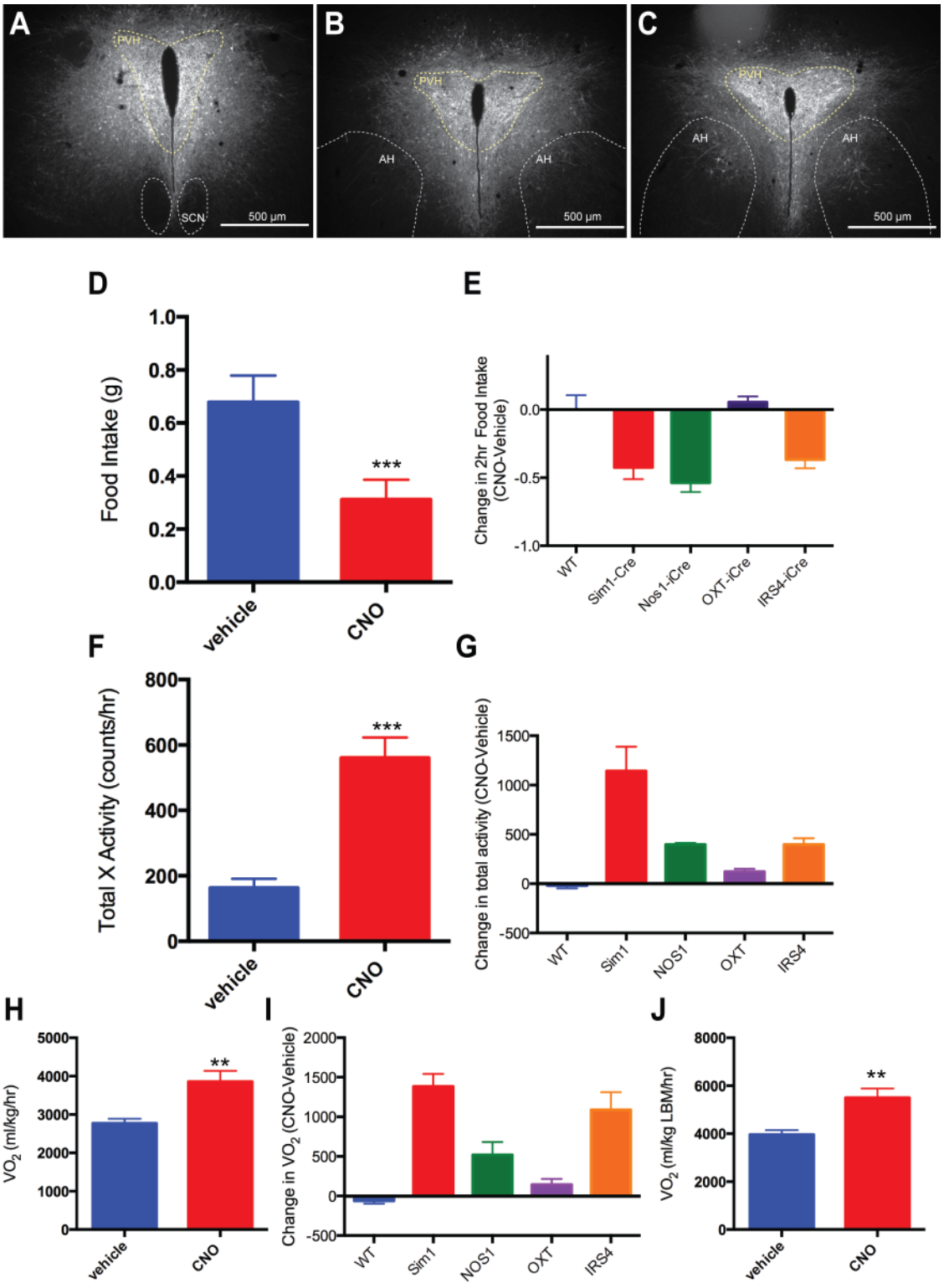
A
PVH
SCN
500 µm
B
PVH
AH
AH
500 µm
C
PVH
AH
AH
500 µm
D
Food Intake (g)
1.0
0.8
0.6
0.4
0.2
0.0
***
vehicle
CNO
E
Change in 2hr Food Intake (CNO-Vehicle)
0.0
-0.5
-1.0
WT
Sim1-Cre
Nos1-iCre
OXT-iCre
IRS4-iCre
F
Total X Activity (counts/hr)
800
600
400
200
0
***
vehicle
CNO
G
Change in total activity (CNO-Vehicle)
1500
1000
500
0
-500
WT
Sim1
NOS1
OXT
IRS4
H
VO2 (ml/kg/hr)
5000
4000
3000
2000
1000
0
**
vehicle
CNO
I
Change in VO2 (CNO-Vehicle)
2000
1500
1000
500
0
-500
WT
Sim1
NOS1
OXT
IRS4
J
VO2 (ml/kg LBM/hr)
8000
6000
4000
2000
0
**
vehicle
CNO

Figure 3.6. Acute activation of IRS4^{PVH} neurons decreases feeding and increases energy expenditure. A-C) IHC for mCherry identifies AAV-hM3Dq expression in IRS4^{PVH} neurons throughout the PVH (yellow dotted line). D) Two-hour food intake was decreased at the onset of dark cycle feeding due to activation of IRS4^{PVH} neurons following an i.p. injection of CNO in comparison to vehicle. E) CNO-induced two-hour feeding suppression was compared across different PVH cell types (WT, Sim1, Nos1 and OXT data obtained from chapter II), suggesting the possibility that food suppression driven by IRS4^{PVH} neuronal activation is comparable to suppression obtained from activating the entire PVH with Sim1^{PVH} neurons. F) Activation of IRS4^{PVH} neurons increases total activity and oxygen consumption (H, J) over a four-hour time period in the absence of food. I) Similar comparisons to previously studied PVH populations suggests that IRS4^{PVH} neuronal activation potentially increases oxygen consumption more than that obtained upon Nos1^{PVH} or OXT^{PVH} neuronal activation, without changing total activity to the same degree as Sim1^{PVH} neurons (G). Average values ± SEM are shown, **p<0.01, ***p<0.001, compared to vehicle values. AH=anterior hypothalamus, SCN=suprachiasmatic nucleus, PVH=paraventricular nucleus of the hypothalamus

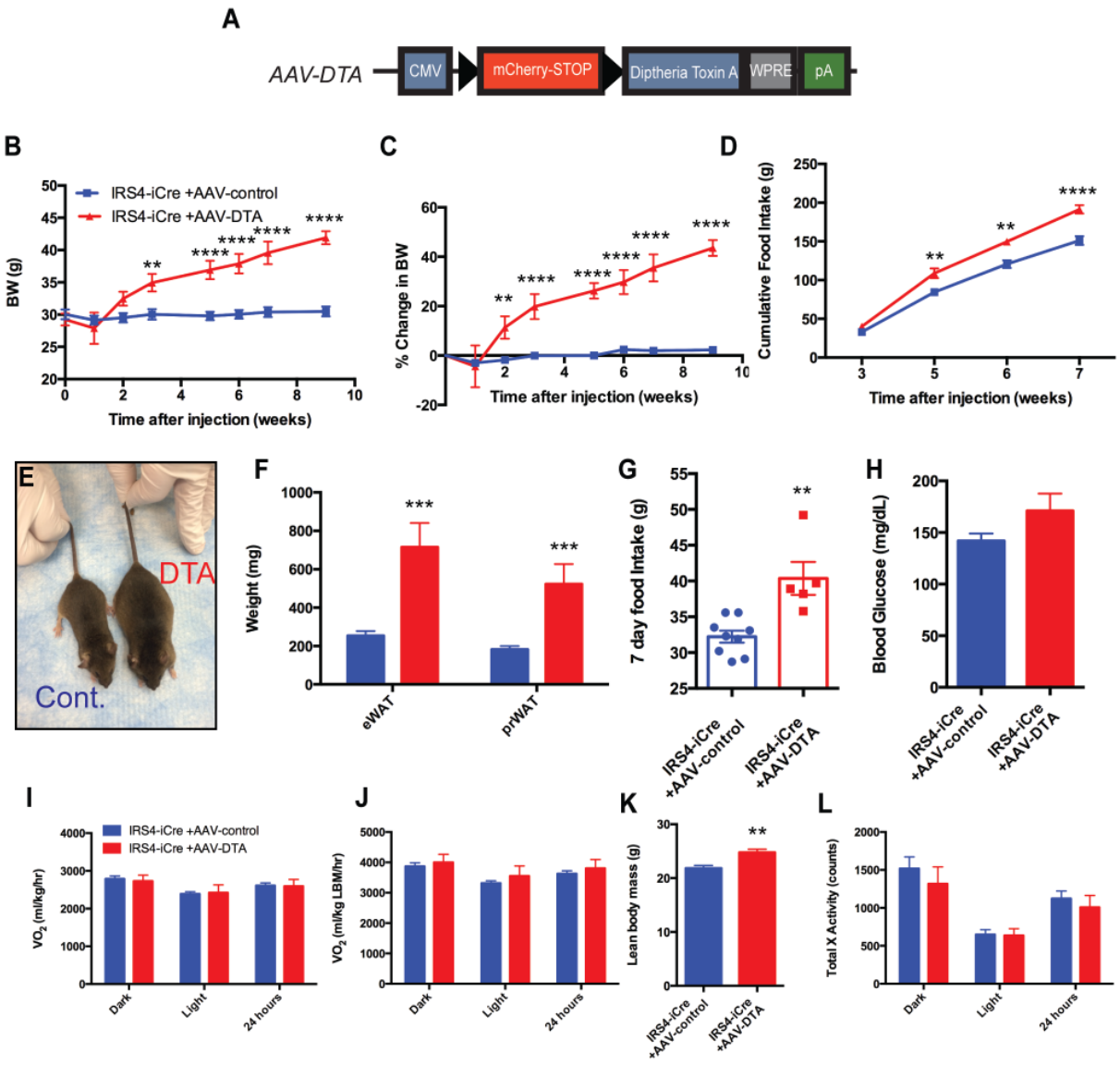
A
AAV-DTA
CMV
mCherry-STOP
Diptheria Toxin A
WPRE
pA
B
IRS4-iCre +AAV-control
IRS4-iCre +AAV-DTA
BW (g)
Time after injection (weeks)
C
% Change in BW
Time after injection (weeks)
D
Cumulative Food Intake (g)
Time after injection (weeks)
E
DTA
Cont.
F
Weight (mg)
eWAT
prWAT
G
7 day food Intake (g)
IRS4-iCre +AAV-control
IRS4-iCre +AAV-DTA
H
Blood Glucose (mg/dL)
IRS4-iCre +AAV-control
IRS4-iCre +AAV-DTA
I
IRS4-iCre +AAV-control
IRS4-iCre +AAV-DTA
VO2 (ml/kg/hr)
Dark
Light
24 hours
J
VO2 (ml/kg LBM/hr)
Dark
Light
24 hours
K
Lean body mass (g)
IRS4-iCre +AAV-control
IRS4-iCre +AAV-DTA
L
Total X Activity (counts)
Dark
Light
24 hours

Figure 3.7. IRS4^{PVH} neurons are necessary for normal feeding and bodyweight. A) A Cre-dependent adeno-associated virus expresses diphtheria toxin A exclusively in Cre-expressing neurons, resulting in Cre-dependent neuronal ablation. B, C) IRS4^{PVH} neuronal ablation in *IRS4-iCre +AAV-DTA* mice results in increased bodyweight in comparison to *IRS4-iCre* mice injected with a control AAV. D) *IRS4-iCre* mice show increased cumulative food intake following IRS4^{PVH} neuronal ablation in comparison to controls. E) *IRS4-iCre* littermate mice injected with either AAV-control (left) or AAV-DTA (right) at 9 weeks post-injection demonstrate the profound obesity resulting from IRS4^{PVH} neuronal ablation, with corresponding increases in epididymal and perirenal fat pad weights (F). G) Prior to the onset of significant obesity (days 14-21), cumulative 7-day food intake (G) and fasted blood glucose (H) was higher in *IRS4-iCre +AAV-DTA* mice in comparison to controls. I-L) Oxygen consumption and total X activity was unchanged due to IRS4^{PVH} neuronal ablation (I, J, L) measured 25-28 days post-injection, while lean body mass was slightly increased in *IRS4-iCre +AAV-DTA* mice (K). Average values ± SEM are shown, **p<0.01, ***p<0.001, ****p<0.0001 compared to AAV-control values (DTA: B-C n=5; D n=4; F, I-L n=3; G n=5; AAV-control: B-D, G n=9; F, H n=8; I-L n=7). Significance was measured using a two-way ANOVA followed by Sidak's multiple comparisons test if necessary (B-D, I, K, L) or an unpaired t-test (F-H, K).

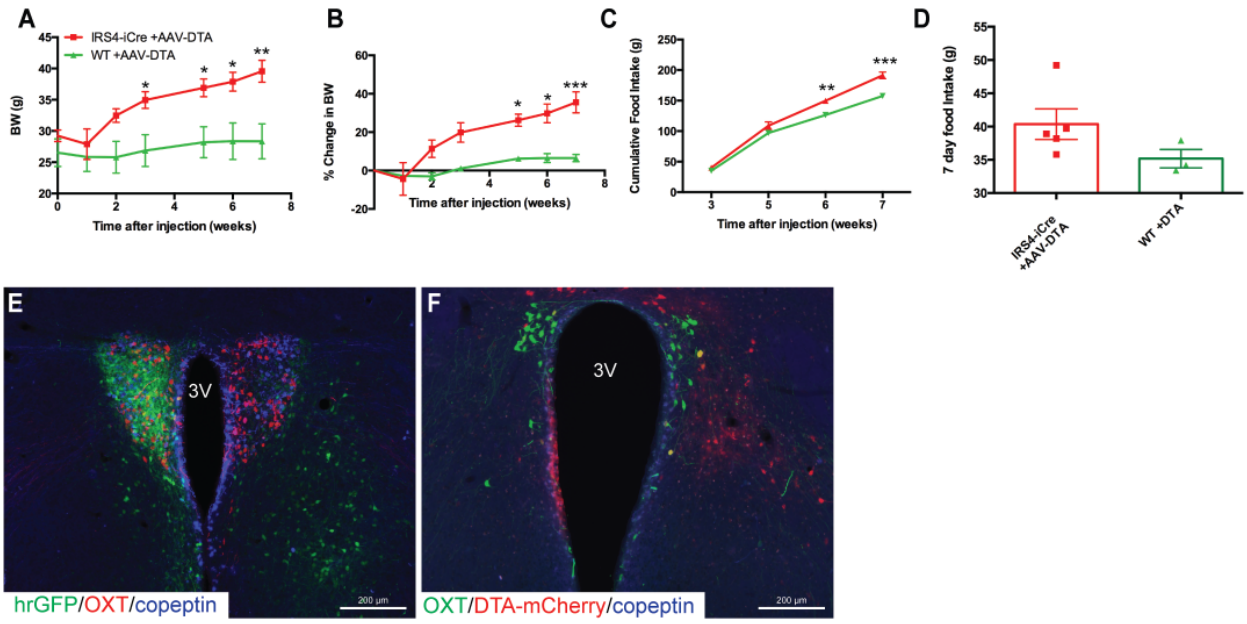
A
IRS4-iCre +AAV-DTA
WT +AAV-DTA
BW (g)
Time after injection (weeks)
B
% Change in BW
Time after injection (weeks)
C
Cumulative Food Intake (g)
Time after injection (weeks)
D
7 day food Intake (g)
IRS4-iCre +AAV-DTA
WT +DTA
E
3V
hrGFP/OXT/copeptin
F
3V
OXT/DTA-mCherry/copeptin

Figure 3.8. PVH-directed injection of AAV-DTA virus in wildtype (*WT*) mice does not cause obesity. A-C) *WT* mice injected with the Cre-dependent AAV-DTA virus (green) do not show changes in bodyweight or food intake (C) in comparison to *IRS4-iCre +AAV-DTA* mice (red). D) 7-day food intake is not elevated in *WT* mice injected with AAV-DTA during 14-21 days post-injection. E) IHC in *IRS4-iCre* mice injected with a Cre-dependent control virus expresses hrGFP in $IRS4^{PVH}$ cells (green) and demonstrates appropriate expression of non-$IRS4^{PVH}$ cells including oxytocin (OXT, red) and copeptin (blue). F) In contrast, IHC in brains from *IRS4-iCre +AAV-DTA* mice display altered PVH architecture with an enlarged third ventricle (3V) and decreased expression of OXT (green) and copeptin (blue). Average values ± SEM are shown, *p<0.05, **p<0.01, ***p<0.001 (*IRS4-iCre*: A-B,D n=5, C n=4; *WT* n=3). Significance was measured using a paired t-test (D, F, H, J) or a two-way ANOVA followed by Sidak's multiple comparisons test (A-C) or an unpaired t-test (D).

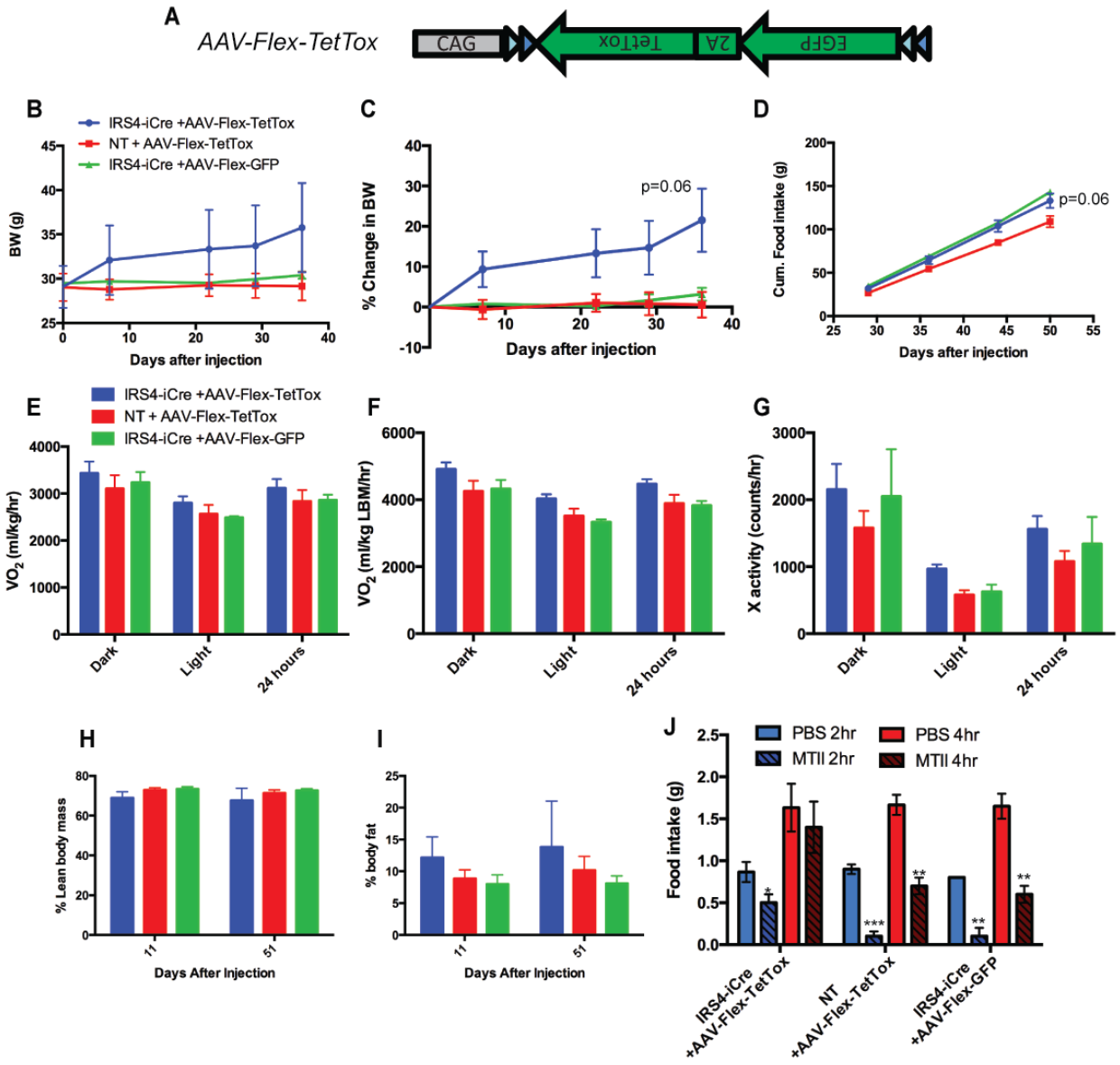
A
AAV-Flex-TetTox
CAG
TetTox
2A
EGFP
B
IRS4-iCre +AAV-Flex-TetTox
NT + AAV-Flex-TetTox
IRS4-iCre +AAV-Flex-GFP
BW (g)
Days after injection
C
% Change in BW
p=0.06
Days after injection
D
Cum. Food intake (g)
p=0.06
Days after injection
E
IRS4-iCre +AAV-Flex-TetTox
NT + AAV-Flex-TetTox
IRS4-iCre +AAV-Flex-GFP
VO2 (ml/kg/hr)
Dark
Light
24 hours
F
VO2 (ml/kg LBM/hr)
Dark
Light
24 hours
G
X activity (counts/hr)
Dark
Light
24 hours
H
% Lean body mass
Days After Injection
I
% body fat
Days After Injection
J
PBS 2hr
PBS 4hr
MTII 2hr
MTII 4hr
Food intake (g)
IRS4-iCre +AAV-Flex-TetTox
NT +AAV-Flex-TetTox
IRS4-iCre +AAV-Flex-GFP

Figure 3.9. IRS4^{PVH} neuronal silencing results in hyperphagic obesity. A) A Cre-dependent tetanus toxin virus (AAV-Flex-TetTox) causes inhibition of synaptic exocytosis in Cre-expressing cells. B-D) IRS4^{PVH} neuronal silencing results in robust obesity due to increased cumulative food intake in comparison to nontransgenic mice injected with AAV-Flex-TetTox (*NT +AAV-Flex-TetTox*) or *IRS4-iCre* mice injected with a control AAV-Flex-GFP virus. E-I) No changes are observed in *IRS4-iCre +AAV-Flex-TetTox* mice in comparison to controls in energy expenditure measurements including oxygen consumption, total X activity, or body composition measured 11 or 51 (body composition only) days after injection. J) While two and four hour dark-cycle food intake is decreased in response to i.p. injection of the melanocortin receptor agonist melanotan II (MTII, 150 ug/mouse) in control mice, this response is diminished in *IRS4-iCre +AAV-Flex-TetTox* mice. Average values ± SEM are shown, **p<0.01, ***p<0.001, ****p<0.0001 (*IRS4-iCre +AAV-Flex-TetTox* D-I: n=4, J-L: n=3; *NT +AAV-Flex-TetTox* D-I: n=4, J-L:n=3; *IRS4-iCre +Flex-GFP* D-K: n=3, L: n=2). Significance was determined using a two-way ANOVA followed by Sidak's multiple comparisons test if necessary.

Chapter IV

Circuit analysis of defined PVH cell-types

Introduction

Neuronal networks in the central nervous system (CNS) have evolved to carry out complex behavioral responses in changing environments to achieve homeostasis and survival. A critical component of an organism's homeostasis is the ability to balance energy intake with energy expenditure. Although significant progress has been made in understanding the composition of neuronal subpopulations important in energy balance, interrogation of the circuits used by these neurons to communicate and ultimately control energy balance parameters largely remains undetermined. Indeed, GWAS studies have implicated the importance of CNS circuits in body weight regulation, since genetic loci controlling synaptic function are disproportionately associated with measures of body mass (1). This suggests the possibility that CNS circuits that were not evolutionarily designed in the presence of energy excess are currently under unusual pressure. Since recent societal changes in feeding behavior and energy expenditure (and therefore, arguably, not genetics) have resulted in a dramatic increase in the obesity prevalence, it is pressing to understand the basic neuroanatomy of the CNS circuits primarily controlling negative energy balance.

The paraventricular nucleus of the hypothalamus (PVH) is the primary hypothalamic output controlling both energy expenditure and feeding (2, 3).

PVH-regulated feeding is in large part driven by inputs from the arcuate nucleus of the hypothalamus (ARC), including the ARC populations producing either agouti related peptide (AgRP) or proopiomelanocortin (POMC) (4-6). AgRP neurons drive feeding behavior through release of the Mc4R-antagonist AgRP at projection sites (7-10). On the other hand, anorexigenic POMC neurons produce and release melanocortins, including α-MSH, that bind melanocortin 4 receptors (Mc4R) in downstream target neurons (11, 12). Mc4R-expressing neurons in the PVH are the one of the main downstream effectors mediating melanocortin-induced satiety (13-15). While the ARC-PVH circuit is the most appreciated in the hypothalamic control of feeding behavior, projections from numerous other hypothalamic sites that sense and control energy status converge on the PVH. These sites include the lateral hypothalamic area (LHA), the ventromedial hypothalamus (VMH), and the dorsomedial hypothalamus (DMH) (16). The PVH integrates these afferent signals and suppresses feeding through projections to hindbrain regions that sense gastrointestinal-derived hormonal signals and neural signals arising from mechanical stretching of the gut (2, 17). Specifically, the hindbrain sites receiving dense PVH innervation include the parabrachial nucleus (PBN), nucleus of the solitary tract (NTS), area postrema (AP) and dorsal motor nucleus of the vagus (DMV) (18-20). Moreover, studies have also identified PVH projections to thoracic spinal cord regions, specifically in the intermediolateral column (IML), suggesting a PVH-IML circuit that may control sympathetic outflow and therefore energy expenditure (Chapter II, Chapter III) (19, 20).

For over a century, neuroanatomical approaches have been used to determine CNS connectivity with the assumption that connections between CNS sites provide

information about the function of different neuronal populations. Recent technical advances have made it possible to map complex circuits involving genetically-identified populations using modified rabies virus techniques in combination with mouse models expressing Cre recombinase in defined cell populations (21, 22). Here, we use modified rabies virus approaches to identify and characterize monosynaptic inputs to genetically-defined PVH subpopulations in order to delineate a PVH circuit that regulates feeding and energy expenditure. To this end, we combine projection-specific modified rabies virus injections in multiple Cre-expressing mouse models to identify inputs to PBN-projecting, NTS-projecting, or IML-projecting PVH subsets. We find that PVH cell groups are highly interconnected; populations expressing neuronal nitric oxide synthase 1 (Nos1) and oxytocin (OXT) both receive dense innervation from other PVH neurons, thereby raising the possibility that parvocellular PVH subsets that project to disparate hindbrain and spinal cord sites are likely functioning as an interconnected PVH network to achieve negative energy balance.

Materials and Methods

Experimental Animals

Sim1-Cre, Nos1-iCre, and OXT-iCre mice were generated as previously described (14, 23, 24)). Adult male mice (8-12 weeks old) were used for all studies. *OXT-iCre* mice that were bred to a Cre-dependent TdTomato reporter line (Ai9, Jackson Labs, 007909) were used to fluorescently label Cre-expressing OXT neurons. All animals were bred and housed within our colony according to guidelines approved by the University of

Michigan Committee on the Care and Use of Animals. All mice were provided *ad libitum* access to food and water and single housed after stereotaxic injection.

Viral preparations

A modified AAV-Flex-TVA-B19G construct was generated due to limited efficacy with previously used helper virus reagents. Specifically, limited rabies virus transduction was observed following co-injection of commercially available AAV-Flex-TVA-mCherry and AAV-Flex-B19G viruses, suggesting that co-infection of both helper viruses in a single cell may be inefficient. Furthermore, the previously generated AAV-Flex-TVA-B19G-GFP construct displayed both weak GFP expression and poor rabies virus efficiency, possibly due to packaging such a large construct into an AAV (25). To remedy this, TVA-B19G was PCR amplified from the pAAV-EF1-TVA-B19G-GFP plasmid (Addgene #26197) and subcloned into a TOPO cloning vector. SpeI and SacI restriction sites were then used to insert the product into the pAAV-hSyn-Flex vector. EnvA-ΔG-mCherry (rabies-mCherry), and EnvA-ΔG-GFP (rabies-GFP) were generated as previously described (Chapter III) (21).

Stereotaxic injections

Stereotaxic injections were performed in *Sim1-Cre*, *Nos1-iCre*, and *OXT-iCre* mice as previously described (Chapter II). Briefly, mice were placed in a digital stereotaxic frame (Model 1900, Kopf Instruments) under isofluorane and provided with pre-surgical analgesia. Viral injections were performed using a pressurized picospritzer system coupled to a pulled glass micropipette. For all experiments (excluding those using

cannulas), 40-50 nl of AAV-Flex-TVA-B19G was unilaterally injected in the PVH (coordinates from bregma: A/P= -.500, M/L= +/- .220, D/V= -4.800). Following three weeks recovery, rabies-mCherry and rabies-GFP were injected in projection sites including the PBN (100 nl, A/P= A/P=-4.770, M/L=+/- 1.35, D/V=-2.8), NTS, and IML. NTS injections were performed as previously described, whereby the fourth ventricle was identified and used as a geographic landmark to determine the site of injection (Chapter II). A glass micropipette was lowered into the site (D/V: -.550) and 50 nl of virus was injected. For injections into the IML, mice were placed in the stereotaxic frame without ear bars. Instead, ear bars were used to raise and stabilize the spinal cord at the level of ~T2-T6. Incisions were made through muscle layers to reveal vertebrae and spinal cord, and muscle held back using micro hemostatic forceps**.** T3-T4 was identified using the T2 vertebral spine and T3/T4 intervertebral disks and the glass pipette was lowered in between T3-T4 towards the midline of the spinal cord (D/V=-.600), where 100 nl of rabies-mCherry virus was injected. Two minutes after the injection was completed, the glass pipette was raised and sutures used to close the wound. Ipsilateral PBN and NTS modified rabies virus injections were performed in relation to helper virus injection, whereas IML injections were performed on the contralateral side due to neuronal decussation.

For studies in which rabies-mCherry was injected into the PVH, cannulas were used to ensure identical PVH hit sites for both viral injections (AAV-Flex-TVA-B19G and rabies-mCherry). For these experiments, *Sim1-Cre* or *OXT-iCre* mice were placed in the stereotaxic frame and the skull drilled at the same PVH coordinates used throughout other experiments. A 4.3mm long guide cannula (Plastics One) was lowered into the

brain and secured using dental cement. Once dental cement had hardened and the cannula was secure (~5 minutes), 200nl of AAV-Flex-TVA-B19G was administered using a Hamilton syringe coupled to tubing and an internal cannula with a 0.5mm overhang (total length=4.8mm). Two minutes following helper virus injection, the internal cannula was removed and a dummy cannula placed in the guide cannula for recovery. Following a three week recovery, dummy cannulas were removed and 75-200 nl of rabies-mCherry injected into the PVH using an internal cannula. Two minutes after virus injection, the internal cannula was removed and dummy cannula replaced until perfusion. For visualization of CRF^{PVH} neurons, colchichine (10 ug, 40 ug/ul) was administered directly to the PVH through the same cannula 36 hours prior to perfusion. Cannula hit sites were histologically verified at the completion of the experiment.

Perfusion and immunohistochemistry (IHC)

For all studies, mice were perfused 7 days following rabies virus injection as previously described to verify viral hit sites for both AAV-Flex-TVA-B19G and rabies-mCherry/rabies-GFP. Briefly, mice were deeply anesthetized with an overdose of pentobarbital (150 mg/kg, IP) and transcardially perfused with PBS followed by 10% neutral buffered formalin. Brains and spinal cords (for IML injections only) were removed, post-fixed, and dehydrated in 30% sucrose before sectioning into 30 µm slices on a freezing microtome (Leica). Coronal brain sections were collected in four representative sections whereas longitudinal thoracic spinal cord sections were collected in three representative sections and stored at -20°C. IHC for 2A peptide was performed to validate appropriate helper virus hit site (data not shown). In the event

that helper virus missed the PVH, data was excluded. mCherry and GFP were detected using with primary antibodies for dsRed (rabbit 1:1000, Clontech, 632496) and GFP (chicken 1:1000, Abcam, ab12970) respectively followed by secondary immunofluorescence (IF) detection with donkey anti-rabbit-Alexa 568 and donkey goat anti-chicken-Alexa 488 (1:200, Invitrogen). For colocalization experiments between rabies-mCherry and ARC POMC neurons, IHC immunostaining was performed using primary antibodies for ACTH (rabbit 1:1000, kindly provided by Dr. Malcolm Low, Parlow AFP-173P) and RFP (rat, 1:1000, Allele Biotechnology ACT-CM-MRRFP10), followed by secondary IF detection with donkey anti-rabbit-Alexa 488 and donkey anti-rat-Alexa 594 (1:200, Invitrogen). In experiments aimed at identifying PVH and SON populations upstream of OXT^{PVH} neurons, IHC was performed for RFP, OXT (rabbit, 1:1500, Bachem, T-4084), copeptin (goat 1:1000, Santa Cruz Biotechnology, sc-7812), neurophysin (goat, 1:1000, Santa Cruz Biotechnology, sc-7810), and CRF (rabbit, 1:1000, Bachem, T-4037) followed by corresponding secondary antibodies (donkey anti-rat-Alexa 594, donkey anti-goat-Alexa 350, and donkey anti-rabbit-Alexa 488 (all 1:200, Invitrogen)). Imaging was performed using an Olympus BX-51 upright microscope with DP30BW camera (Olympus, Figures 4.1C-J, 4.6D, 4.7), Nikon 90i upright microscope (Nikon) with CoolSNAP HQ2 CD camera (Photometrics, Figures 4.1K-N, 4.6), or an Olympus BX-53 upright microscope (Olympus) with G6000 camera (Q imaging, Figures 4.2-5).

Results

Modified rabies virus identifies inputs to $Sim1^{PVH}$ neurons

Using a variety of non cell-type specific retrograde viral tracing reagents, previous reports suggest broad inputs to the PVH from hypothalamic structures including the ARC, DMH, and LHA, as well as both forebrain (POA, BNST) and hindbrain (NTS, RVLM) sites (16, 26-31). In order to validate the viral technologies modified for this study, we aimed to map neuronal inputs to all PVH neurons using the *Sim1-Cre* mouse model in combination with modified rabies virus reagents. To this end, a Cre-dependent "helper virus" (AAV-Flex-TVA-B19G, Figure 4.1A) was injected in the PVH of *Sim1-Cre* mice to express both the TVA receptor and the B19 glycoprotein (B19G) in all PVH neurons. Three weeks following helper virus injection, modified rabies virus (rabies-mCherry) was injected in the PVH. Since the TVA receptor is required for modified rabies virus infection, rabies-mCherry expression is dependent on prior helper virus expression (Chapter III, Figure 3.5). Moreover, rabies-mCherry has been generated with mCherry expression instead of the native B19G, therefore requiring B19G expression from the helper virus for retrograde transmission (Figure 4.1B). Importantly, since helper virus injection is limited to the PVH, neurons upstream do not express B19G unless they: 1) are within the injection site and 2) produce Cre recombinase (21). Therefore, this approach allows for visualization of rabies-mCherry labeled monosynaptic inputs to $Sim1^{PVH}$ neurons. Indeed, rabies-mCherry expression is identified throughout the PVH, thereby tagging primary-infected PVH neurons (Figure 4.1C, 1D). Additionally, neurons of the supraoptic nucleus, classically thought to be entirely magnocellular, are labeled by rabies-mCherry, therefore identifying a direct SON-PVH circuit. Rabies-mCherry also identifies BNST and POA inputs to the PVH (Figure 4.1E, 1F), validating previous reports (28). Importantly, the well-defined ARC-

PVH circuit is also identified using this approach, since rabies-mCherry is expressed widely throughout the ARC (Figure 4.1G-J) (4). Additional hypothalamic structures innervating the PVH include the VMH, DMH, and LHA (Figure 4.1G-J). Lastly, to confirm the identity of the ARC neurons synaptically connected to the PVH, we performed IHC for adrenocorticotropic hormone (ACTH), a cleavage product of POMC. Indeed, rabies-mCherry colocalizes with some ACTH cells throughout the ARC, further confirming the specificity of the modified rabies virus technology in a classically defined circuit (Figure 4.1K-N).

Terminal-restricted modified rabies virus injection identifies projection-specific circuits engaging the PVH

We hypothesized that PVH projection targets represent different subsets of PVH populations, and that afferent inputs to these populations will therefore be distinct. If so, this would imply divergent circuit control of different PVH outputs and therefore potentially identify regulators of distinct aspects of energy balance (feeding vs. energy expenditure). In order to determine this, we performed helper virus injection in the PVH of *Sim1-Cre* mice as before. Rather than re-injecting rabies virus injection in the PVH, rabies-mCherry was delivered to the NTS, a known projection target of the PVH. In the same mouse, a similar modified rabies virus expressing GFP (rabies-GFP) was injected in the PBN (Figure 4.2A). Since the TVA receptor can be expressed throughout axons and on terminals, both rabies-mCherry and rabies-GFP can infect $Sim1^{PVH}$ cells projecting to the NTS or PBN, respectively (30) (Chapter III). Using this method, $Sim1^{PVH}$ cells expressing rabies-GFP and rabies-mCherry are largely distinct (Figure

4.2B-2D). Since Nos1^{PVH} neurons comprise some, but not all (e.g. not including IRS4^{PVH}), of the PVH projections to hindbrain and spinal cord regions, we aimed to identify if some inputs to projection-specific Nos1^{PVH} neurons were less than that observed with analysis of the entire PVH. Thus, the same experiment was performed in *Nos1-iCre mice*, with helper virus injection in the PVH (*Nos1-iCre +AAV-Flex-TVA-B19G*) followed by modified rabies virus injection in the PBN (rabies-GFP) or NTS (rabies-mCherry). Similarly, Nos1^{PVH} populations projecting to the NTS or PBN are largely non-overlapping since rabies-mCherry and rabies-GFP cells have minimal colocalization throughout the PVH (Figure 4.2E-G). Importantly, previous results indicate that both rabies-mCherry and rabies-GFP can enter and express in the same PVH cell, strongly suggesting that PVH circuits engaging the PBN or NTS are distinct with limited axonal collateralization (Chapter III, Figure 3.5). Since B19G is expressed in these PVH cells, rabies-mCherry and rabies-GFP can travel to neurons upstream and therefore identify monosynaptic inputs to NTS-projecting or PBN-projection PVH cells with rabies-mCherry or rabies-GFP visualization, respectively (Figure 4.3A). Surprisingly, inputs to NTS-projecting and PBN-projecting Sim1^{PVH} neurons are in similar nuclei, yet are different neuronal populations. Large numbers of rabies-mCherry and rabies-GFP cells are found in the BNST and POA (Figure 4.3B) as well as the SON (Figure 4.3D). Hypothalamic areas with neurons upstream of NTS-projecting PVH neurons include the ARC and DMH, in addition to fewer neurons in the VMH and LHA (Figure 4.3F). Rabies-GFP identifies inputs to PBN-projecting PVH neurons including the VMH, DMH, and some ARC neurons. Rabies-mCherry and rabies-GFP cells are also located, albeit in much smaller numbers, in midbrain regions including the

periaqueductal gray (PAG) and zona incerta (ZI) (Figure 4.3H). Injection sites can be visualized due to neuronal gliosis at the site of injection for rabies-GFP in the PBN (Figure 4.3J) and rabies-mCherry in the NTS (Figure 4.3L). Additionally, rabies-mCherry cells are expressed in the PBN, suggesting a PBN-PVH-NTS circuit (Figure 4.3J). In comparison to the regulation of the entire PVH, inputs to NTS-projecting or PBN-projecting $Nos1^{PVH}$ neurons are outstandingly similar. Gross analysis of sites upstream of the smaller $Nos1^{PVH}$ population indicates that inputs to projection-defined $Nos1^{PVH}$ populations are largely the same, but rabies-GFP and rabies-mCherry show little colocalization (Figure 4.3C, E, G, I, K, M).

Projection-specific modified rabies virus approach reveals strikingly similar circuits engaging distinct PVH populations

While results obtained from dual rabies virus injection in disparate projection sites identified distinct circuits regulating PVH populations, rabies-GFP routinely identified fewer neurons than rabies-mCherry. Although previous control results demonstrated that rabies-GFP and rabies-mCherry are capable of co-labeling PVH neurons, few populations upstream co-labeled rabies-mCherry and rabies-GFP (Chapter III, Figure 3.5). This highlights the possibility of different viral efficiencies between preparations of rabies-mCherry and rabies-GFP, with underreporting of neural populations labeled with GFP. For this reason, rabies-mCherry alone was injected in *Sim1-Cre +AAV-Flex-TVA-B19G* mice in different projection sites and results compared (Figure 4.4A-C). Surprisingly, extensive rabies-mCherry expression is observed in the PVH, appearing to label almost all PVH neurons, despite different rabies-mCherry injection sites (Figure

4.4G-I). Additionally, rabies-mCherry identifies similar populations upstream of $Sim1^{PVH}$ neurons projecting to the NTS, PBN, or IML. Dense rabies-mCherry neuronal labeling is identified in the BNST and POA throughout all groups (Figure 4.4D-F). Correspondingly, hypothalamic sites including the SON (Figure 4.4G-I), ARC, DMH, and VMH are all upstream of NTS-projecting, PBN-projecting, and IML-projecting $Sim1^{PVH}$ neurons (Figure 4.4J-L). While rabies-mCherry identifies that the PBN is upstream of NTS-projecting and IML-projecting neurons (Figure 4.4M-O), few NTS neurons express rabies-mCherry (Figure 4.4P-R).

Since $Sim1^{PVH}$ neurons comprise the entire PVH, we sought to characterize inputs to $Nos1^{PVH}$ neurons, a smaller population still capable of controlling both feeding and energy expenditure. Thus, rabies-mCherry injection was performed in the NTS, PBN, or IML of *Nos1-iCre +AAV-Flex-TVA-B19G* mice (Figure 4.5A-C). Sites throughout the CNS were largely similar to $Sim1^{PVH}$ results, with BNST and POA forebrain regions upstream of all $Nos1^{PVH}$ populations (Figure 4.5D-F). Once again, rabies-mCherry expression in the PVH seemingly marked almost all PVH neurons, in addition to the SON (Figure 4.5G-I). Hypothalamic regulation of $Nos1^{PVH}$ populations originates from the same sites as when studying the entire PVH, with rabies-mCherry expression in the ARC, DMH, LHA and VMH (Figure 4.5J-L). While the PBN is upstream of NTS-projecting $Nos1^{PVH}$ neurons, rabies-mCherry is not identified in the PBN of *Nos1-iCre +AAV-Flex-TVA-B19G* mice injected with rabies-mCherry in the IML, suggesting a potential disparity between hindbrain inputs to IML-projecting $Nos1^{PVH}$ neurons from the entire IML-projecting $Sim1^{PVH}$ neuronal population (Figure 4.5M-O). While neuronal gliosis identifies the rabies-mCherry injection site in experiments aimed

to label Nos1^{PVH} inputs to the NTS, few rabies-mCherry neurons are identified upstream of projection-specific PVH neurons (Figure 4.5P-R).

Monosynaptic inputs to OXT^{PVH} neurons arise primarily from other PVH neuronal populations

As noted previously, communication among Cre^{+} PVH populations can confound results, highlighting the problem of using modified rabies virus techniques in sites with local, intranuclear connections in combination with densely expressed, and therefore less distinct, neuronal populations. Therefore, we hypothesized that further limiting the PVH population under investigation could simplify the circuitry of PVH populations and better highlight inputs to defined PVH subpopulations. Thus, we aimed to characterize neuronal inputs to OXT^{PVH} neurons, a small subset of the Nos1^{PVH} field. Therefore, we performed helper virus injection in the PVH of *OXT-iCre* mice (*OXT-iCre +AAV-TVA-B19G*), followed by rabies-mCherry injection in the same site three weeks later (Figure 4.6A). Rabies-mCherry identified numerous PVH neurons directly upstream of the OXT^{PVH} neuronal population, with many rabies-mCherry cells in the PVH not co-labeling OXT peptide (Figure 4.6B). Since the PVH is a heterogenous structure consisting of many different, largely nonoverlapping, neuropeptide populations, we aimed to test if some of the PVH inputs to OXT^{PVH} neurons include vasopressin (AVP) neurons in the PVH (26). Certainly, many rabies-mCherry neurons co-express OXT, indicating primary infected OXT^{PVH} neurons (white arrows, Figure 4.6B-C). In addition, some non-OXT rabies-mCherry neurons also express copeptin, the carrier molecule for AVP (yellow arrows, Figure 4.6B, C), suggesting direct AVP^{PVH} innervation of OXT^{PVH} neurons.

Although few rabies-mCherry neurons are identified outside of the PVH, the SON is the primary extra-PVH site with rabies-mCherry localization (Figure 4.6D). The SON is comprised entirely of AVP and OXT neurons that are critical in regulating peripheral circulating levels of AVP and OXT via the posterior pituitary. Rabies-mCherry localization appears to be in the vicinity of AVP^{SON} neurons, though co-labeling is hard to identify due to copeptin localization primary in axons rather than cell bodies (Figure 4.6E-G). While few rabies-mCherry neurons are identified in OXT^{SON} vicinity, at least one rabies-mCherry neuron co-labels OXT (Figure 4.6F). This highlights the potential for AVP^{SON}, and minimal OXT^{SON}, innervation and regulation of OXT^{PVH} neurons.

To further characterize the intra-PVH circuitry engaging OXT^{PVH} neurons, the same rabies virus procedure was performed in *OXT-iCre +AAV-Flex-TVA-B19G* mice in addition to PVH-directed treatment of colchicine 36 hours prior to perfusion in order to identify neurons expressing corticotropin-releasing factor (CRF). CRF is rapidly trafficked to terminals, therefore requiring colchicine, a peptide transport inhibitor, for cell-body visualization (32). Indeed, rabies-mCherry colocalizes with CRF^{PVH} neurons (white arrows, Figure 4.6H). Rabies-mCherry colocalization with OXT^{PVH} neurons (blue) identifies primary infected neurons (yellow arrows), which are separate from CRF^{PVH} neurons (green), indicating that some CRF^{PVH} neurons are directly upstream of OXT^{PVH} neurons.

OXT^{PVH} projections to the NTS were previously thought to be a component of the ARC-PVH-NTS circuit, though recent studies suggest that OXT peptide expression in the NTS are fibers of passage (Chapter II)(19). Still, we aimed to test this circuit using modified rabies virus techniques. *OXT-iCre* mice were crossed to a Cre-dependent

TdTomato reporter (*OXT-iCre, Td*) to visualize all OXT^{PVH} cells and reduce the possibility of decreased OXT peptide expression as a result of rabies expression in cells. *OXT-iCre, Td* mice were injected with helper virus in the PVH followed by rabies-GFP injection in the NTS three weeks later (Figure 4.7A). Certainly, some OXT^{PVH} neurons co-express rabies-GFP, therefore identifying primary NTS inputs or fibers of passage (white arrows, Figure 4.7B, 7C). Similar to results obtained with both helper and rabies viruses injected directly into the PVH, there are many non-OXT rabies-GFP PVH cells, likely identifying inputs to OXT^{PVH} neurons with axonal projections in the NTS. However, few rabies-GFP cells are identified outside of the PVH (Figure 4.7D-F). This is in stark contrast to the densely labeled CNS inputs to NTS-projecting $Nos1^{PVH}$ or $Sim1^{PVH}$ neurons, suggesting the capability for PVH circuit dissection using these approaches.

Discussion

Although significant advances have been made in the understanding of the PVH's role in controlling energy balance, far less is understood about the afferent control of PVH populations projecting to hindbrain and spinal cord regions. Certainly, the ARC-PVH circuit has been a primary area of research, since ARC POMC and AgRP neurons clearly control feeding primarily through the PVH (8, 9, 14, 30, 33). Previously, it was hypothesized that the ARC-PVH-NTS circuit was the primary hypothalamic regulator of satiety (34). However, recent advances using optogenetic techniques suggest that $Mc4R^{PVH}$ connections to the PBN control feeding suppression (9). Yet, there is a large gap in the understanding of how distinct circuits engage different PVH

populations that are ultimately connected to the PBN, NTS, or IML. Using recent advancements in genetic mouse models and neuroscience technologies, our studies begin to answer some of these questions and demonstrate the complexity of inputs to genetically-defined PVH circuits. We demonstrate that PVH populations are highly interconnected, highlighting the potential for a large-scale PVH network in the regulation of different PVH projection sites.

Until recently, reagents used for retrograde tracing were not dependent on Cre recombinase and therefore did not have the ability to map inputs to cell-type specific PVH populations. More recently, modified rabies virus approaches have been generated to accomplish this task (21, 22). Using a novel Cre-dependent helper virus capable of co-expressing both the rabies glycoprotein and TVA receptor in Cre-expressing cells, we characterized inputs to $Sim1^{PVH}$ neurons. We demonstrate that inputs to PVH neurons are largely similar to results obtained with other approaches, including the canonical $POMC^{ARC}$-PVH circuit (4, 30). Next, we aimed to determine which sites specifically engage centrally-projecting parvocellular PVH circuits. While results from dual rabies virus injection in the same mouse suggest distinct circuit regulation of NTS-projecting PVH populations in comparison to PBN-projecting PVH neurons, technical limitations surrounding rabies virus efficacy limit our ability to make definitive statements about these results. Routinely, rabies-GFP injections in projection sites identified fewer GFP-labeled neurons than those expressing rabies-mCherry. Although rabies-mCherry and rabies-GFP can be co-expressed in the same neuron, it is possible that rabies-mCherry is more efficient than rabies-GFP. Previous control studies indicate that while both rabies-GFP and rabies-mCherry can co-express in some

cells, the ability of cells upstream of the primary infection to express both viruses seems impaired (Chapter III). Taken together, it is apparent that dual rabies virus approaches in the same mouse are limited in scope.

Using a single rabies virus approach, monosynaptic inputs to projection-specific PVH populations were strikingly similar. Moreover, despite different injection sites, it was apparent that rabies-mCherry routinely illuminated almost all PVH neurons. Therefore, it is likely that different Cre^+ PVH populations were not only synapsing in distinct hindbrain sites, but also communicating with one another in a complex intra-PVH network. In this scenario, since helper virus expresses in all Cre^+ neurons in the PVH, B19G is expressed in local PVH Cre^+ neurons. Therefore, rabies-mCherry labels CNS sites not only upstream of Cre^+ neurons projecting to a distinct site but also all inputs to local, synaptically connected, Cre^+ PVH neurons (Figure 4.4S). Depending on the level of PVH interconnectivity, this technique could essentially mark all inputs to the PVH despite projection-defined rabies-mCherry injection. Indeed, electrophysiologic data consistently suggests intra-PVH communication, since glutamatergic interneurons are sometimes required for changes in PVH electrical activity observed in response to a variety of receptor agonists (29, 35, 36). Additionally, dendrodentric synapses have been identified between thyrotropin releasing hormone (TRH) producing neurons in the PVH, though the ability of modified rabies virus to travel retrogradely through dendrodentric synapses is unknown (37).

Therefore, to both limit the primary Cre^+ population infected with rabies-mCherry and further characterize PVH interconnectivity, we performed similar rabies-mCherry experiments in the OXT^{PVH} population, a small subset of the $Nos1^{PVH}$ field. Once again,

dense intra-PVH labeling was observed upstream of OXT^{PVH} neurons, further supporting intra-PVH circuitry as the likely reason for similar extensive rabies-mCherry signaling in $Nos1^{PVH}$ and $Sim1^{PVH}$ rabies studies. Additionally, identification of direct input from AVP^{PVH} and CRH^{PVH} neurons onto the OXT^{PVH} population suggests a complex regulation of distinct PVH populations by adjacent neurons. With this in mind, it is intriguing to consider the close proximity of dissimilar PVH populations in the control of a variety of physiologic functions not only related to energy balance but also including blood pressure control, stress responses, and reproduction. The diverse nature of these functions are also highly interrelated; certainly these circuits should be connected at some level given the necessity of energy intake or sympathetic output for a variety of physiologic demands. Whether the PVH mediates the coordination of such behaviors by multifaceted intra-PVH networks is a fascinating possibility that will require further investigation.

OXT^{PVH} neurons have long been implicated in the control of feeding behavior, presumably through an ARC-OXT^{PVH}-NTS connection (34, 38). However, numerous studies to date have questioned the ability for OXT^{PVH} neurons to directly control feeding behavior (9, 15). Our studies further prove that ARC populations are not synaptically connected to OXT^{PVH} neurons, both through identifying inputs to the entire OXT^{PVH} neuronal population as well as “NTS-projecting” OXT^{PVH} neurons. Since there are few, if any, OXT^{PVH} terminals in the NTS, it is likely that rabies-GFP labeled OXT^{PVH} neurons are marked by TVA-expressing fibers of passage headed through the NTS towards the spinal cord (Chapter II, Figure 2.4). Taken together, it is clear that OXT^{PVH} neurons primarily receive innervation from local PVH circuits and the SON, and not the

ARC or other hypothalamic structures. Although the significance of this novel SON input to the PVH is unknown, the similar neuropeptide populations in the SON and PVH implicate this connection in the coordinated control of peptide release in the neurohypophysis and corresponding endocrine regulation. Previous results also indicate that the SON is upstream of other non-OXT PVH populations (e.g. IRS4), therefore suggesting the possibility for SON regulation of parvocellular PVH function in the control of energy balance parameters, though this remains to be determined (Chapter III).

Overall, here we provide a novel anatomical framework for understanding the regulation of PVH subsets by sites throughout the hypothalamus, forebrain, and brainstem. It is clear that dense interconnectivity occurs at the level of the PVH, and that these intra-PVH networks have the potential to regulate PVH outputs at diverse brainstem and spinal cord projection targets. As the primary hypothalamic output, the PVH is well situated to coordinate a multitude of different responses in order to achieve homeostasis. While these studies highlight the potential ability of this node to respond and function as an organized structure, further studies are needed to test the significance of this interaction. Furthermore, while the regulation of the smaller OXT^{PVH} population was identified using these techniques, troubleshooting with modified rabies virus approaches will need to be performed in future experiments to address interconnected PVH networks, potentially through identifying smaller genetic PVH populations with limited overlap. Ultimately, these approaches have the potential to identify novel circuits capable of regulating discrete energy balance parameters through

disparate projection targets, thereby providing useful targets for obesity and its comorbidities.

References

1. Locke AE, Kahali B, Berndt SI, Justice AE, Pers TH, et al. 2015. Genetic studies of body mass index yield new insights for obesity biology. *Nature*. 518(7538):197–206
2. Saper CB, Loewy AD, Swanson LW, Cowan WM. 1976. Direct hypothalamo-autonomic connections. *Brain Research*. 117(2):305–12
3. Schwartz MW, Woods SC, Porte D, Seeley RJ, Baskin DG. 2000. Central nervous system control of food intake. *Nature*. 404(6778):661–71
4. Cowley MA, Pronchuk N, Fan W, Dinulescu DM, Colmers WF, Cone RD. 1999. Integration of NPY, AGRP, and melanocortin signals in the hypothalamic paraventricular nucleus: evidence of a cellular basis for the adipostat. *Neuron*. 24(1):155–63
5. Broberger C, Johansen J, Johansson C, Schalling M, Hökfelt T. 1998. The neuropeptide Y/agouti gene-related protein (AGRP) brain circuitry in normal, anorectic, and monosodium glutamate-treated mice. *Proceedings of the National Academy of Sciences*. 95(25):15043–48
6. Wang D, He X, Zhao Z, Feng Q, Lin R, et al. 2015. Whole-brain mapping of the direct inputs and axonal projections of POMC and AgRP neurons. *Front Neuroanat*. 9:40
7. Lu D, Willard D, Patel IR, Kadwell S, Overton L, et al. 1994. Agouti protein is an antagonist of the melanocyte-stimulating-hormone receptor. *Nature*. 371(6500):799–802
8. Atasoy D, Betley JN, Su HH, Sternson SM. 2012. Deconstruction of a neural circuit for hunger. *Nature*. 488(7410):172–77
9. Garfield AS, Li C, Madara JC, Shah BP, Webber E, et al. 2015. A neural basis for melanocortin-4 receptor-regulated appetite. *Nat. Neurosci.* 18(6):863–71
10. Krashes MJ, Koda S, Ye C, Rogan SC, Adams AC, et al. 2011. Rapid, reversible activation of AgRP neurons drives feeding behavior in mice. *J. Clin. Invest.* 121(4):1424–28
11. Hruby VJ, Lu D, Sharma SD, Castrucci AL, Kesterson RA, et al. 1995. Cyclic lactam alpha-melanotropin analogues of Ac-Nle4-cyclo[Asp5, D-Phe7,Lys10] alpha-melanocyte-stimulating hormone-(4-10)-NH2 with bulky aromatic amino acids at position 7 show high antagonist potency and selectivity at specific melanocortin receptors. *J. Med. Chem.* 38(18):3454–61
12. Cheung CC, Clifton DK, Steiner RA. 1997. Proopiomelanocortin neurons are direct targets for leptin in the hypothalamus. *Endocrinology*. 138(10):4489–92
13. Xu Y, Wu Z, Sun H, Zhu Y, Kim ER, et al. 2013. Glutamate mediates the function of melanocortin receptor 4 on sim1 neurons in body weight regulation. *Cell Metab.* 18(6):860–70
14. Balthasar N, Dalgaard LT, Lee CE, Yu J, Funahashi H, et al. 2005. Divergence of melanocortin pathways in the control of food intake and energy expenditure. *Cell*. 123(3):493–505
15. Shah BP, Vong L, Olson DP, Koda S, Krashes MJ, et al. 2014. MC4R-expressing glutamatergic neurons in the paraventricular hypothalamus regulate feeding and are synaptically connected to the parabrachial nucleus. *Proc. Natl. Acad. Sci.*

U.S.A. 111(36):13193–98
16. Sawchenko PE, Swanson LW. 1983. The organization and biochemical specificity of afferent projections to the paraventricular and supraoptic nuclei. *Prog. Brain Res.* 60:19–29
17. Grill HJ, Hayes MR. 2012. Hindbrain neurons as an essential hub in the neuroanatomically distributed control of energy balance. *Cell Metab.* 16(3):296–309
18. Tokita K, Inoue T, Boughter JD. 2009. Afferent connections of the parabrachial nucleus in C57BL/6J mice. *Neuroscience*. 161(2):475–88
19. Biag J, Huang Y, Gou L, Hintiryan H, Askarinam A, et al. 2012. Cyto- and chemoarchitecture of the hypothalamic paraventricular nucleus in the C57BL/6J male mouse: a study of immunostaining and multiple fluorescent tract tracing. *J. Comp. Neurol.* 520(1):6–33
20. Sawchenko PE, Swanson LW. 1982. Immunohistochemical identification of neurons in the paraventricular nucleus of the hypothalamus that project to the medulla or to the spinal cord in the rat. *J. Comp. Neurol.* 205(3):260–72
21. Wickersham IR, Lyon DC, Barnard RJO, Mori T, Finke S, et al. 2007. Monosynaptic restriction of transsynaptic tracing from single, genetically targeted neurons. *Neuron*. 53(5):639–47
22. Wall NR, Wickersham IR, Cetin A, La Parra De M, Callaway EM. 2010. Monosynaptic circuit tracing in vivo through Cre-dependent targeting and complementation of modified rabies virus. *Proc. Natl. Acad. Sci. U.S.A.* 107(50):21848–53
23. Leshan RL, Greenwald-Yarnell M, Patterson CM, Gonzalez IE, Myers MG. 2012. Leptin action through hypothalamic nitric oxide synthase-1-expressing neurons controls energy balance. *Nat. Med.* 18(5):820–23
24. Wu Z, Xu Y, Zhu Y, Sutton AK, Zhao R, et al. 2012. An obligate role of oxytocin neurons in diet induced energy expenditure. *PLoS ONE*. 7(9):e45167
25. Watabe-Uchida M, Zhu L, Ogawa SK, Vamanrao A, Uchida N. 2012. Whole-brain mapping of direct inputs to midbrain dopamine neurons. *Neuron*. 74(5):858–73
26. Swanson LW, Sawchenko PE. 1983. Hypothalamic integration: organization of the paraventricular and supraoptic nuclei. *Annu. Rev. Neurosci.* 6(1):269–324
27. Horst ter GJ, Luiten PG. 1986. The projections of the dorsomedial hypothalamic nucleus in the rat. *Brain Res. Bull.* 16(2):231–48
28. Ulrich-Lai YM, Jones KR, Ziegler DR, Cullinan WE, Herman JP. 2011. Forebrain origins of glutamatergic innervation to the rat paraventricular nucleus of the hypothalamus: differential inputs to the anterior versus posterior subregions. *J. Comp. Neurol.* 519(7):1301–19
29. Follwell MJ, Ferguson AV. 2002. Cellular mechanisms of orexin actions on paraventricular nucleus neurones in rat hypothalamus. *The Journal of Physiology*. 545(Pt 3):855–67
30. Betley JN, Cao ZFH, Ritola KD, Sternson SM. 2013. Parallel, redundant circuit organization for homeostatic control of feeding behavior. *Cell*. 155(6):1337–50
31. Ziegler DR, Edwards MR, Ulrich-Lai YM, Herman JP, Cullinan WE. 2012. Brainstem origins of glutamatergic innervation of the rat hypothalamic paraventricular nucleus. *J. Comp. Neurol.* 520(11):2369–94

32. Rho JH, Swanson LW. 1989. A morphometric analysis of functionally defined subpopulations of neurons in the paraventricular nucleus of the rat with observations on the effects of colchicine. *Journal of Neuroscience*. 9(4):1375–88
33. Huszar D, Lynch CA, Fairchild-Huntress V, Dunmore JH, Fang Q, et al. 1997. Targeted disruption of the melanocortin-4 receptor results in obesity in mice. *Cell*. 88(1):131–41
34. Blevins JE, Schwartz MW, Baskin DG. 2004. Evidence that paraventricular nucleus oxytocin neurons link hypothalamic leptin action to caudal brain stem nuclei controlling meal size. *Am. J. Physiol. Regul. Integr. Comp. Physiol.* 287(1):R87–R96
35. Daftary SS, Boudaba C, Tasker JG. 2000. Noradrenergic regulation of parvocellular neurons in the rat hypothalamic paraventricular nucleus. *Neuroscience*. 96(4):743–51
36. Csáki A, Kocsis K, Halász B, Kiss J. 2000. Localization of glutamatergic/aspartatergic neurons projecting to the hypothalamic paraventricular nucleus studied by retrograde transport of [3H]D-aspartate autoradiography. *Neuroscience*. 101(3):637–55
37. van den Pol AN. 1982. The magnocellular and parvocellular paraventricular nucleus of rat: intrinsic organization. *J. Comp. Neurol.* 206(4):317–45
38. Blevins JE, Eakin TJ, Murphy JA, Schwartz MW, Baskin DG. 2003. Oxytocin innervation of caudal brainstem nuclei activated by cholecystokinin. *Brain Research*. 993(1-2):30–41

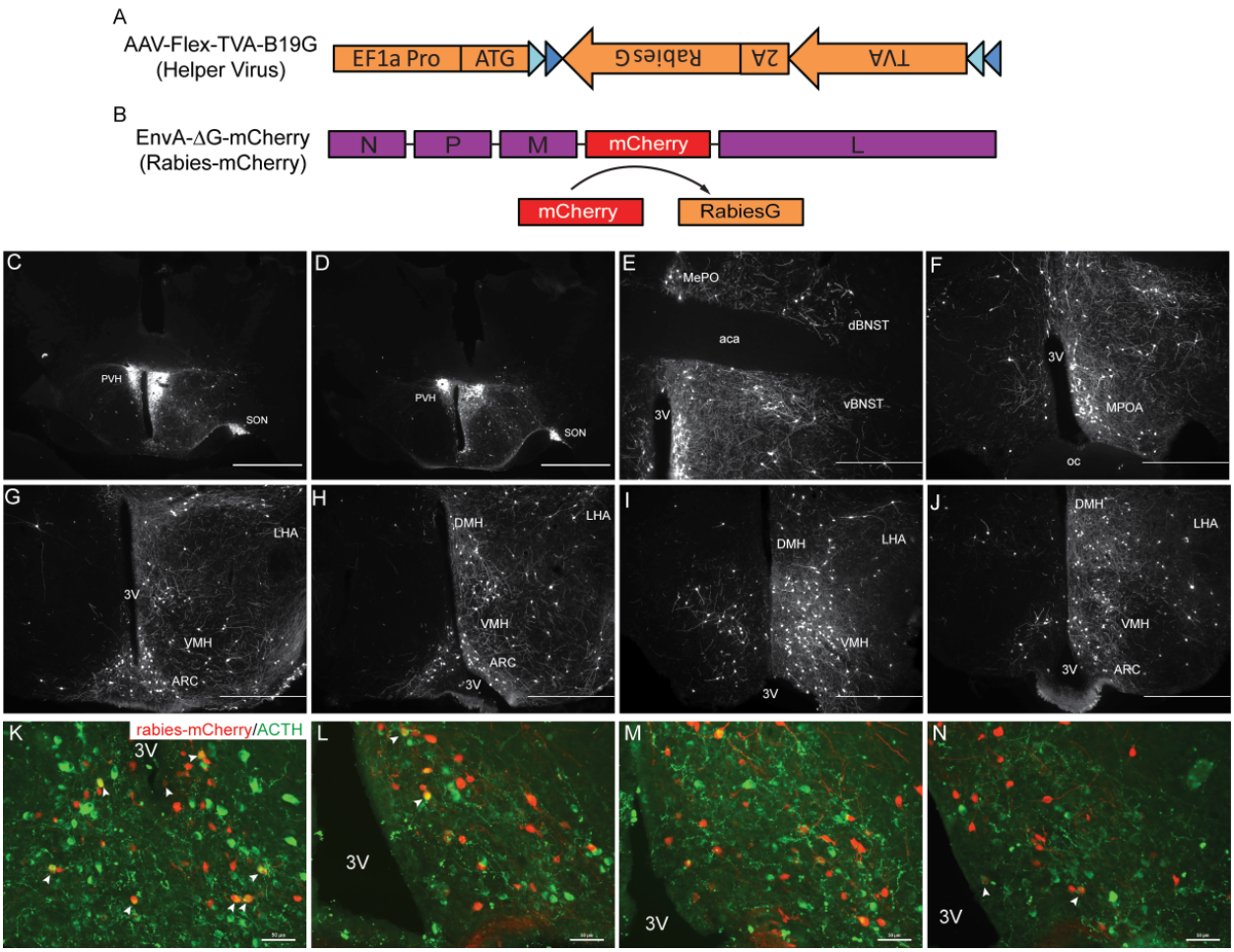
A
AAV-Flex-TVA-B19G
(Helper Virus)
EF1a Pro
ATG
RabiesG
2A
TVA
B
EnvA-ΔG-mCherry
(Rabies-mCherry)
N
P
M
mCherry
L
mCherry
RabiesG
C
PVH
SON
D
PVH
SON
E
MePO
aca
dBNST
vBNST
3V
F
3V
MPOA
oc
G
LHA
3V
VMH
ARC
H
DMH
LHA
VMH
ARC
3V
I
DMH
LHA
VMH
3V
J
DMH
LHA
VMH
3V
ARC
K
rabies-mCherry/ACTH
3V
L
3V
M
3V
N
3V

Figure 4.1. Modified rabies virus allows for identification of monosynaptic inputs to Cre-expressing PVH populations. A) Using a 2A linker, a helper virus was generated to express the TVA receptor and B19 glycoprotein (B19G/rabiesG) in Cre-expressing cells. B) Modified rabies virus expresses mCherry instead of the endogenous B19G, therefore requiring prior injection of AAV-Flex-TVA-B19G. C-D) Immunohistochemistry (IHC) identifies dense rabies-mCherry expression throughout the PVH of *Sim1-Cre +AAV-Flex-TVA-B19G* mice injected with rabies-mCherry in the PVH. Rabies-mCherry expression in the SON identifies SON projections to $Sim1^{PVH}$ neurons. E-J) Sites identified upstream of the PVH include the bed nucleus of the stria terminalis (BNST, E-F), preoptic area (POA, E-F), arcuate nucleus (ARC, G-J), ventromedial hypothalamus (VMH, G-H), and lateral hypothalamic area (LHA, G-I). K-N) IHC was performed for ACTH and rabies-mCherry demonstrating $POMC^{ARC}$ regulation of the PVH using this approach. 3V=third ventricle, aca=anterior part of anterior commissure, MePO=median preoptic area, MPOA=medial preoptic area, DMH=dorsomedial hypothalamus, oc=optic chiasm.

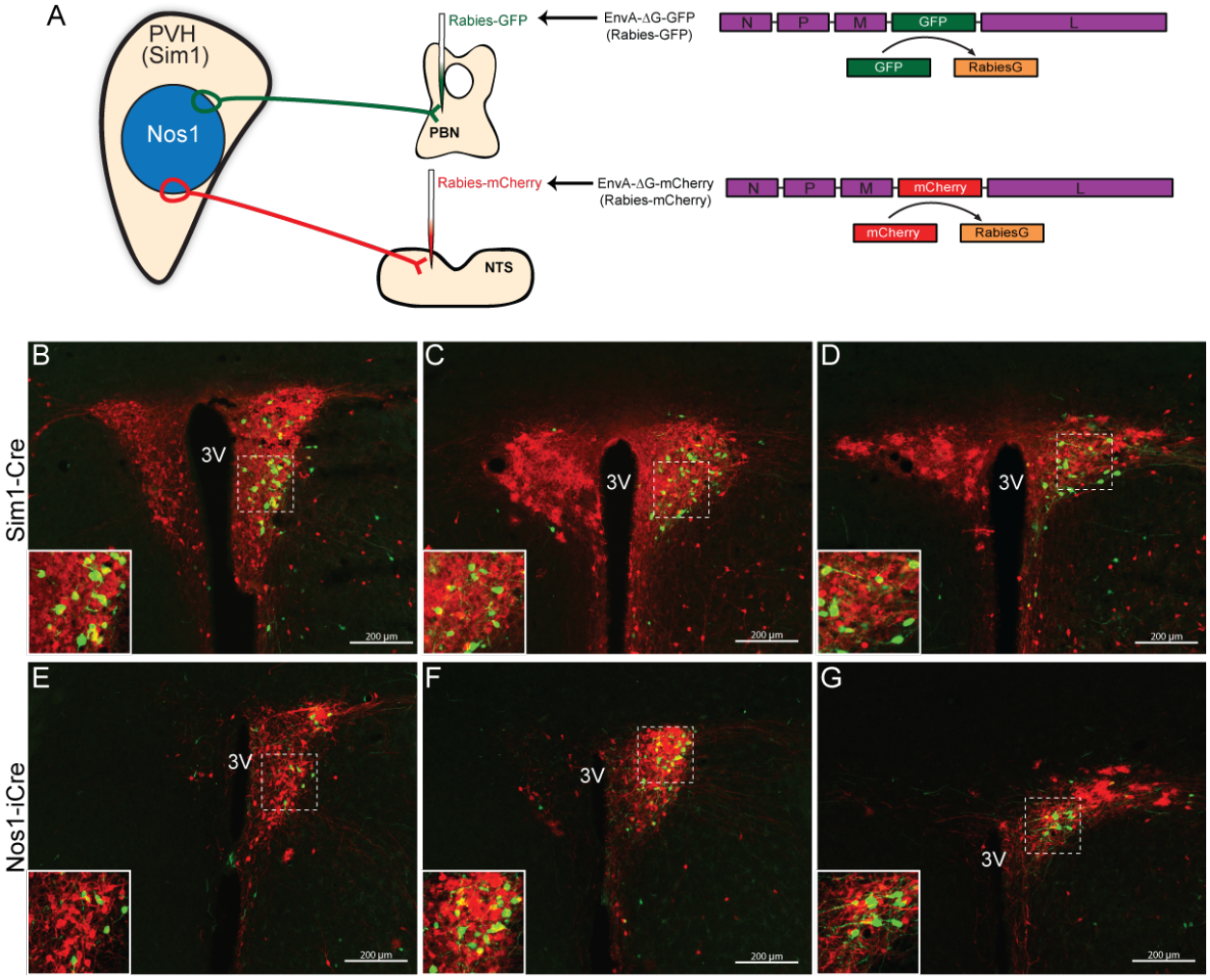
A
PVH
(Sim1)
Nos1
PBN
NTS
Rabies-GFP
EnvA-ΔG-GFP
(Rabies-GFP)
N
P
M
GFP
L
GFP
RabiesG
Rabies-mCherry
EnvA-ΔG-mCherry
(Rabies-mCherry)
N
P
M
mCherry
L
mCherry
RabiesG
Sim1-Cre
Nos1-iCre
B
C
D
E
F
G
3V
200 μm

Figure 4.2. Terminal-specific modified rabies virus injection identifies PVH populations regulating PBN and NTS outputs. A) *Sim1-Cre +AAV-Flex-TVA-B19G* and *Nos1-iCre +AAV-Flex-TVA-B19G* mice were injected with rabies-GFP in the PBN and rabies-mCherry in the NTS to determine if PVH neurons collateralize to different projection sites. B-D) IHC throughout the PVH demonstrates little overlap between rabies-mCherry, identifying NTS-projecting $Sim1^{PVH}$ neurons, and rabies-GFP, labeling PBN-projecting $Sim1^{PVH}$ neurons. E-G) Similar distribution of rabies-mCherry and rabies-GFP is observed in the PVH of *Nos1-iCre +AAV-Flex-TVA-B19G* mice. Dashed boxes indicate regions that are digitally enlarged and shown as insets. 3V=third ventricle

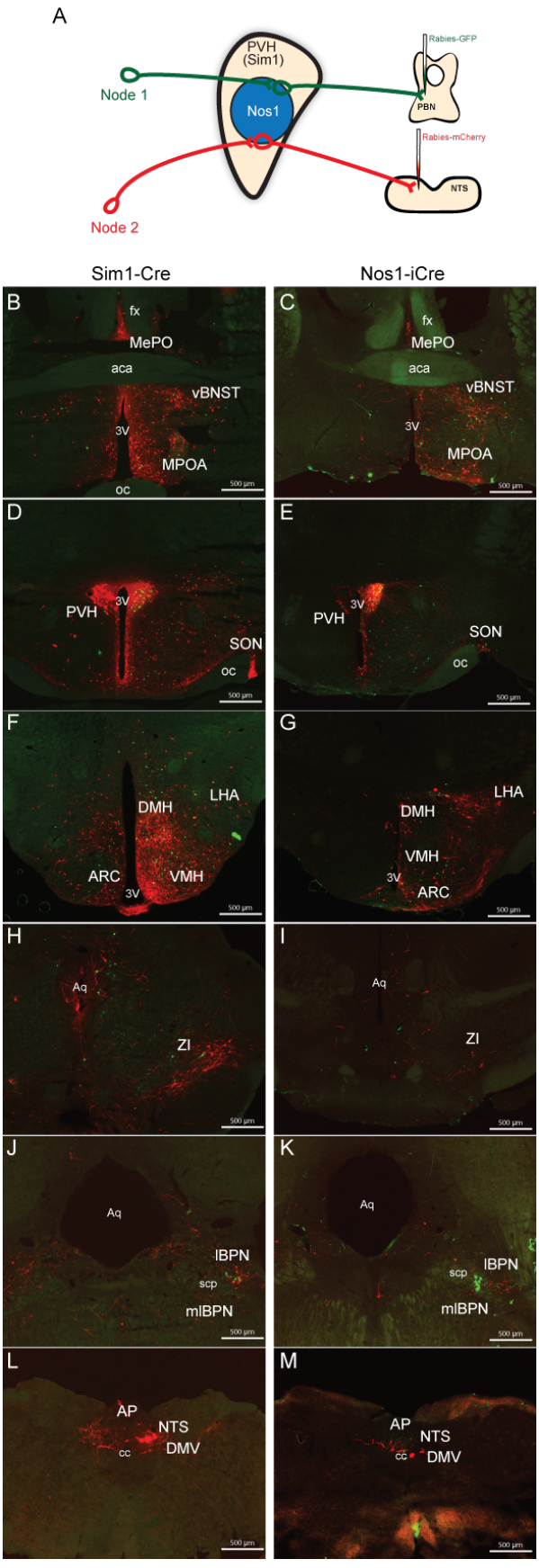
A
PVH
(Sim1)
Node 1
Nos1
Rabies-GFP
PBN
Rabies-mCherry
NTS
Node 2
Sim1-Cre
Nos1-iCre
B
fx
MePO
aca
vBNST
3V
MPOA
oc
C
fx
MePO
aca
vBNST
3V
MPOA
D
PVH
3V
SON
oc
E
PVH
3V
SON
oc
F
DMH
LHA
ARC
VMH
3V
G
LHA
DMH
VMH
3V
ARC
H
Aq
ZI
I
Aq
ZI
J
Aq
lBPN
scp
mlBPN
K
Aq
scp
lBPN
mlBPN
L
AP
NTS
cc
DMV
M
AP
NTS
cc
DMV

Figure 4.3 Inputs to NTS-projecting or PBN-projecting PVH populations are distinct. A) Monosynaptic inputs to PBN-projecting Sim1^{PVH} and Nos1^{PVH} populations are identified with rabies-GFP, whereas sites upstream of NTS-projecting Sim1^{PVH} and Nos1^{PVH} neurons are labeled by rabies-mCherry. B-H) IHC for GFP and mCherry identifies little overlap in neuronal populations upstream of Sim1^{PVH} populations projecting to the PBN or NTS, respectively. J, L) Rabies-GFP (J) and rabies-mCherry (L) injection sites are identified by glial damage. C-I) Similar localization of rabies-mCherry and rabies-GFP is demonstrated by neurons upstream of the smaller Nos1^{PVH} population when rabies-GFP was injected in the PBN (K) and rabies-mCherry into the NTS (M). fx=fornix, aq=aqueduct, scp=superior cerebellar peduncle, cc=central canal, DMV=dorsal motor nucleus of the vagus, AP=area postrema, ZI=zona incerta

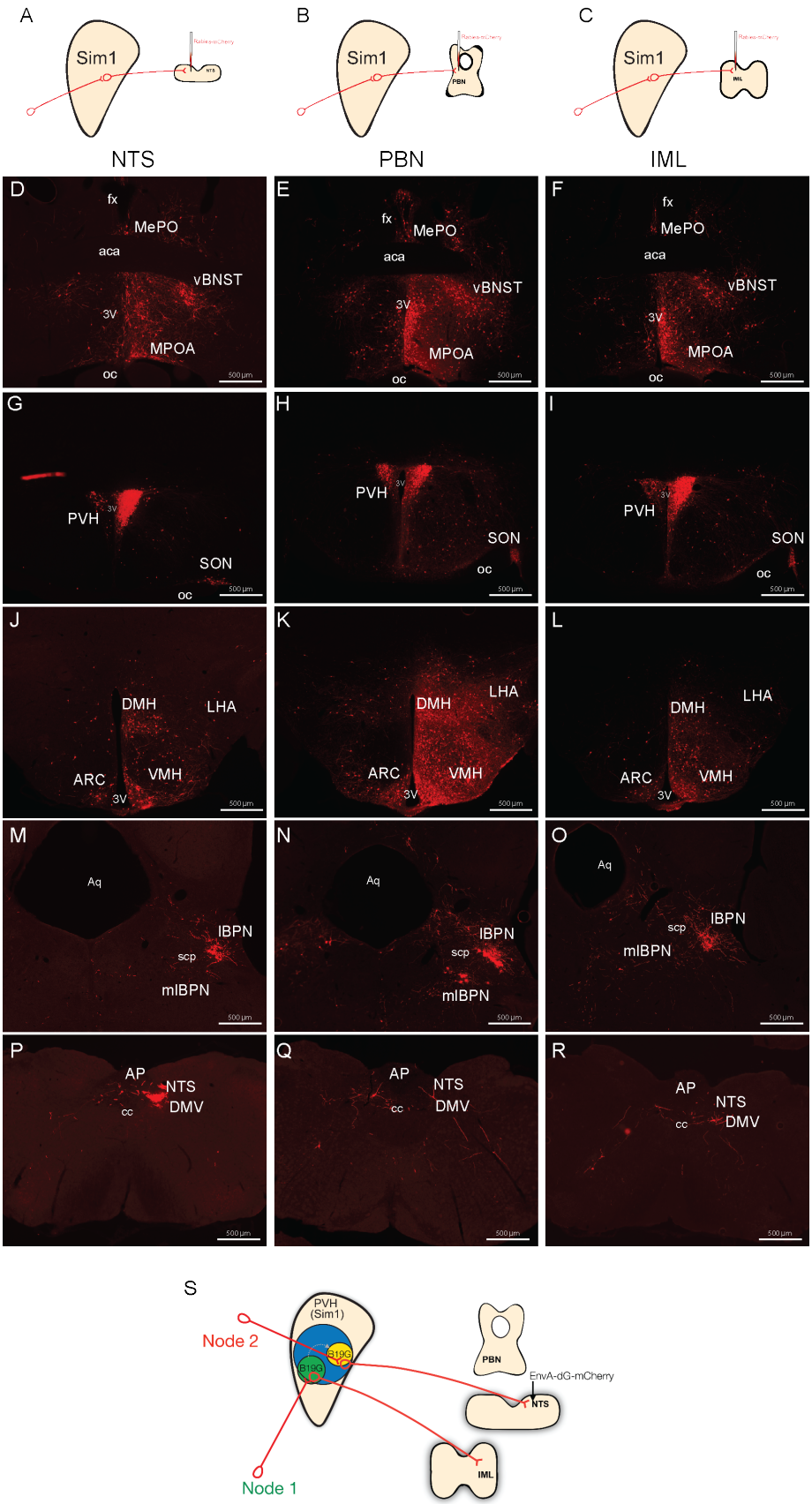
A
Sim1
NTS
B
Sim1
PBN
C
Sim1
IML
D
fx
MePO
aca
vBNST
3V
MPOA
oc
E
fx
MePO
aca
vBNST
3V
MPOA
oc
F
fx
MePO
aca
vBNST
3V
MPOA
oc
G
PVH
3V
SON
oc
H
PVH
3V
SON
oc
I
PVH
3V
SON
oc
J
DMH
LHA
ARC
VMH
3V
K
DMH
LHA
ARC
VMH
3V
L
DMH
LHA
ARC
VMH
3V
M
Aq
IBPN
scp
mIBPN
N
Aq
IBPN
scp
mIBPN
O
Aq
IBPN
scp
mIBPN
P
AP
NTS
DMV
cc
Q
AP
NTS
DMV
cc
R
AP
NTS
DMV
cc
S
PVH
(Sim1)
Node 2
B19G
B19G
PBN
EnvA-dG-mCherry
NTS
IML
Node 1

Figure 4.4. Projection-specific rabies-mCherry injection reveals similar inputs to Sim1^{PVH} neurons projecting to the NTS, PBN, or IML. A-C) *Sim1-Cre +AAV-Flex-TVA-B19G* mice were injected with rabies-mCherry in the NTS (A), PBN (B), or IML (C) to compare inputs to projection-defined Sim1^{PVH} neurons. D-F) Similar localization of rabies-mCherry is observed in BNST and POA neurons upstream of NTS-projecting (D), PBN-projecting (E), or IML-projecting (F) Sim1^{PVH} neurons. G-I) Despite different rabies-mCherry injection sites, dense rabies-mCherry expression is observed throughout the PVH. J-L) ARC, VMH, DMH, and LHA populations are all upstream of Sim1^{PVH} neurons projecting to different sites. M, O) PBN neurons lie upstream of NTS-projecting (M) and IML-projecting (O) Sim1^{PVH} neurons. N, P) Gliosis identifies rabies-mCherry injection site in experiments testing inputs to PBN-projecting (N) or NTS-projecting (P) Sim1^{PVH} neurons (N). Q-R) Few NTS neurons lie upstream of parvocellular Sim1^{PVH} neurons. S) Diagram depicting possible caveat with projection-specific modified rabies virus approaches. Since B19G is expressed in all Sim1-Cre^{+} neurons in the PVH, including neurons not projecting to the rabies-mCherry injection site, intra-PVH connectivity allows for multi-synaptic retrograde transmission of rabies-mCherry.

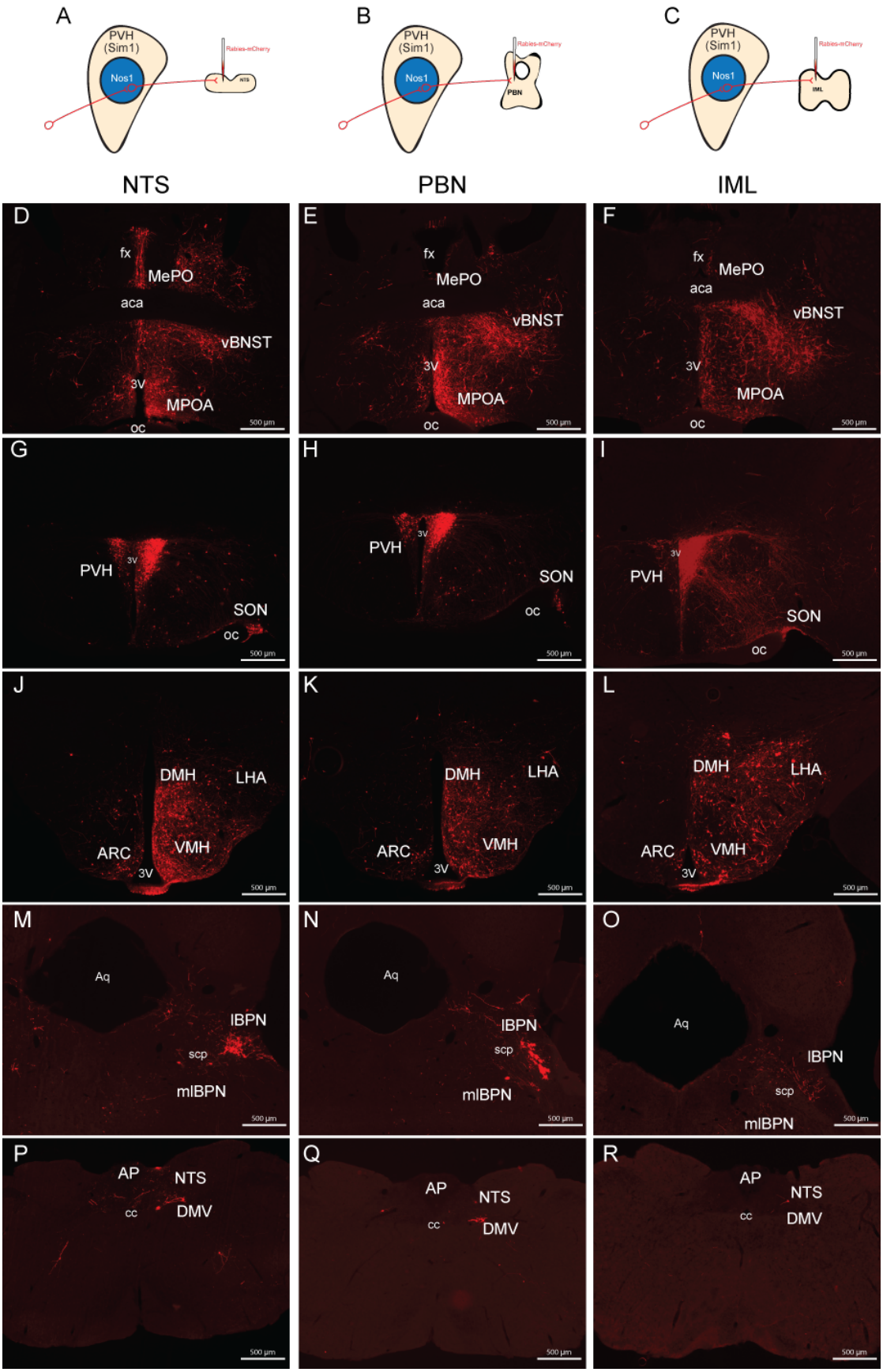
A
PVH (Sim1)
Nos1
Rabies-mCherry
NTS
B
PVH (Sim1)
Nos1
Rabies-mCherry
PBN
C
PVH (Sim1)
Nos1
Rabies-mCherry
IML
NTS
PBN
IML
D
fx
MePO
aca
vBNST
3V
MPOA
oc
500 μm
E
fx
MePO
aca
vBNST
3V
MPOA
oc
500 μm
F
fx
MePO
aca
vBNST
3V
MPOA
oc
500 μm
G
PVH
3V
SON
oc
500 μm
H
PVH
3V
SON
oc
500 μm
I
PVH
3V
SON
oc
500 μm
J
DMH
LHA
ARC
VMH
3V
500 μm
K
DMH
LHA
ARC
VMH
3V
500 μm
L
DMH
LHA
ARC
VMH
3V
500 μm
M
Aq
lBPN
scp
mlBPN
500 μm
N
Aq
lBPN
scp
mlBPN
500 μm
O
Aq
lBPN
scp
mlBPN
500 μm
P
AP
NTS
cc
DMV
500 μm
Q
AP
NTS
cc
DMV
500 μm
R
AP
NTS
cc
DMV
500 μm

Figure 4.5. Inputs to projection-defined Nos1^{PVH} neurons reveal intra-PVH network. A-C) Rabies-mCherry injection was performed in distinct projection sites of Nos1^{PVH} neurons, a subset of the Sim1^{PVH} neuronal field, in *Nos1-iCre +AAV-Flex-TVA-B19G* mice. Forebrain (D-F) and hypothalamic (J-L) inputs to NTS-projecting, PBN-projecting, or IML-projecting Nos1^{PVH} neurons are similar to those observed from the entire PVH (using *Sim1-Cre*, Figure 4.4). G-I) Rabies-mCherry identifies dense labeling in the PVH despite different rabies-mCherry injection sites. M,O) PBN neurons are upstream of NTS-projecting Nos1^{PVH} neurons (M), whereas rabies-mCherry expression is largely absent in the PBN of mice with IML-directed rabies-mCherry injections (O). N, P) Glial damage identifies rabies-mCherry injection sites in the PBN (N) and NTS (P). Q-R) Few NTS neurons are upstream of Nos1^{PVH} neurons projecting to the PBN or IML.

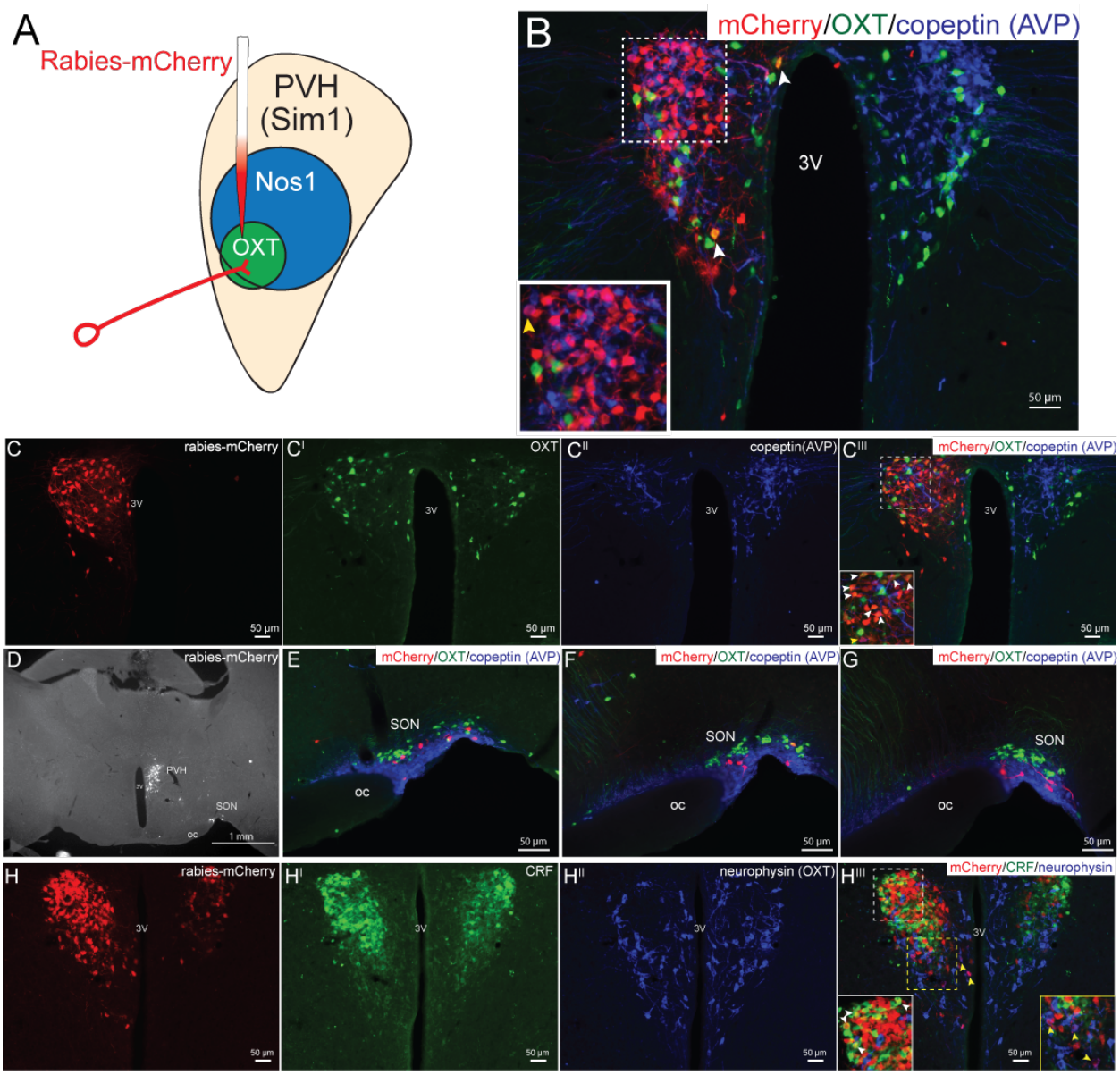
A
Rabies-mCherry
PVH
(Sim1)
Nos1
OXT
B
mCherry/OXT/copeptin (AVP)
3V
50 µm
C
rabies-mCherry
C'
OXT
C''
copeptin(AVP)
C'''
mCherry/OXT/copeptin (AVP)
D
rabies-mCherry
PVH
SON
oc
1 mm
E
mCherry/OXT/copeptin (AVP)
SON
oc
F
mCherry/OXT/copeptin (AVP)
SON
oc
G
mCherry/OXT/copeptin (AVP)
SON
oc
H
rabies-mCherry
H'
CRF
H''
neurophysin (OXT)
H'''
mCherry/CRF/neurophysin

Figure 4.6. Intra-PVH circuits are upstream of OXT^{PVH} neurons. A) Monosynaptic inputs to OXT^{PVH} neurons, a small subset of the $Nos1^{PVH}$ neuronal population, are identified using PVH-directed injection of rabies-mCherry in *OXT-iCre +AAV-Flex-TVA-B19G* mice. B-C) Rabies-mCherry labeling demonstrates that monosynaptic inputs to OXT^{PVH} neurons (green, white arrows) are largely from non-OXT^{PVH} populations, including those expressing copeptin, the carrier molecule for AVP (blue, yellow arrows). D). Although few non-PVH sites lie upstream of OXT^{PVH} neurons, expression of rabies-mCherry is obxserved in the SON. E-G) Rabies-mCherry identifies SON inputs to OXT^{PVH} neurons largely in the vicinity of AVP^{SON} neurons (blue). H) PVH-directed colchichine in *OXT-iCre +AAV-Flex-TVA-B19G* mice with rabies-mCherry injection in the PVH allows for detection of CRF^{PVH} neurons (green) that co-express rabies-mCherry (white arrows), demonstrating CRF^{PVH} regulation of OXT^{PVH} neurons (identified by neurophysin, blue). Co-localization of neurophysin and mCherry identifies primary infected OXT^{PVH} neurons (yellow arrows). Dashed boxes indicate regions that are digitally enlarged and shown as insets. 3V=third ventricle, SON=supraoptic nucleus, CRF=cortiocotropin releasing factor, OXT=oxytocin, AVP=vasopressin

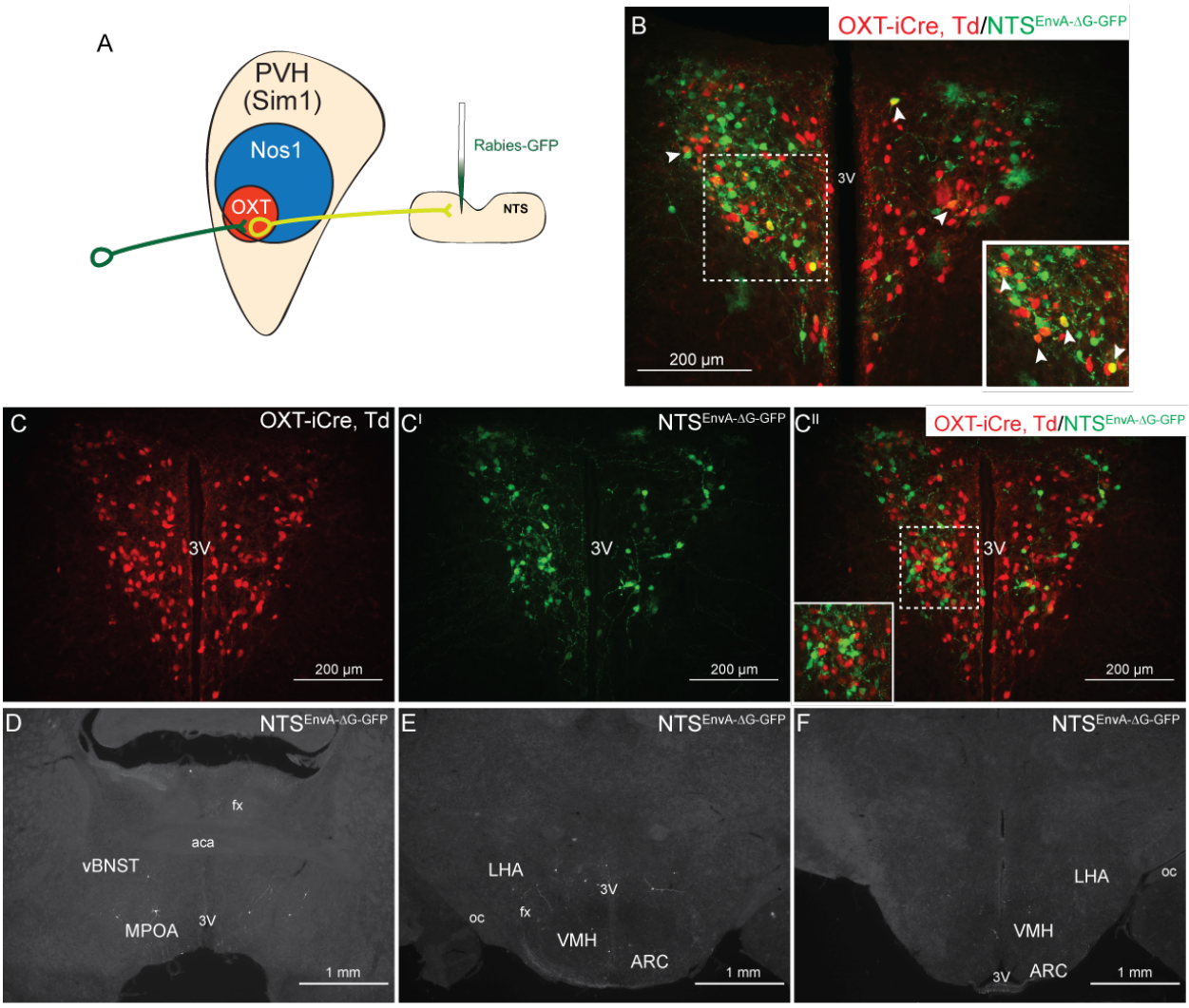
A
PVH
(Sim1)
Nos1
OXT
Rabies-GFP
NTS
B
OXT-iCre, Td/NTS EnvA-ΔG-GFP
3V
200 μm
C
OXT-iCre, Td
3V
200 μm
C'
NTS EnvA-ΔG-GFP
3V
200 μm
C''
OXT-iCre, Td/NTS EnvA-ΔG-GFP
3V
200 μm
D
NTS EnvA-ΔG-GFP
fx
aca
vBNST
MPOA
3V
1 mm
E
NTS EnvA-ΔG-GFP
LHA
3V
oc
fx
VMH
ARC
1 mm
F
NTS EnvA-ΔG-GFP
LHA
oc
VMH
3V
ARC
1 mm

Figure 4.7. Intra-PVH regulation of OXT^{PVH} neuronal populations projecting through the NTS. A) Rabies-GFP was injected in the NTS of *OXT-iCre,Td +AAV-Flex-TVA-B19G* mice to determine inputs to OXT^{PVH} neurons connected to the NTS, likely via OXT^{PVH} fibers of passage. B-C) Co-localization of OXT-iCre, Td neurons (red) with rabies-GFP (green) identifies NTS-projecting OXT^{PVH} neurons (white arrows). D-F) Limited rabies-GFP expression is observed outside of the PVH, demonstrating that inputs to OXT^{PVH} neurons projecting through the NTS are regulated by sites within the PVH. Dashed boxes indicate regions that are digitally enlarged and shown as insets.

Chapter V

Discussion: Distinct PVH subpopulations control energy balance in an intra-PVH network

Early lesioning studies that destroyed the cellular components of the PVH demonstrated a critical role for this complex nucleus in restraining food intake (1, 2). Since PVH neurons are heterogeneous and largely distinct, interrogation of the entire PVH, such as what occurs with anatomical lesions, does not discriminate the capabilities of different PVH circuits to regulate disparate functions, including feeding behavior and energy expenditure. Studies to date have interrogated both the neurocircuitry and function of the neuropeptidergic PVH neurons through the use of nonspecific tracing reagents in combination with knock-out rodent models in an attempt to link potential function with PVH projection targets (3-6). These studies suggested that known neuropeptide populations encompass just 25% of the PVH neurons projecting to hindbrain or spinal cord regions, highlighting a significant gap in our knowledge of the neurochemical identity of PVH circuits regulating autonomic function (7).

Significant questions remain regarding the ability of PVH neurons to control energy balance parameters: does a single PVH population regulate feeding suppression, or can this be achieved by multiple, redundant PVH neuronal subpopulations? Do PVH neurons increase energy expenditure, and if so, which neurons coordinate this response? What are the afferent circuits engaging PVH

subpopulations? Which circuits are used by PVH neurons to carry out diverse physiologic responses, and are these circuits mutually exclusive? In this dissertation, I have addressed some of these questions with the use of novel genetic mouse models in combination with viral reagents to clarify the circuitry and function of PVH cell-types in energy balance control.

Multiple PVH populations can control feeding suppression and energy expenditure

With these studies, we characterize different genetically-marked PVH subpopulations that are largely independent of one another (with the exception of OXT^{PVH} neurons). Our initial experiments suggested that a non-OXT $Nos1^{PVH}$ neuronal population was the primary PVH controller of feeding behavior. Additional studies demonstrate that $IRS4^{PVH}$ neurons, an independent population that does not express Nos1 or OXT, are also sufficient for feeding and energy expenditure regulation. This demonstrates the capacity of multiple, separate PVH populations to control both these parameters and suggests that PVH populations may act redundantly in energy balance regulation. Moreover these distinct neuronal subsets also send dense projections to the same hindbrain and spinal regions, providing a potential mechanism for PVH neuronal subpopulations to each control feeding and energy expenditure parameters, respectively. These initial studies testing sufficiency demonstrated that Nos1 and IRS4 are novel markers of independent PVH populations capable of achieving similar physiologic effects in terms of energy balance regulation.

As the primary pre-autonomic hypothalamic output, it would make sense for PVH circuits to be redundant in nature (8, 9). Coordinating a robust sympathetic response is necessary in a variety of physiologic responses, and suppression of feeding must be achieved at some point during meal ingestion due to the immediate physical limitations of energy intake. With the increasing prevalence of substantial energy intake and corresponding diseases such as obesity, these, potentially redundant, circuits would provide multiple avenues for therapeutic intervention. Future studies employing cell-specific RNA analysis in these different PVH subpopulations could identify the molecular identity of $IRS4^{PVH}$ and $Nos1^{PVH}$ neurons and therefore exploit multiple pathways for intervention.

While our initial chemogenetic activation studies suggest redundancy in the capability of PVH populations to control energy balance parameters, other studies testing the necessity of $IRS4^{PVH}$ neurons in feeding regulation call this theory into question. Indeed, neuronal silencing or ablation of $IRS4^{PVH}$ neurons, a population separate from $Nos1^{PVH}$ neurons, results in robust obesity due to hyperphagia. Therefore, this suggests that while activation of $Nos1^{PVH}$ neurons is sufficient to drive changes in feeding behavior, perhaps this response is dependent on intra-PVH networks requiring $IRS4^{PVH}$ neuronal activity. This theory is further supported by the fact that OXT^{PVH} neurons, a subset of the $Nos1^{PVH}$ population, are not necessary for feeding behavior. Indeed, we demonstrate dense interconnected PVH neurons upstream of hindbrain-projecting $IRS4^{PVH}$ or $Nos1^{PVH}$ neurons. Certainly, depending on the level of PVH interconnectivity, chemogenetic approaches used throughout these studies to activate specific PVH subsets could essentially activate large PVH

populations that are not limited to the subset in question. Whether these interconnected populations are required for the feeding effects observed upon chemogenetic activation is unknown.

Despite the sufficiency of IRS4^{PVH} neurons to drive increased energy expenditure, silencing or ablation of these neurons demonstrates that the IRS4^{PVH} population is not necessary for normal energy expenditure. These results highlight the potential for PVH subsets to be sufficient, but not necessary, in individual energy balance parameters. Moreover, these results suggest that other PVH populations are the relevant regulators of energy expenditure, in the absence of redundancy. Though undetermined in these studies, if Nos1^{PVH} neurons are necessary for energy expenditure regulation, it would suggest that PVH energy expenditure circuits are not redundant, and that Nos1^{PVH} neurons are the necessary output in energy expenditure regulation. To this point, previous reports testing the necessity of OXT and/or OXT^{PVH} neurons, a Nos1^{PVH} subset, suggest the importance of sympathetic output by these neurons in the prevention of diet-induced obesity. Similarly, in the context that Nos1^{PVH} neurons are sufficient, but not necessary for feeding regulation, this would demonstrate a lack of redundancy in PVH circuits controlling feeding, since IRS4^{PVH} neurons are clearly necessary in feeding regulation. With this model, PVH circuits would not be redundant, since the Nos1^{PVH} population would control energy expenditure and IRS4^{PVH} neurons would mediate feeding suppression (Figure 5.1). Yet, due to intra-PVH networks, these neuronal populations could change both energy balance parameters, likely via activation of one another. Future experiments ablating or silencing Nos1^{PVH} neurons would aid in determining the necessity of Nos1^{PVH} neurons in comparison to

the IRS4^{PVH} population, and further our understanding of the potential connections between these populations in the regulation of physiologic outputs. Since current technology limits our ability to detect small decreases in energy expenditure, future studies investigating the necessity of these populations in energy expenditure regulation would benefit by determining if PVH subset silencing affects cold-induced increases in sympathetic output.

Our studies show that multiple PVH neuronal populations are capable of controlling distinct energy balance parameters. This raises the possibility that the PVH populations studied may share some degree of overlap. In Nos1^{PVH} studies, a Cre-dependent reporter mouse was used in combination with immunohistochemical identification of different PVH subtypes. Therefore, PVH subtype analysis may be confounded somewhat by developmental expression of Cre activity by PVH cell types. Certainly, Nos1 immunoreactivity (IR) in adult mice labels far fewer neurons than those identified by Cre-dependent reporter mice. It is unknown if this discrepancy is due to limited Nos1 antibody efficacy. Therefore, since we determined that OXT^{PVH} neurons are a Nos1^{PVH} neuronal subset using reporter mice, it is possible that these populations show limited overlap in the adult mouse. However, studies using antibodies for both OXT peptide and Nos1 peptide in the same brain suggest this is unlikely. The characterization of Nos1^{PVH} versus IRS4^{PVH} neuronal populations is more difficult, since antibodies for IRS4 peptide are unavailable, and germline recombination of reporter constructs crossed to *IRS4-iCre* mice limits the use of reporter mice to identify IRS4^{PVH} neurons. Since our studies used PVH-directed viral reagents dependent on the active expression of Cre recombinase in adult mice, characterization of Cre-expressing PVH

neurons is likely best achieved via injection of a Cre-dependent reporter virus in the PVH of *IRS4-iCre* or *Nos1-iCre* mice. While IRS4^{PVH} neurons identified with this approach demonstrate distinct IRS4^{PVH} and Nos1^{PVH} neuronal populations, future studies employing *in situ* hybridization could also be used to validate the extent of overlap.

PVH circuit mechanisms underlying energy balance control

While these studies identify the projection targets that the PVH may engage to alter feeding and energy expenditure, the specific circuitry used by PVH subpopulations to control different physiologic outcomes has not been determined. It is likely that projections to thoracic spinal cord regions that regulate sympathetic output (i.e. IML) represent the main PVH output driving increased energy expenditure (7, 10, 11). Conversely, direct connections to hindbrain regions capable of sensing gastrointestinal-derived mechanical and peripheral energy status signals are probably coordinating the PVH-mediated satiety response (12, 13). Yet, which hindbrain site mediates this effect is unknown. Theories of PVH projections to the NTS as the primary circuit coordinating melanocortin-induced satiety were recently brought into question, since Mc4R^{PVH} neuronal projections to the PBN, but not the NTS, appear to be the relevant PVH circuit controlling feeding suppression (14). However, the optogenetic approaches used to decipher the functional relevance of these circuits should be interrogated, since terminal-specific activation of PVH projection targets does not eliminate the possibility of action potential back-propagation (15). In addition, we have shown that PVH populations projecting throughout the CNS are highly interconnected. It is therefore

possible that optogenetic activation of $Mc4R^{PVH}$ terminals in one projection site (i.e. PBN) could result in the unintended activation of other local PVH neurons with wider projection targets (i.e. NTS, IML). Future studies could employ terminal-specific inhibitory optogenetic approaches, thereby eliminating the possibility of action potential back-propagation and the potential large-scale PVH neuronal activation following activation of one PVH subset. These studies would therefore clarify the role of specific PVH subset projection targets in controlling feeding behavior and energy expenditure.

Future studies will be required to determine the mechanism used by $IRS4^{PVH}$ and $Nos1^{PVH}$ neurons to regulate feeding suppression. Melanocortinergic input to the PVH, a primary site of *Mc4R* expression, is widely considered to be the likely mechanism of PVH-controlled satiety regulation (6, 16, 17). Certainly, $Mc4R^{PVH}$ neuronal function is necessary for normal feeding control (6, 18). Yet, $Mc4R^{PVH}$ neurons are a relatively small proportion of the entire PVH, and have little overlap with neuropeptidergic PVH neuronal populations hypothesized to control feeding behavior (18). Though unstudied in this dissertation, it is possible that the $Nos1^{PVH}$ and $IRS4^{PVH}$ populations contain Mc4R, and therefore are a component of the Mc4R-mediated satiety response. Due to the lack of antibodies specific to Mc4R or IRS4 peptides, the overlap between these populations is unknown. $Nos1^{PVH}$ and $IRS4^{PVH}$ populations likely contain non-Mc4R neurons, since chemogenetic activation of these populations alters energy expenditure whereas activation of the $Mc4R^{PVH}$ neuronal population does not. While previous approaches used genetic mouse models to eliminate or re-express *Mc4R* on genetically-identified PVH populations, this approach would have limited application for $IRS4^{PVH}$ or $Nos1^{PVH}$ neurons since extra-PVH expression of IRS4, Nos1, and Mc4R is

broad, therefore making it difficult to limit studies to the PVH. Future experiments using more specific CRISPR/Cas9 reagents could abrogate these problems in order to determine the necessity of Mc4R on IRS4^{PVH} or Nos1^{PVH} neurons.

OXT^{PVH} neuronal circuits do not control feeding behavior

Substantial research indicates that OXT^{PVH} neurons project to the NTS and coordinate a satiety response (4, 5, 19). Moreover an increasing number of therapeutic approaches are using OXT administration in humans to suppress feeding and therefore treat obesity (20). OXT^{PVH} neurons were initially highlighted as a viable candidate for PVH-mediated feeding suppression, since obese *Sim1* haploinsufficient mice routinely demonstrated disproportionate decreases in *Oxt* expression (21, 22). Moreover, central administration of OXT in rodents can suppress feeding (23, 24). Recent studies highlighted the necessity of OXT neuronal inhibition to achieve AgRP-induced feeding suppression using viral reagents driving transgene expression from a relatively short OXT promoter element (19).

The evidence for OXT^{PVH} neuronal projections to hindbrain structures came from co-labeling of NTS-injected retrograde tracing reagents with OXT-IR in the PVH (4, 5, 7). However, the ability of these retrograde tracing reagents to infect fibers of passage has been documented, suggesting the possibility that these connections are potentially fibers of passage headed to the spinal cord (25, 26). Indeed, using a novel *OXT-iCre* mouse model, we demonstrate dense OXT^{PVH} innervation of the IML, and few synaptic terminals in the NTS arising from OXT^{PVH} neurons. In addition, NTS-directed injection of latex microspheres which are transported in a retrograde fashion fail to label OXT-IR

in the PVH. Moreover, our studies clearly demonstrate that OXT^{PVH} neuronal activation cannot alter feeding behavior. Recently, studies employing the same *OXT-iCre* mice used in our studies validated that OXT^{PVH} neurons are not synaptically connected to AgRP neurons, and that OXT^{PVH} neuronal inhibition is not required for AgRP-induced feeding (14). Our rabies virus results support these findings, since ARC populations are not monosynaptically connected to OXT^{PVH} neurons. These studies highlight the importance of using the *OXT-iCre* mouse model rather than the previously used viral approaches that are likely less specific to the OXT^{PVH} neuronal population.

Our results demonstrate the inability of OXT^{PVH} neuronal activation to change feeding behavior; this is in contrast to previous studies that demonstrate feeding suppression following pharmacologic administration of OXT in rodents and humans (20, 23, 24). Anorexic responses to high dose oxytocin administration could possibly be due to off-target pharmacologic effects or engagement of OXTR in peripheral sites. However, since we were unable to dissociate between central and pituitary-projecting OXT^{PVH} neurons, our chemogenetic activation studies may have also increased circulating OXT; this was still unable to change feeding behavior. It is important to note that OXT production is not limited to the PVH and that OXT^{SON} neurons are the primary source of circulating OXT. While this suggests the unlikely potential for non-PVH OXT to coordinate peripheral OXTR-mediated anorexia, additional experiments employing chemogenetic or optogenetic activation of OXT^{SON} neurons would be required to test this hypothesis.

Intra-PVH networks

Using a combination of modified rabies virus approaches, we demonstrate that PVH subpopulations are highly interconnected, and that this network has the potential to regulate multiple sites downstream of the PVH. Consistently, we demonstrate that rabies virus tracing identifies dense local PVH inputs to NTS-projecting, IML-projecting or PBN-projecting PVH neurons. While these studies do not test the functional implications of this interconnected network, it is plausible that multiple neuronal subpopulations within the PVH (e.g. Nos1, IRS4, OXT) all communicate different information relevant to energy balance in order to achieve a coordinated physiologic response. Although the separate $IRS4^{PVH}$ and $Nos1^{PVH}$ neuronal populations have similar functions and projection targets, the presence of an intra-PVH network further suggests the possibility that these pathways are not redundant but instead are coordinated in a complex local circuit to ultimately drive a functional output. Studies testing the necessity of $IRS4^{PVH}$ neuronal activity demonstrate this, since $IRS4^{PVH}$ neurons are required for the feeding response, even though $Nos1^{PVH}$ neurons, a population capable of decreasing feeding, should be unaffected in this situation. Future studies exploring the electrophysiology of non-$IRS4^{PVH}$ neurons following $IRS4^{PVH}$ neuronal ablation or silencing would provide valuable information regarding the importance of interconnected PVH circuits in coordinating energy balance.

The relevance of dense connectivity between the highly heterogenous PVH populations, likely both magnocellular and parvocellular, in the regulation of circuits projecting to hindbrain and spinal cord sites makes sense in the overall regulation of energy balance. PVH neurons are not only important in the regulation of feeding and

energy expenditure but are also essential in the control of a variety of physiologic and behavioral responses, including reproduction, stress responses, anxiety-related behaviors, blood pressure control, and growth (27-29). Certainly, these diverse physiologic functions are highly interrelated and should be communicating to coordinate appropriate homeostatic responses. While previous studies demonstrated that PVH populations had the capability of communicating with one another, they did not demonstrate that these PVH circuits were ultimately connected to hindbrain and spinal cord structures (30, 31). Thus, these studies greatly advance our understanding of the circuit mechanisms potentially used by the PVH to control complex physiologic outcomes. Moreover, this positions the PVH, a primary controller of feeding behavior, as a potential integrator of a variety of circuits and signals that coordinates appropriate feeding responses depending on the current physiologic state. More specifically, these intra-PVH networks have the potential to mediate a variety of physiologic paradigms that result in dysregulated energy balance such as anorexia, stress-induced feeding, dehydration-induced anorexia, and bulimia, to name a few. Therefore, further interrogation of the relevance of these interconnected circuits in a variety of behavioral paradigms associated with energy balance would greatly advance our understanding of PVH-controlled feeding behavior and energy expenditure.

Given the dense interconnectivity among PVH populations, it is tempting to consider the endogenous neuronal activity patterns of PVH subpopulations, especially as it relates to energy balance control. While PVH populations clearly communicate with one another, such as the demonstrated AVP^{PVH} neuronal innervation of OXT^{PVH} neurons, we did not determine the neuronal physiology of these connections. Since

PVH neuronal populations are predominately glutamatergic, it is tempting to hypothesize that neuronal activation of AVP^{PVH} neurons would increase the activity of OXT^{PVH} neurons. From a broader perspective, activation of one PVH subtype could therefore result in large-scale neuronal activity of the entire PVH. It is also possible that glutamate in PVH neurons could bind metabotropic glutamate receptors (mGluR) to achieve pre-synaptic inhibition. Though relatively unstudied, this would provide intra-PVH networks the ability to either activate or inhibit distinct circuits in order to carry out complex physiologic parameters. In addition to glutamate, intra-PVH connections likely use neuropeptides to communicate, though changes in neuronal activity resulting from neuropeptide release would be on a slower time scale than fast-acting neurotransmitters. Future studies employing *ex vivo* and/or *in vivo* calcium imaging techniques could test these hypotheses and further our understanding of the underlying activity patterns used by interconnected PVH networks to potentially regulate energy balance.

Our initial goal with the modified rabies virus tracing system was to determine if PVH circuits engaging distinct hindbrain sites (i.e. PBN vs. NTS) overlapped. Unfortunately, we found that rabies-GFP viral efficacy was lower than rabies-mCherry, limiting our ability to make definitive conclusions about the extent of overlap between the populations upstream of NTS-projecting or PBN-projecting PVH neurons. Moreover, we were unable to determine if PVH neurons collateralize to distinct projection targets, since rabies-GFP and rabies-mCherry labeling identified not only primary PVH neurons projecting to the PBN or NTS, but also the intra-PVH network upstream of these PVH neurons. Previous reports have employed a TVA-only helper

virus in order to determine if PVH populations collateralize to more than one projection site, since terminal-specific injection of modified rabies virus allows for visualization of primary PVH neurons and their projection targets (14, 32). For example, the lack of rabies-labeled terminals in the NTS of mice in which rabies tracing was performed in PBN-projecting $Mc4R^{PVH}$ neurons suggests that $Mc4R^{PVH}$ neurons do not send collateral projections to both the PBN and NTS (14). Yet, the reagents used in these studies employed a TVA-only helper virus that also expresses mCherry for visualization of injection site, limiting its use to rabies-GFP variants only. Given that our results suggest lower efficacy of the rabies-GFP virus, this approach likely underestimates $Mc4R^{PVH}$ populations projecting the PBN and their axons. To ameliorate this problem, future studies will employ a novel Cre-dependent TVA-HA helper virus that allows the use of rabies-mCherry in addition to labeling the injection site by HA-IR. With this approach, we will determine if PVH subpopulations collateralize to multiple projection sites, as well as further characterize the primary PVH neuronal subpopulations projecting to distinct sites.

Our results clearly demonstrate that numerous hypothalamic and forebrain sites densely innervate PVH subpopulations. However, the presence of a highly interconnected PVH network hinders our ability to generate discrete circuit maps of the afferent inputs engaging projection-specific PVH subpopulations. Specifically, we determined that intra-PVH connections between Cre^{+} populations likely resulted in multi-synaptic retrograde transmission of modified rabies virus. Therefore, while we attempted to specifically label inputs to PBN-projecting, NTS-projecting, or IML-projecting PVH neurons, these results largely reflected rabies virus tracing from all Cre^{+}

neurons in the PVH (Chapter IV, Figure 4.4S). Although this reflects a significant limitation of the projection-specific rabies virus approach, it also emphasizes the degree of interconnectivity between PVH populations that are ultimately upstream of distinct hindbrain or spinal cord sites. Future studies attempting to identify monosynaptic inputs to projection-defined PVH subpopulations would benefit from interrogating smaller PVH subsets and prior clarification of limited connectivity between Cre-expressing populations.

Overall, our studies demonstrate the importance of interrogating genetically-defined PVH circuits in the characterization of the PVH's ability to control energy balance. While multiple PVH subpopulations are capable of controlling feeding and energy expenditure, we highlight the potential for intra-PVH networks to regulate these distinct parvocellular PVH populations projecting throughout the brain. The significance of this interconnectivity cannot be understated, since heterogenous PVH neuronal populations regulate a variety of physiologic responses. The potential for a circuit connection between these responses in a single anatomical site such as the PVH could provide an inroad to understanding complex behaviors associated with energy balance control. Furthermore, the characterization of genetic populations within this complex PVH network has the potential for identification of therapeutic markers and/or approaches to a variety of complex diseases associated with dysregulated energy balance. Our discoveries highlight the complexity of examining the cellular biology of heterogenous nuclei such as the PVH. Emerging technological approaches including *in vivo* calcium imaging, optogenetics, and terminal-specific chemogenetic reagents will greatly enhance our ability to understand the endogenous network activity and

relevance of PVH circuits used to coordinate the homeostatic regulation of energy balance. Additionally, the development of intersectional genetic tools with multiple recombinases (Cre, Flp, Dre) will allow for finer scale dissection of complex nuclei such as the PVH. After all, much like the proportion of previously characterized centrally-projecting PVH populations discovered by Sawchenko *et. al.*, our current understanding of PVH circuits is likely less than 25% of all the mechanisms used by this nucleus to coordinate the complex regulation of energy balance.

References

1. Gold RM. 1973. Hypothalamic obesity: the myth of the ventromedial nucleus. *Science*. 182(4111):488–90
2. Sims JS, Lorden JF. 1986. Effect of paraventricular nucleus lesions on body weight, food intake and insulin levels. *Behav. Brain Res.*
3. Marsh DJ, Hollopeter G, Huszar D, Laufer R, Yagaloff KA, et al. 1999. Response of melanocortin-4 receptor-deficient mice to anorectic and orexigenic peptides. *Nat. Genet.* 21(1):119–22
4. Blevins JE, Eakin TJ, Murphy JA, Schwartz MW, Baskin DG. 2003. Oxytocin innervation of caudal brainstem nuclei activated by cholecystokinin. *Brain Research*. 993(1-2):30–41
5. Blevins JE, Schwartz MW, Baskin DG. 2004. Evidence that paraventricular nucleus oxytocin neurons link hypothalamic leptin action to caudal brain stem nuclei controlling meal size. *Am. J. Physiol. Regul. Integr. Comp. Physiol.* 287(1):R87–R96
6. Balthasar N, Dalgaard LT, Lee CE, Yu J, Funahashi H, et al. 2005. Divergence of melanocortin pathways in the control of food intake and energy expenditure. *Cell*. 123(3):493–505
7. Sawchenko PE, Swanson LW. 1982. Immunohistochemical identification of neurons in the paraventricular nucleus of the hypothalamus that project to the medulla or to the spinal cord in the rat. *J. Comp. Neurol.* 205(3):260–72
8. Saper CB, Loewy AD, Swanson LW, Cowan WM. 1976. Direct hypothalamo-autonomic connections. *Brain Research*. 117(2):305–12
9. Schwartz MW, Woods SC, Porte D, Seeley RJ, Baskin DG. 2000. Central nervous system control of food intake. *Nature*. 404(6778):661–71
10. Bamshad M, Song CK, Bartness TJ. 1999. CNS origins of the sympathetic nervous system outflow to brown adipose tissue. *Am. J. Physiol.* 276(6 Pt 2):R1569–78
11. Caverson MM, Ciriello J, Calaresu FR. 1984. Paraventricular nucleus of the hypothalamus: an electrophysiological investigation of neurons projecting directly to intermediolateral nucleus in the cat. *Brain Research*. 305(2):380–83
12. Grill HJ, Hayes MR. 2012. Hindbrain neurons as an essential hub in the neuroanatomically distributed control of energy balance. *Cell Metab.* 16(3):296–309
13. Berthoud HR, Blackshaw LA, Brookes SJH, Grundy D. 2004. Neuroanatomy of extrinsic afferents supplying the gastrointestinal tract. *Neurogastroenterol. Motil.* 16 Suppl 1(s1):28–33
14. Garfield AS, Li C, Madara JC, Shah BP, Webber E, et al. 2015. A neural basis for melanocortin-4 receptor-regulated appetite. *Nat. Neurosci.* 18(6):863–71
15. Sternson SM, Atasoy D, Betley JN, Henry FE, Xu S. 2016. An Emerging Technology Framework for the Neurobiology of Appetite. *Cell Metab.* 23(2):234–53
16. Kishi T, Aschkenasi CJ, Lee CE, Mountjoy KG, Saper CB, Elmquist JK. 2003. Expression of melanocortin 4 receptor mRNA in the central nervous system of the rat. *J. Comp. Neurol.* 457(3):213–35

17. Krashes MJ, Lowell BB, Garfield AS. 2016. Melanocortin-4 receptor-regulated energy homeostasis. *Nat. Neurosci.* 19(2):206–19
18. Shah BP, Vong L, Olson DP, Koda S, Krashes MJ, et al. 2014. MC4R-expressing glutamatergic neurons in the paraventricular hypothalamus regulate feeding and are synaptically connected to the parabrachial nucleus. *Proc. Natl. Acad. Sci. U.S.A.* 111(36):13193–98
19. Atasoy D, Betley JN, Su HH, Sternson SM. 2012. Deconstruction of a neural circuit for hunger. *Nature*. 488(7410):172–77
20. Zhang H, Wu C, Chen Q, Chen X, Xu Z, et al. 2013. Treatment of obesity and diabetes using oxytocin or analogs in patients and mouse models. *PLoS ONE*. 8(5):e61477
21. Kublaoui BM, Gemelli T, Tolson KP, Wang Y, Zinn AR. 2008. Oxytocin deficiency mediates hyperphagic obesity of Sim1 haploinsufficient mice. *Mol. Endocrinol.* 22(7):1723–34
22. Tolson KP, Gemelli T, Gautron L, Elmquist JK, Zinn AR, Kublaoui BM. 2010. Postnatal Sim1 deficiency causes hyperphagic obesity and reduced Mc4r and oxytocin expression. *J. Neurosci.* 30(10):3803–12
23. Olson BR, Drutarosky MD, Chow MS, Hruby VJ, Stricker EM, Verbalis JG. 1991. Oxytocin and an oxytocin agonist administered centrally decrease food intake in rats. *Peptides*. 12(1):113–18
24. Arletti R, Benelli A, Bertolini A. 1989. Influence of oxytocin on feeding behavior in the rat. *Peptides*. 10(1):89–93
25. Chen S, Aston-Jones G. 1995. Evidence that cholera toxin B subunit (CTb) can be avidly taken up and transported by fibers of passage. *Brain Research*. 674(1):107–11
26. Dado RJ, Burstein R, Cliffer KD, Giesler GJ. 1990. Evidence that Fluoro-Gold can be transported avidly through fibers of passage. *Brain Research*. 533(2):329–33
27. Swanson LW, Sawchenko PE. 1983. Hypothalamic integration: organization of the paraventricular and supraoptic nuclei. *Annu. Rev. Neurosci.* 6(1):269–324
28. Ferguson AV, Latchford KJ, Samson WK. 2008. The paraventricular nucleus of the hypothalamus - a potential target for integrative treatment of autonomic dysfunction. *Expert Opin. Ther. Targets*. 12(6):717–27
29. Coote JH. 1995. Cardiovascular function of the paraventricular nucleus of the hypothalamus. *Biol. Signals*. 4(3):142–49
30. Daftary SS, Boudaba C, Szabó K, Tasker JG. 1998. Noradrenergic excitation of magnocellular neurons in the rat hypothalamic paraventricular nucleus via intranuclear glutamatergic circuits. *Journal of Neuroscience*. 18(24):10619–28
31. Csáki A, Kocsis K, Halász B, Kiss J. 2000. Localization of glutamatergic/aspartatergic neurons projecting to the hypothalamic paraventricular nucleus studied by retrograde transport of [3H]D-aspartate autoradiography. *Neuroscience*. 101(3):637–55
32. Betley JN, Cao ZFH, Ritola KD, Sternson SM. 2013. Parallel, redundant circuit organization for homeostatic control of feeding behavior. *Cell*. 155(6):1337–50

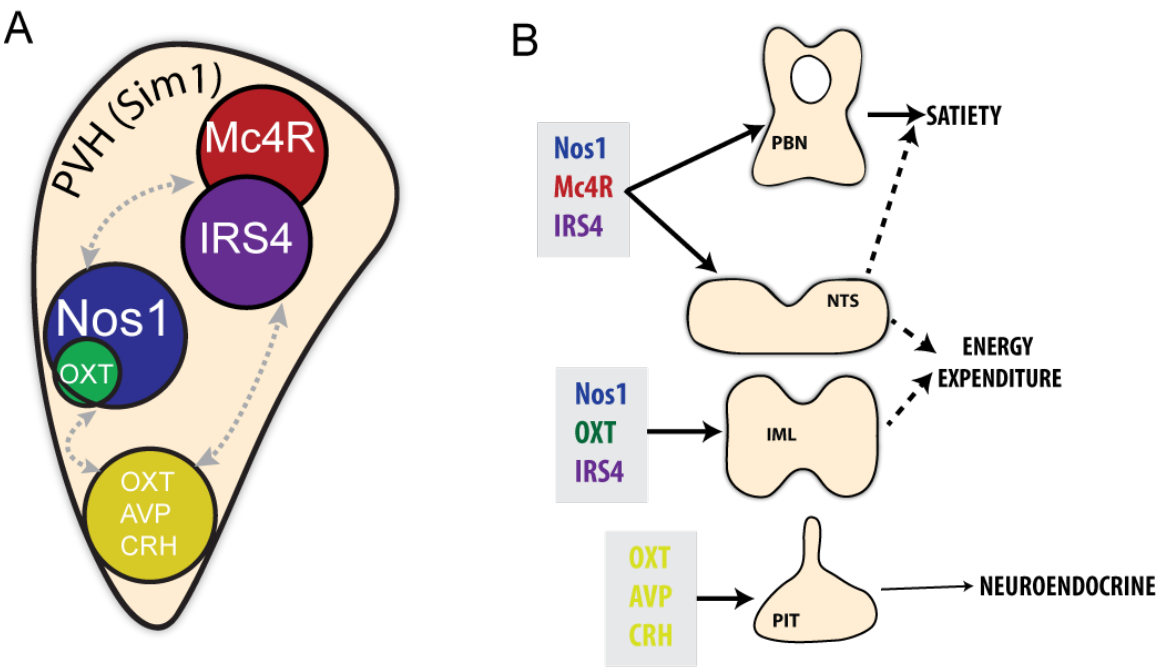
A
PVH (Sim1)
Mc4R
IRS4
Nos1
OXT
OXT
AVP
CRH
B
Nos1
Mc4R
IRS4
PBN
SATIETY
NTS
ENERGY
EXPENDITURE
Nos1
OXT
IRS4
IML
OXT
AVP
CRH
PIT
NEUROENDOCRINE

Figure 5.1. Distinct neurocircuits in an intra-PVH network regulate feeding and energy expenditure. A) Model of hypothesized interactions between independent PVH populations demonstrates the potential interconnectivity between $Nos1^{PVH}$, $IRS4^{PVH}$, $Mc4R^{PVH}$, and endocrine PVH neurons (yellow). B) Model for potential circuit mechanisms employed by PVH subpopulations in the regulation of satiety, energy expenditure, and endocrine output. Since $Mc4R^{PVH}$ projections to the PBN have been implicated in the control of feeding suppression, it is likely that $Nos1^{PVH}$ and/or $IRS4^{PVH}$ projections to this site mediate the satiety response. The function of $Nos1^{PVH}$, $IRS4^{PVH}$, and $Mc4R^{PVH}$ neuronal projections to the NTS are unknown, but might mediate energy expenditure and/or feeding suppression. On the other hand, PVH projections to the IML originate from OXT^{PVH}, $Nos1^{PVH}$ and $IRS4^{PVH}$ neurons, and likely coordinate sympathetic output and corresponding energy expenditure regulation. Neuroendocrine PVH neurons (including CRH, OXT, and AVP) regulate pituitary function via direct projections pituitary projections or the hypophyseal portal system.